Solitons on lattices and curved space-time

Vinay Kotecha

Solitons on Lattices and Curved Space-Time

Vinay Kotecha

A Thesis presented for the degree of
Doctor of Philosophy

Department of Mathematical Sciences
University of Durham
England

February 2001

To my parents,

Solitons on Lattices and Curved Space-time

Vinay Kotecha

Abstract

This thesis is concerned with solitons (solutions of certain nonlinear partial differential equations) in certain cases when the underlying space is either a lattice or curved. Chapter 2 of the thesis is concerned with the outcome of collisions between a kink (a 1-dimensional soliton) and an antikink for certain topological discrete (TD) systems. The systems considered are the TD sine-Gordon and the TD ϕ^4. For the TD sine-Gordon system it is found that the kink can support an internal shape mode which plays an important role during the collisions. In particular, this mode can be excited during collisions and this leads to spectacular resonance effects. The outcome of any particular collision has sensitive dependence on the initial conditions and could be either a trapped kink-antikink state, a "reflection" or a "transmission". Such resonance effects are already known to exist for the conventional discrete ϕ^4 system, and the TD ϕ^4 system is no different, though the results for the two are not entirely similar.

Chapter 3 considers the question of the existence of explicit travelling kink solutions for lattice systems. In particular, an expression for such a solution for the integrable lattice sine-Gordon system is derived.

In Chapter 4, by reducing the Yang-Mills equations on the $(2+2)$-dimensional ultrahyperbolic space-time, an integrable Yang-Mills-Higgs system on $(2+1)$ dimensional de Sitter space-time is derived. It represents the curved space-time version of the Bogomolny equations for monopoles on $\mathbb{R}^3$. Using twistor methods, various explicit solutions with gauge groups U(1) and SU(2) are constructed. A multi-soliton SU(2) solution is also presented.

Declaration

This thesis is based on the work done by the author between October 1997 and December 2000 under the supervision of Professor R.S. Ward in the Department of Mathematical Sciences, at University of Durham. No part of it has been previously submitted for any degree at any university.

No claim of originality is being made for chapter 1 or the introductory sections of chapters 2, 3 and 4, and sections (2.2), (3.2) and (4.2). The remainder of the thesis is believed to be original. Part of the results of chapter 2 have been submitted for publication, and exist as a preprint *nlin.PS/0102037*. Part of the results of chapter 4 are published in *J Math Phys*.

Acknowledgements

I would like to thank my supervisor Prof Richard Ward for suggesting the research projects I have worked on, and for his help and advice throughout my time in Durham. I have learnt many things from him. I would also like to thank my office mates Linda Baker, Stuart Cherry, Clare Dunning and Matt Szyndel for many interesting diversions from work. I would like to thank Dave Hickin for interesting conversations regarding solitons on a curved space-time setting, and finally I would like to thank the various members of the department who turned up for Friday Football, and indeed the members of the Maths 5-A-side football team. May your fortunes change in the coming season.

Outside of the department, I would like to thank my house mates Karl Lyons and Steve Kirk for providing a good household environment and also to the Durham University Shotokan Karate Club for increasing my interest in karate. Lastly but not least, I would like to thank my parents for their support throughout my life.

Thanks are also due to the Engineering and Physical Sciences Research Council for a research studentship.

Contents

List of Figures

Chapter 1

Introduction

Solitary waves were first discovered in the context of hydrodynamics, by John Scott Russell in 1834, who whilst supervising a project in an Edinburgh canal discovered what he later described as a "great wave of translation" [3]. What Russell saw was essentially this: an elevated mass of water with the property that it travelled without any change in its shape or speed, and with only a slight decrease in amplitude. He realised that what he saw was a genuinely new phenomenon, and after subsequent experiments in a smaller version of the canal in his back-garden, he concluded that the decrease in amplitude is due to friction. This observation led to the definition of a solitary wave: a lump-like coherent structure which travels without any change in its shape, speed or amplitude. Such an object is sometimes also incorrectly referred to as a soliton. But a soliton, strictly speaking, satisfies an additional condition that it is unaffected by interactions: two interacting solitons pass through each other with their size, shape and speed unchanged by the interaction. The only interaction memory is a phase-shift (or a time-delay): each soliton would have been centered at a different location had it travelled without any interaction at all. Moreover, solitons (unlike solitary waves) are stable under perturbations [4].

Solitons (or solitary waves) tend to occur as solutions of certain nonlinear equations. The nonlinearity plays an important role in their existence. Indeed, we are familiar with coherent lump-like objects (wave-packets) which occur as solutions of linear field equations (such as the linear time-dependent Schrödinger equation). But such packets disperse in a time scale proportional to k^2, where k is the wavenumber.

The presence of a nonlinear term counteracts the action of the dispersive (linear) term, and a soliton structure emerges if the action of these two terms are perfectly balanced.

There are in fact different kinds of solitons. They can be topological or integrable. Topological solitons owe their existence to the role played by the global topology of the field. They are not solitons in the sense described above but rather solitary waves; it is nonetheless common practice to refer to them as solitons. Integrable solitons on the other hand occur because the nonlinear system in question is completely integrable. One consequence of this feature is that soliton solutions of such systems have infinitely many conserved quantities, and this in turn is what is responsible for the soliton's stability [4].

Since this thesis is concerned with both integrable and topological solitons, we will now consider them in detail.

1.1 Topological Solitons

Topological solitons are generally a consequence of a non-trivial mapping between the internal field space and the manifold of real space. The soliton itself can be regarded as a heteroclinic connection between two any vacuum states of the theory. The stability of the soliton (the fact that it does not decay into a lower energy solution) can be attributed to a conserved nonzero charge. This charge may be the Noether charge which is associated with a continuous symmetry of the theory, or it may be the so-called topological charge, Q. The topological charge is nonzero if the field configuration is a member of a non-trivial homotopy class; it is essentially a consequence of the boundary condition, that the total energy is finite, so it does not generate a symmetry of the Lagrangian. Note that when we say a 'field' we mean a map from the space-time manifold $M \times \mathbb{R}$ to some target space manifold, Φ, *i.e.* $\phi : M \times \mathbb{R} \longrightarrow \Phi$, whilst a configuration is a particular leaf in the time foliation of ϕ, *i.e.* $\phi^c : M \longrightarrow \Phi$. So, topological solitons exist if some homotopy class of Φ is non-trivial. Φ and M can be any smooth manifolds: In chapters 2 and 3 of this thesis, we will consider M to be be a 1-dimensional lattice, *i.e.* $M = \{nh \in \mathbb{R} | n \in \mathbb{Z}\}$,

where $n \in \mathbb{Z}$ and h is the distance between any two points, $h = x_{n+1} - x_n$; whereas in chapter 4, M will be a curved manifold.

Many of the features of topological solitons are more transparent in lower dimensional systems such as the ϕ^4 model [44], sine-Gordon system [5], etc. The sine-Gordon system plays a central role in chapter 2 of this thesis. We will therefore describe this system here, and at the same time use it to illustrate some of the major features of topological solitons.

The fundamental object in the sine-Gordon system is a field $\phi(x,t)$, (*i.e.* a map $\phi : \mathbb{R} \times \mathbb{R} \longrightarrow S^1$) and the model itself is given by the Lagrangian density[1],

$$\mathcal{L}[\phi] = \frac{1}{2}(\partial_\mu \phi)(\partial^\mu \phi) - V(\phi), \tag{1.1}$$

with the potential $V(\phi) = 1 - \cos\phi$. We use the following conventions here and in chapter 2: $x^\mu = (x,t)$, $\partial_\mu = \partial/\partial x^\mu$; indices are raised or lowered using the metric tensor $g_{\mu\nu} = \text{diag}\,(-1,1)$, and repeated indices are summed over. The alternating tensor $\epsilon_{\mu\nu}$ is defined so that $\epsilon_{01} = 1$.

The action for the Lagrangian density may be calculated using the equation

$$S = \int \mathcal{L}[x,t]dx\,dt, \tag{1.2}$$

and the field equation then follows from Hamilton's principle of least action $\delta S = 0$,

$$\partial_\mu \partial^\mu \phi + \sin\phi = 0. \tag{1.3}$$

Note that the Lagrangian is symmetric under $\phi \longrightarrow \phi + 2n\pi$ and $\phi \longrightarrow -\phi$. Equation (1.3) has the trivial solutions $\phi^{(n)} = 2n\pi$. These are the degenerate minima of $V(\phi)$. These minima play an important role in the classification of soliton solutions: Suppose we have a smooth non-singular finite energy solution to (1.3), $\phi(x,t)$. For $\phi(x,t)$ to have finite energy we require $\phi(-\infty,t)$ and $\phi(\infty,t)$ to be one of the vacuum

[1]The name sine-Gordon is intended to be a pun on Klein-Gordon and is attributed to Martin Kruskal. The equation first arose in the study of differential geometry: it describes the properties of pseudo-spherical surfaces [6].

states, $\phi^{(n)}$. If $\phi(x,t)$ is smooth, then these values of $\phi(\pm\infty,t)$ are stationery under the evolution equation (1.3). That is, any one particular value of the vacuum taken by $\phi(\infty,t)$ or $\phi(-\infty,t)$ cannot be continuously deformed into any other. So we have that $\phi(x,t)$ must belong to a (topological) sector given by $(2m\pi, 2n\pi)$, $m,n \in \mathbb{Z}$. Since the target manifold $\Phi \simeq S^1$, we have $n-m = 1,0$ *i.e.* we consider fields modulo 2π. The trivial solutions $\phi = 2n\pi$ belong to the sectors for which $n = m$ and are not topological. The remaining sectors contain solutions that interpolate between two vacuum states, $(2m\pi, 2n\pi)$. A solution that belongs to this sector is a topological soliton and is classified by a topological charge, Q. For instance, for the first sector $(0, 2\pi)$,

$$Q = \frac{1}{2\pi}[\phi(\infty,t) - \phi(-\infty,t)] = \pm 1. \tag{1.4}$$

The solitons with $Q = 1$ and -1 are known as kinks and anti-kinks respectively. The charge Q has the associated conserved current,

$$j^\mu = \epsilon^{\mu\nu}\partial_\nu\phi. \tag{1.5}$$

Clearly, $\partial_\mu j^\mu = 0$, and

$$Q = \int j^0\, dt = \int_{\mathbb{R}} \frac{\partial\phi}{\partial x}\, dx. \tag{1.6}$$

An explicit expression for the kink (or the anti-kink) can be obtained using a remarkable argument due to Bogomolny [7]. The argument involves (essentially) completing the square in the expression of the total energy of a topological solution $\phi(x,t)$. For convenience let us set $\psi(x,t) = \phi(x,t)/2$. The total energy of the static configuration $\psi(x)$ is given by

$$E = \frac{1}{4}\int_{-\infty}^{\infty} (\psi_x^2 + \sin^2\psi)dx, \tag{1.7}$$

so completing the square gives

$$0 \leq \frac{1}{4}\int_{-\infty}^{\infty}(\psi_x - \sin\psi)^2 dx \tag{1.8}$$

$$= E + \frac{1}{2}\int_{-\infty}^{\infty}(\cos\psi)_x dx \tag{1.9}$$

$$= E - 1, \tag{1.10}$$

where the last equality is obtained by imposing the kink boundary conditions $\psi(-\infty) = 0$ and $\psi(\infty) = \pi$. This argument shows that the energy of a static configuration $\psi(x)$ is bounded below by 1. The bound is saturated by functions which satisfy the equation

$$\frac{d\psi}{dx} = \sin\psi. \tag{1.11}$$

This is a first order equation and can be easily solved. Equation (1.11) is known as the Bogomolny equation and shows the power of the Bogomolny argument: a solution of a second order nonlinear equation is being obtained by solving a first order equation. Equation (1.11) has the general solution

$$\psi(x) = 2\tan^{-1} e^{x-x_0}, \tag{1.12}$$

where x_0 is a constant of integration [4]. Equation (1.12) is the expression of the static kink referred to above. An expression for the anti-kink can be obtained by using the appropriate anti-kink boundary conditions in the Bogomolny argument.

Figure 1.1 shows a plot of the kink $\psi(x)$ together with its energy density function $E[\psi(x)]$. Note that we have taken $x_0 = 0$. For other values of x_0 we find that the center of the kink (defined to be the point at which $\psi = \pi/2$) is located at x_0. So x_0 can be interpreted as the position of the kink.

This is a convenient place to conclude the introduction to the sine-Gordon system. We will return to it again in chapter 2. We have seen some of the features of topological solitons, namely that the solutions are classified by an integer called the topological charge, and the existence of a Bogomolny bound which is saturated by the solitons. Both of these facts can be regarded as being relevant to the stability

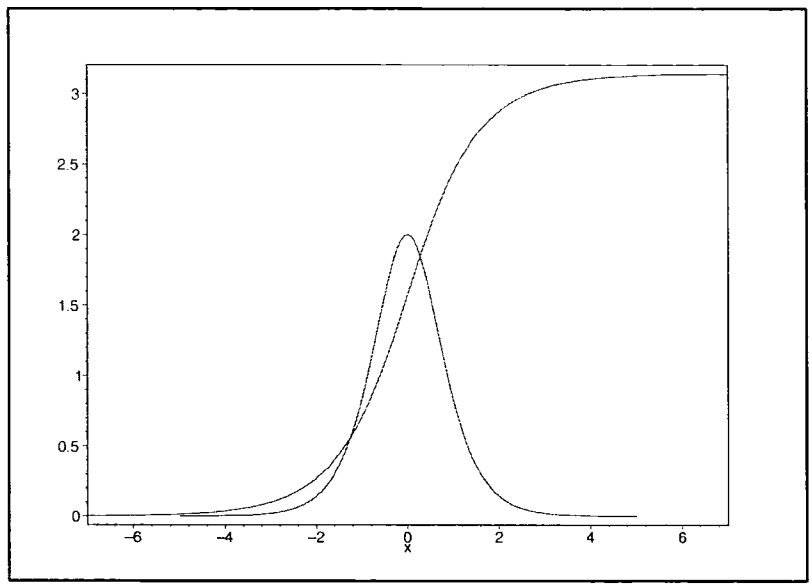

Figure 1.1: A plot showing the profile of the kink $\psi(x)$ and its potential energy density function $E[\psi(x)]$.

of the soliton; and they can be linked to the following space of configurations which minimize the potential,

$$\mathbf{M} = \{\phi^c : V(\phi^c) = \text{minimum}\}. \tag{1.13}$$

$\mathbf{M}$ is known as the vacuum manifold. Field theories that have topological soliton solutions fall into two classes, (1) theories for which the boundary conditions of ϕ^c is non-trivial, and (2) theories for which ϕ^c is restricted to a non-trivial manifold (so the boundary conditions of ϕ^c tends to be trivial). Let us consider the space manifold to be $\mathbb{R}^d$. So for case (1) we have maps $\phi^c : S^{d-1} \longrightarrow \mathbf{M}$. Here S^{d-1} is the unit sphere in $\mathbb{R}^d$, representing the directions in $\mathbb{R}^d$ where the field approaches a vacuum. For the second case, we have maps $\phi^c : S^d \longrightarrow \mathbf{M}$, where S^d is the natural compactification of $\mathbb{R}^d$, and $\mathbf{M}$ is non-trivial. An important fact is that the vacuum manifold $\mathbf{M}$ can be divided into disjoint path components, so points within a given component can be joined together by some map $\phi^c \in \mathbf{M}$, but points in distinct components cannot. This is what is responsible for the solitons's stability: for a topological soliton to be stable we need the map $\phi^c : S^n \longrightarrow \mathbf{M}$ to be stable under deformations. A smooth deformation of ϕ^c is a 1-parameter family of (finite

energy) configurations ϕ^c_ζ; ϕ^c_ζ depends smoothly on ζ and for $\zeta = 0$, $\phi^c_\zeta = \phi^c$. Such deformations could be the deformations used in Hamilton's principle of least action, or the deformations created by the time evolution of the system (through the equation of motion), or even a continuous gauge transformation. A map ϕ^c would be stable under these deformations if it cannot be continuously deformed into a constant map. For type (1) field theories such maps would belong to a non-trivial component of $\mathbf{M}$ given by the homotopy group $\pi_{d-1}(S^n)$; for type (2) theories we would require that $\pi_d(S^n)$ is non-trivial. Topological solitons which belong to the former homotopy group are known as monopoles and ones belonging to the latter are called textures. The sine-Gordon soliton we considered earlier is therefore an example of a texture.

Finally, before we end this section, we discuss the physical motivation behind studying topological solitons. Topological solitons have seen major applications in two areas of physics: condensed matter theory and particle physics. The applications in condensed matter physics provided the first verification of the ideas on solitons and topology. Solitons in this area are used to model a vast range of phenomena, including crystal dislocations, charge density waves, magnetic domain walls, Josephson junctions, wave pulses in fibre optics, etc [8]. Many of these phenomena require the underlying space to be discrete. It is not always possible to find exact static soliton solutions in this case. It is even more difficult to find solutions which are explicitly time-dependent (*i.e.* where velocity occurs as a parameter rather than being fixed from the outset.)[2]. Sometimes the solution of the analogous continuum system (if there is one) is used in the simulations. But this approximation is less effective in higher dimensions. Application of higher dimensional solitons in condensed matter physics are therefore more difficult to find. In 2 space dimensions, topological solitons usually exist because the field is restricted to a non-trivial manifold. In certain cases the addition of a gauge field to the theory also yields solitons. An example of a theory where this occurs is the abelian line vortex [9], which has applications in superconductivity. Models which require the former are known as σ-models. A famous example of this, in 3 dimensions, is the Skyrme model [10]

[2]This issue forms the subject of chapter 3

where one considers the map $\phi^c : S^3 \longrightarrow \mathrm{SU(N)}$. The Skyrme model may be derived as the low energy limit of QCD in the limit where the number of quark colours is large [11]. It is a field theory where the carriers of the strong nuclear force are pions $(\pi^0, \pi^{\pm})$, and protons and neutrons occur as solitons. The role of the baryon number B is played by the topological charge $B \in \pi_3(\mathrm{SU(N)}) \simeq \mathbb{Z}$. Numerical solutions for multi-solitons have been found for baryons with $1 \leq B \leq 9$. Plots of the constant baryon-density surfaces show the baryons to have the shape and symmetries of regular polehedra, with the $B = 2$ baryon having the symmetry of a torus, $B = 3$ of a tetrahedron, etc [12]. The properties of the quantized multi-skyrmions agree well with empirical observation [13], [14].

As already mentioned, sometimes the inclusion of a gauge field to a theory yields solitons. Gauge theories feature prominently in particle theory. The standard model is a gauge theory with gauge group SU(3)×SU(2)×U(1). A key ingredient in this theory is the Higgs boson. The Higgs potential has a continuous degenerate vacuum which is a non-trivial gauge orbit [15]. At low energies, the Higgs boson has to choose a particular vacuum, leaving the theory invariant only under the U(1) subgroup of electromagnetism. This process is known as spontaneous symmetry breaking and is necessary for mass-generation for the electroweak bosons $(W^{\pm}, Z^0)$. Recent experimental evidence suggests that we may have seen such a particle in nature (though at present the evidence is believable only to 2.6 standard deviations, *i.e.* there is a 0.6% chance that it is background effects rather than the Higgs [16]). Spontaneous symmetry breaking may have occurred at earlier times in the Universe as well, and in particular earlier there may have been a Grand Unified Theory gauge group which was subsequently broken to the standard model gauge group. If this was the case, then spontaneous symmetry breaking would have occurred via the Kibble mechanism [17], and this would have created cosmological objects such as cosmic strings, defects and monopoles. These are all examples of topological solitons but have at present not been seen in nature. However, in chapter 4 we will look at the monopole in different setting, namely on a $(2 + 1)$-dimensional de Sitter space-time. This may have little physical ramifications, but is nonetheless an interesting mathematical problem.

1.2 Integrable Solitons

An integrable soliton is a solution of a nonlinear partial differential (or difference) equation which is completely integrable; the global topology of the field now plays a secondary role. The meaning of complete integrability for a partial differential equation is not altogether clear[3]. The reason for this is that any such definition needs to encompass the vast range of mathematical phenomena exhibited by integrable systems. Roughly speaking though, an integrable system is a system "whose solutions can in principle be constructed explicitly" [19]. There are a number of ways of constructing solutions of an integrable equation. The particular method one employs depends more on the problem at hand than the taste of the user. Indeed, this is one of the problems in the study of integrable systems that needs to be overcome: finding a way of knowing *a priori* which method to employ for a given integrable equation, or finding a method that will yield a solution for any integrable equation. In the absence of this we will mention some of the features of integrable systems. They can be regarded as forming 'tests' for an integrable system:

- An equation is regarded to be integrable if many exact solutions can be obtained by a solution generating method such as the inverse scattering transform (IST) [20], the Hirota bilinear-operator method [21], the Zakharov-Shabat method [26] or certain twistor methods [22].

- An equation is said to be integrable if it can be written as the compatibility condition of two linear operators [23], $L(x,t,\zeta)$, and $M(x,t,\zeta)$ say, where

$$\frac{\partial \phi}{\partial x} = L(x,t,\zeta)\phi, \tag{1.14}$$

$$\frac{\partial \phi}{\partial t} = M(x,t,\zeta)\phi. \tag{1.15}$$

[3]Compare this with the situation for ordinary differential equations where Liouville's definition of integrability applies: a Hamiltonian system with n degrees of freedom is said to be integrable if there exists $(n-1)$ independent and globally-defined functions, which are all in involution with each other and with the Hamiltonian.

The original nonlinear equation then amounts to the compatibility condition of L and M, obtained by taking the space derivative of (1.15) and subtracting that from the time derivative of (1.14),

$$\frac{\partial L}{\partial t} - \frac{\partial M}{\partial x} + [L, M] = 0, \tag{1.16}$$

and this equation should hold for each ζ. Equation (1.16) is known as the zero curvature condition because $L(x, t, \zeta)$ and $M(x, t, \zeta)$ can be considered to be the connection coefficients for a trivial vector bundle $\mathbb{R}^{1+1} \times \mathbb{C}^2$; here $\mathbb{R}^{1+1}$ is the space-time and $\mathbb{C}^2$ is the space of ϕ. Equations (1.14) and (1.15) then show that ϕ is covariantly constant, and equation (1.16) says that the (L, M) connection has zero curvature.

- An ordinary differential equation is said to be integrable if it passes the Painleve test *i.e.* it can be reduced to one of the Painleve equations [24]. But this usually requires a change of coordinates and it is not always apparent what to use.

In order to provide a certain amount of foundation for chapter 3, we will illustrate the basic idea behind the IST [20]:

$$\phi(x, 0) \longrightarrow S(x, 0) \longrightarrow S(x, t) \longrightarrow \phi(x, t). \tag{1.17}$$

We start with an initial condition of a nonlinear partial differential equation $\phi(x, 0)$ and transform it to the initial scattering data $S(x, 0)$ using a transform that is analogous to the Fourier transform. The scattering data is then evolved using a simple relation. Finally, to obtain a solution of the nonlinear equation we apply the inverse transform to $S(x, t)$. This method uses the observation that the evolution of the scattering data is simpler than the evolution of the field. The method has been successfully used to construct soliton solutions for many integrable systems, including the sine-Gordon system [25].

Integrable systems tend to occur mostly in $(1 + 1)$ dimensions, of which the sine-Gordon system is an example. Some other examples are the nonlinear Schrödinger

equation [26], the Bousinessq equation [27], and the Korteweg de Vries equation [28] (which describes approximately the "great wave of translation" seen by Russell). There are also some examples in $(2+1)$-dimensions, namely, the Davey-Stewartson equation [29], the Kadomtsev-Patviashvili equation [30], etc [24]. For all of these systems one can find exact expressions for single and multi-soliton solutions. A characteristic feature of these solutions is that they have an infinite number of conserved symmetries and so the solitons have an infinite number of conserved quantities[4]. In some sense this is what is responsible for the soliton's stability during interactions, though as noted already, these interactions are usually trivial compared to the dynamics of topological solitons.

Some integrable systems in $(1+1)$-dimensions are Lorentz invariant so for such systems one can obtain time dependent solitons by simply Lorentz boosting the static solitons. In higher dimensions, integrability seems not to be compatible with Lorentz invariance. There is however a semi-Lorentz invariant system in $(2+1)$-dimensions [32], and the Yang-Mills system in 4-dimensions is also Lorentz invariant. But, in particular, there is no known integrable system in $(3+1)$-dimensions which is Lorentz invariant [24]. This coupled with the fact that integrable systems tend to have trivial dynamics means that they have limited scope for use in particle theory.

The motivation behind studying integrable systems is therefore largely mathematical. One area of mathematical interest at present is the idea that integrable systems are unified in some sense. The idea is known as Ward's conjecture and says that all the known integrable systems occur as (algebraic or dimensional) reductions of the self-dual Yang-Mills equations [33]. By dimensional reduction we mean that we would look for solutions of the sdYM equations which are invariant under some group of conformal transformations. The self-dual Yang-Mills equations then lead to (integrable) equations in a lower dimensional space.

1.2.1 The Unifying Integrable Equation

The self-dual Yang-Mills equation is an integrable equation in 4-space [22]. The fundamental object is the Yang-Mills field which is defined as

[4]This can be established using the Miura map [31].

$$F_{\mu\nu} = \partial_\mu A_\nu - \partial_\nu A_\mu - [A_\mu, A_\nu], \tag{1.18}$$

where $\mu = 0, 1, 2, 3$ are the coordinates on the 4-space, A_μ is the gauge potential taking values in the Lie algebra of a gauge group G. The self-dual Yang-Mills equations are given by

$$F = *F, \tag{1.19}$$

where $*$ is the Hodge star defined on the 4-space. In terms of components they can be written as

$$F_{\mu\nu} = \frac{1}{2}\sqrt{g}\epsilon_{\mu\nu\alpha\beta}F^{\alpha\beta}, \tag{1.20}$$

where $g = \det g_{\mu\nu}$ and $g_{\mu\nu}$ is the metric on 4-space.

We will consider equation (1.20) in terms of null coordinates $(w, \bar{w}, z, \bar{z})$: If (x, y, s, t) are the coordinates on 4-space $M = \mathbb{R}^4$, then the null coordinates are given by

$$w = x + iy, \quad \bar{w} = x - iy, \quad z = t + is, \quad \bar{z} = t - is.$$

The self-dual Yang-Mills equations in these coordinates become

$$\begin{aligned} F_{wz} &= 0, \\ F_{\bar{w}\bar{z}} &= 0, \\ F_{w\bar{w}} + F_{z\bar{z}} &= 0. \end{aligned} \tag{1.21}$$

Note that the self-dual Yang-Mills equations are invariant under the gauge transformation,

$$A_\mu \longrightarrow gA_\mu g^{-1} + (\partial_\mu g)g^{-1}, \tag{1.22}$$

for any $g(x^\mu) \in G$.

Equations (1.21) can be regarded as the compatibility condition of the Lax pair

$$\begin{aligned}(\partial_w + \zeta\partial_{\bar{z}})\Psi &= (A_w + \zeta A_{\bar{z}})\Psi, \\ (\partial_z - \zeta\partial_{\bar{w}})\Psi &= (A_z - \zeta A_{\bar{w}})\Psi,\end{aligned} \tag{1.23}$$

where ζ is the spectral parameter and Ψ is a vector in some representation of the Lie algebra of G. The compatibility condition is expressed as a polynomial in ζ,

$$(\partial_w + \zeta\partial_{\bar{z}})(A_z - \zeta A_{\bar{w}}) - (\partial_z - \zeta\partial_{\bar{w}})(A_w + \zeta A_{\bar{z}}) = [A_w + \zeta A_{\bar{z}}, A_z - \zeta A_{\bar{w}}], \tag{1.24}$$

and equations (1.21) are retrieved by comparing coefficients of the powers of ζ. Equations (1.23) show that the self-dual Yang-Mills equations form an integrable system. To see how other integrable systems arise as reductions of (1.23), consider, as an example, the euclidean sine-Gordon system, $\phi_{xx}+\phi_{tt} = \sin\phi$. Take $w = \bar{w} = x$ and $z = \bar{z} = t$. Then the gauge potentials, $A_\mu \in \mathrm{sl}(2,\mathbb{C})$ given by

$$A_w = \frac{1}{4}\begin{pmatrix} -\phi_x & -2\sin(\phi/2) \\ 2\sin(\phi/2) & \phi_x \end{pmatrix}, \quad A_{\bar{w}} = \frac{1}{4}\begin{pmatrix} -\phi_x & 2\sin(\phi/2) \\ -2\sin(\phi/2) & \phi_x \end{pmatrix},$$

$$A_z = \frac{1}{4}\begin{pmatrix} \phi_t & -2\cos(\phi/2) \\ -2\cos(\phi/2) & -\phi_t \end{pmatrix}, \quad A_{\bar{z}} = \frac{1}{4}\begin{pmatrix} \phi_t & 2\cos(\phi/2) \\ 2\cos(\phi/2) & -\phi_t \end{pmatrix}.$$

satisfy (1.21) provided $\phi_{xx} + \phi_{tt} - \sin\phi = 0$. This is an example of dimensional reduction where the Yang-Mills equation is reduced by a time-like and null Killing vectors. Alternatively, one could obtain the sine-Gordon equation by a mixture of algebraic and dimensional reduction as follows:

Let the gauge potentials A_μ be a function only of w and $\bar{w}$, and be su(2)-valued. By using certain gauge freedom we can set $A_{\bar{w}} = 0$. The remaining gauge potentials form a Lax pair

$$\begin{aligned}\partial_w\Psi &= (A_w + \zeta A_{\bar{z}})\Psi, \\ \partial_{\bar{w}}\Psi &= -\zeta^{-1}A_z\Psi.\end{aligned} \tag{1.25}$$

If we choose the gauge potentials to be given by

$$A_w = c\sigma_3, \quad A_z = (a+b)\sigma_2, \quad A_{\bar{z}} = \sigma_1,$$

where the σ_i are the Pauli matrices and a, b and c are functions of w and $\bar{w}$ only, then the Lax pair (1.25) is given by

$$\partial_w a = -2ibc, \quad \partial_w b = 2iac,$$

$$\partial_{\bar{w}} c = 2ib. \tag{1.26}$$

The solution of (1.26) is $a^2 + b^2 = k$, where k is a constant. Choosing $k = 1$, $a = \cos\phi$ and $b = \sin\phi$ gives $c = \frac{1}{2}i\partial_w\phi$. Substituting this into (1.26) then gives the sine-Gordon equation.

At present, it is generally believed that the self-dual Yang-Mills equations play a useful unifying role in the theory of integrable systems, and that Ward's conjecture may be true.

This concludes our introduction on solitons. Although we have considered solitons on flat spaces only, this introduction forms a good basis for the rest of the thesis where we will consider solitons on lattices and curved space backgrounds. In chapter 2 we will consider kink dynamics on a 1-dimensional lattice. In particular, we will look at the outcome of the kink-anti-kink interactions in the topological discrete sine-Gordon system. In chapter 3 we will consider the question of the existence of travelling kink solutions on lattice. By using the inverse scattering transform we derive an expression for such a solution for the integrable lattice sine-Gordon system. In chapter 4 we have obtained, via a reduction of the self-dual Yang-Mills system, a (2+1)-dimensional integrable system on a curved space background. Several explicit solutions are constructed, and some of them are found to be topological in nature. Each chapter is self-contained and ends with concluding remarks.

Chapter 2

Kink-antikink Interactions in Topological Discrete Systems

2.1 Introduction

As we mentioned in the introduction, solitons have seen many applications in condensed matter physics [8]. In many cases it is necessary to consider the solitons on a 1-dimensional spatial lattice (time is still continuous). Moreover, it is necessary to model interactions of the soliton with other objects such as impurities, defects, phonons, antisolitons, or other solitons. In (1+1)-dimensional field theories, these interactions have sometimes been quite spectacular, particularly if the 1-dimensional soliton, or the kink, supports extra modes of vibration. This mode can be excited during an interaction and this leads to a "resonance effect" [34]. This effect has been seen in both continuous and lattice systems [34], [35], [36], [37], [38], [39], [40], [41]. These resonance effects give rise to "windows" in the space of impact velocity, *i.e.* there are certain intervals of velocities in this space for which the kinks form a bound state, known as a bion, and others for which the kinks scatter off each other. This phenomenon was first observed by Ablowitz *et al* [37] for various Klein-Gordon-type systems.

In this chapter we will consider interactions of a kink with an antikink in a particular type of lattice systems, namely topological discrete systems. Such systems were introduced in 1994 [42] and are particularly interesting because the lattice system

retains many of the features of the corresponding continuum system. In particular, the lattice system maintains the Bogomolny bound. The resulting Bogomolny equation is typically a first-order difference equation which can be easily solved. For the case of the topological discrete sine-Gordon system (TDSG), the solution is analogous to the well-known continuum sine-Gordon static kink solution (1.12).

The chapter is divided into six sections of which the first three are background material. In section 2 we will review kink-antikink interactions in the (continuum) ϕ^4 and the continuum sine-Gordon systems. We will introduce Campbell *et al's* "resonance energy exchange mechanism" in section 2.1.3. This is essentially an explanation of the resonance effects of kink-antikink interactions seen in many non-integrable systems. In section 3 we present details of the TDSG system. In section 4 we present the results of kink-antikink interactions in the TDSG. Section 5 will contain the corresponding results for the topological discrete ϕ^4 system [42], and section 6 contains some concluding remarks.

2.1.1 The Continuum ϕ^4 Model

We begin by mentioning some details for the ϕ^4 model[1]. The model is defined by the Lagrangian density

$$\mathcal{L}[\phi] = \frac{1}{2}(\partial_\mu\phi)(\partial^\mu\phi) - \frac{1}{4}(\phi^2 - 1)^2, \tag{2.1}$$

and the equation of motion is

$$\partial_\mu\partial^\mu\phi + \phi(\phi^2 - 1) = 0. \tag{2.2}$$

Equation (2.2) has three trivial solutions, $\phi = 0$ and $\phi = \pm 1$. The solutions $\phi = \pm 1$ correspond to the classical vacua of the theory. In addition, there are the static kink solutions,

$$\phi_{K(\bar{K})} = \pm \tanh\left(\frac{x \pm b}{\sqrt{2}}\right), \tag{2.3}$$

where b is a constant. A time-dependent solution can be obtained by Lorentz boosting this static solution. This kink solution is essentially an interpolation between

[1]The conventions have been outlined in chapter 1.

the two vacua so that asymptotically, as $x \to \pm\infty$, $\phi \to \pm 1$. The negative solution is the antikink, with the reverse boundary condition, $\phi \to \mp 1$ as $x \to \pm\infty$. These boundary conditions give the kink finite total energy.

The ϕ^4 kink is qualitatively very similar to the sine-Gordon kink. But unlike the sine-Gordon kink which is a true soliton, the ϕ^4 kink is not. The interaction of the kink and anti-kink, for instance, does not result in the kink and anti-kink passing through each other unscathed, as the "soliton condition" demands. But rather, they reflect off each other after undergoing a complicated sequence of bouncing. This process is not elastic and the kinks emit radiation. In some cases they form a trapped breather-like state. We will review next the results of such kink-anti-kink interactions in the ϕ^4 model.

2.1.2 Kink-antikink Interactions in ϕ^4 Model

Since the ϕ^4 model is not integrable one has little hope of finding exact solutions that describe kink-antikink interactions. One therefore has to resort to numerical simulations of the interactions. This can be done by discretizing the equation of motion and using appropriate initial conditions. Such simulations have been done in the past [34], [35], [36], [37]. We consider the results of Anninos *et al* [36]. Anninos *et al* solve a discretized version of (2.2),

$$\ddot{\phi}_n = \frac{1}{12(\Delta x)^2}(-\phi_{n-2} + 16\phi_{n-1} - 30\phi_n + 16\phi_{n+1} - \phi_{n+2}) - \phi_n(\phi_n^2 - 1). \quad (2.4)$$

This is solved on a discrete spatial grid with periodic boundary conditions. Here Δx is the grid spacing so the n^{th} point on the grid is given by $x_n = n\Delta x$. The second-order spatial derivative is computed using a fourth-order centre difference scheme. The initial condition corresponds to a widely separated kink and antikink moving towards each other with velocity v at $t = 0$, *i.e*

$$\begin{aligned} \phi(x,0) &= \tanh(x+b)/\sqrt{2} - \tanh(x-b)/\sqrt{2} - 1, \quad (2.5) \\ \dot{\phi}(x,0) &= -v((\mathrm{sech}^2(x+b)/\sqrt{2} + \mathrm{sech}^2(x-b)/\sqrt{2})). \end{aligned}$$

Equation (2.4) describes a set of coupled second-order ordinary differential equations for ϕ_n which can be solved numerically, for instance using a 4th-order Runge-Kutta

scheme [43]. The results show that the outcome of an interaction depends sensitively on the impact velocity of the kinks. The end result however is always either a "reflection", or a bion. The bion is a breather-like state and oscillates for a long time, but eventually decays into radiation.

One can summarise the results of the interaction by considering the space of impact velocity. It is found that for some intervals of velocities in this space, the interaction is a scattering whose net result is a reflection. For other intervals the net result is a bion. These intervals are known as "windows". The windows for the reflection and bion cases alternate along this space of impact velocity. Moreover, the edges of the windows show a similar pattern of alternating windows. In fact, the edge of the window forms a self-similar fractal [36].

Although the global outcome of the scattering is a reflection, the actual interaction of the kinks is a bit more complicated. It involves the kinks "bouncing" off each other more than once. In general, after the first collision the kinks move back a finite distance and then come back for a second collision. After the second collision the kinks either escape to infinity or come back for more collisions. Each of these collisions is known as a bounce, so that an interaction involving 2 collisions is known as a 2-bounce event. The simulations have shown up to 30-bounce events.

2.1.3 Resonant Energy Exchange Mechanism

The results of the simulations can be explained using Campbell *et al*'s "resonant energy exchange mechanism" [34]. Their idea is to treat solitary waves as deformable particles which have extra modes of vibration. These modes are known as shape oscillations. When two particles collide some of the energy in the translational mode is transferred to the lowest-energy vibration mode. The bound state is formed only if sufficient energy is transferred from the particle's translational mode to this vibration mode.

One can understand the two-bounce behaviour using this idea in the following way. The first collision transfers sufficient energy from the translational mode to the internal shape mode so that the kinks are now weakly bound. Since they are only weakly bound they retain their usual shape as they start to separate. But since they

are bound they only separate to a short distance and they come back for a second collision. The second collision transfers energy back from the internal mode to the translational mode and the kinks are then free to escape.

One can show that the ϕ^4 kink has an internal mode by linearising the equation of motion about the kink solution [44]. Consider a small perturbation $\eta(x,t)$ such that

$$\phi \approx \phi_K(x) + \eta(x,t). \tag{2.6}$$

Substituting (2.6) into the field equation (2.2) and linearizing gives the equation for the fluctuations around the kink,

$$\frac{\partial^2\eta}{\partial t^2} - \frac{\partial^2\eta}{\partial x^2} + (3\tanh^2\frac{x}{\sqrt{2}} - 1)\eta = 0. \tag{2.7}$$

We can then solve for the normal modes by setting

$$\eta(x,t) = e^{i\omega t}\chi(x). \tag{2.8}$$

Substituting this into (2.7) gives the eigenvalue equation,

$$\left(-\frac{d^2}{dx^2} - 3\,\mathrm{sech}^2\frac{x}{\sqrt{2}} + 2\right)\chi(x) = \omega^2\chi(x). \tag{2.9}$$

This is the Schrodinger equation with a reflectionless potential. Its solution can be found in [45]. Equation (2.9) has two discrete eigenvalues and a continuum of eigenvalues. The discrete eigenvalues and their corresponding eigenvectors are given by,

$$\omega_0^2 = 0;\ \ \chi_0(x) = \mathrm{sech}^2\frac{x}{\sqrt{2}},$$

and

$$\omega_1^2 = 3/2;\ \ \chi_1(x) = \tanh\frac{x}{\sqrt{2}}\mathrm{sech}\frac{x}{\sqrt{2}}.$$

The continuous spectrum of eigenvalues is given by $\omega_k^2 = 2+k^2$, for $k^2 > 0$. The corresponding eigenvectors are $\chi_k \sim e^{ikx}$ multiplied by a Jacobi polynomial in $\tanh x$. The first discrete eigenvalue $\omega_0 = 0$ is the translational mode, due to the translational symmetry of (2.2). The second discrete eigenvalue, ω_1, is the frequency of the shape mode.

For the kink-antikink 2-bounce event, the shape modes annihilate at a certain phase angle of the internal vibrations, given by,

$$\omega_1 T = 2\pi m + \theta, \tag{2.10}$$

where T is the time between the two collisions, m is an integer (the window number) and θ is a phase shift. This means that transfer of energy from the shape mode to the translational mode happens whenever (2.10) holds. This result is not analytically derived by Campbell *et al* but their numerical results confirm the relation.

2.1.4 The Continuum sine-Gordon System

The salient features of this system have already been described in the preceding chapter. Since the sine-Gordon kink is an exact soliton, an interacting kink and antikink simply "pass through" each other. Furthermore, the sine-Gordon kink has no localised vibration mode. It does however support a short-lived quasimode which is exicted by the perturbations arising from the process of discretization of the system [47], [48], [49].

In addition to the kink solutions (1.12), the sine-Gordon equation admits a doublet solution (a breather), which is spatially localised and time periodic,

$$\phi_B(x,t) = 4\tan^{-1}\left[\frac{v\sin(t/(1+v^2)^{\frac{1}{2}})}{\cosh(vx/(1+v^2)^{\frac{1}{2}})}\right]. \tag{2.11}$$

Here $\omega = \frac{1}{\sqrt{(1+v^2)}}$ is the angular frequency. Furthermore, equation (1.3) admits a solution that explicitly describes the interaction of a kink and antikink,

$$\phi_{K\bar{K}}(x,t) = 4\tan^{-1}\left[\frac{\sinh(\gamma u t)}{u\cosh(\gamma x)}\right], \tag{2.12}$$

where $\gamma = (1-u^2)^{-1/2}$.

For $t << -u^{-1}$, (2.12) reduces to

$$\phi_{K\bar{K}} \approx 4\tan^{-1}\exp\gamma(x+u(t+\Delta/2)) - 4\tan^{-1}\exp\gamma(x-u(t+\Delta/2)), \tag{2.13}$$

representing a Lorentz boosted kink and antikink approaching each other with speed u; and for $t >> u^{-1}$ we get

$$\phi_{K\bar{K}} \approx 4\tan^{-1}\exp(\gamma(x+u(t-\Delta/2)) - 4\tan^{-1}\exp(\gamma(x-u(t-\Delta/2)), \tag{2.14}$$

representing a kink and antikink moving away from each other with speed u. The quantity Δ is the phase shift or time delay and is the sole effect of the interaction. By writing (2.13) in terms of u rather than Δ, we see that

$$\Delta = (2/u\gamma)\ln u. \tag{2.15}$$

This quantity Δ is negative, suggesting that there is an attractive potential between the kinks. The magnitude of this potential can be calculated using equation (2.12) [50]. We define the kinks to be located where $\phi = \pi$, then

$$\sinh(\gamma u t) = u\cosh(\gamma x). \tag{2.16}$$

For $u << 1$, $\gamma \approx 1$, and

$$\sinh ut = u\cosh x. \tag{2.17}$$

For $x >> 0$, this equation has an iterative solution of the form

$$x = ut - \ln u - \exp(-2ut). \tag{2.18}$$

Equation (2.18) can be used to calculate the force between the kinks,

$$F = M\ddot{x} = -4u^2\exp(-2x), \tag{2.19}$$

where we have used the fact that $M = 1$, and to leading order, $x = ut$. The potential between the kinks is then given by

$$U(s) = -2u^2\exp(-s), \tag{2.20}$$

where $s = 2x$ is the separation between the kink and antikink.

2.1.5 Kink Vibrational Mode

There are reports suggesting that sine-Gordon kink can support a long-lived localised vibrational mode [47], [48]. This mode was first found by Rice using a collective coordinate method that treats the length of the kink and the centre of mass position of the kink as collective coordinates [47]. The quasimode frequency for the sine-Gordon kink was found to be $2\pi\omega_R = (12/\pi^2)^{1/2}(l_o/\pi)$, where l_o is the length of

the kink. Boesch and Willis then extended this work by using a different collective coordinates method. Their method is known as the projection operator method [48]. The advantage of this method is that one is able to take into the account the effects of radiation and dressing on a moving kink. The numerical value of the quasimode frequency was found by changing the slope of the kink slightly and then following the subsequent damped oscillations. A Fourier analysis of these oscillations showed that the frequency is just above (but close to) the lower phonon band edge. Recent numerical studies, however, claim that such a mode does not exist but that there is in fact another quasimode (*i.e.* other than the one predicted by Rice) which is excited when the kink is placed on the lattice [49].

The sine-Gordon quasimode plays no part in kink-antikink interactions. The slope of the kink during such an interaction changes in a way that does not excite the mode and no radiation is emitted during the process. However, one expects the quasimode to be excited during kink-phonon and kink-impurity interactions, and also when the kink is placed on a lattice. In the latter case the mode is excited because it is able to resonate with the Peierls-Nabarro potential.

2.2 Lattice systems

Lattice systems are important for two reasons. Firstly, we may want to solve a non-linear partial differential equation system which cannot be solved analytically. This would involve discretising the system and then solving the equations numerically. Secondly, we may want to model a physical process explicitly on a lattice rather than continuous space. These two cases are different in the sense that the first case requires the corresponding lattice system to be as close to the continuum case as possible. That is, we would like to minimise the effects of discretization on the lattice system. For the second case, these effects may be important to the physical model. An important example of such a discretization effect is the Peierls-Nabarro (PN) potential barrier. In general the PN barrier is numerically equal to the difference in energy of a static kink located exactly on a lattice site and one located halfway between two sites. It arises essentially because in a given lattice system, the static

kink cannot take any arbitrary position on the lattice: it can be located either exactly on a lattice site, or half-way between two sites. The kink energy is maximum if the kink is located exactly on a lattice site and minimum if it is half-way between sites. This means that a kink travelling along a lattice will experience an oscillating potential well and will radiate. It may eventually get pinned between sites, when the PN barrier is insurmountable.

There are other features of continuum systems which one can also have in discretized systems, such as integrability, the topological stability of the soliton, etc. One can usually maintain these by a careful choice of discretization [42], [52]. In the next section we will describe a lattice sine-Gordon system which maintains the Bogomolny bound of the continuum system. One consequence of this is that the discrete model is a much better approximation to the continuum sine-Gordon system. For example, one gets an exact static kink solution on the lattice, and also there is no PN barrier [42].

2.2.1 Topological Discrete Sine-Gordon System

Topological discrete models were introduced in [42], [53], [54], [55], [56]. They are basically lattice systems which maintain the Bogomolny bounds of their continuum counterparts. The upshot of this is that there is usually an exact expression of the soliton available and the lattice system is a better approximation to the continuum system. The topologically discrete sine-Gordon (TDSG) system [42] is defined by the Lagrangian

$$L = \frac{h}{4}\sum_{n\in Z}(\dot{\psi_n}^2 - (D_n^2 + F_n^2)), \tag{2.21}$$

where the kinetic energy is $E_K = \frac{h}{4}\sum \dot{\psi}_n^2$ and the potential energy is $E_P = \frac{h}{4}\sum(D_n^2 + F_n^2)$.

The quantities D_n and F_n are given by

$$D_n = \frac{2}{h}\sin\frac{1}{2}(\psi_{n+1} - \psi_n) \quad \text{and} \quad F_n = \sin\frac{1}{2}(\psi_{n+1} + \psi_n), \tag{2.22}$$

giving

$$E_P = \frac{h}{4}\sum \frac{4}{h^2}\sin^2\frac{1}{2}(\psi_{n+1} - \psi_n) + \sin^2\frac{1}{2}(\psi_{n+1} + \psi_n). \tag{2.23}$$

$\psi_n = \psi(x)$ at the n^{th} lattice site and $\psi_{n+1} = \psi(x+h)$, where h is the lattice spacing. The first term in equation (2.23) represents an attractive force analogous to the Hooke force. The second term is a substrate potential, found by taking an average of the potential of the two nearest neighbours.

In the continuum limit, as $h \to 0$, $D_n \to \psi_x$, and $F_n \to \sin\psi$, and one recovers the standard expression of the continuum potential

$$E_P^{cont}(\psi) = \frac{1}{4}\int_{-\infty}^{\infty} (\psi_x^2 + \sin^2\psi)\, dx. \tag{2.24}$$

The main feature of this model is the choice of the derivative on the lattice. This choice is motivated by the Bogomolny argument of the continuum system, presented in the preceding chapter. In particular, equation (1.10) is replaced with the discrete analogue,

$$-\Delta\cos\psi_n = -\frac{\cos\psi_{n+1} - \cos\psi_n}{h} = D_n F_n, \tag{2.25}$$

with the kink boundary conditions

$$\lim_{n\to-\infty}\psi_n = 0 \quad \text{and} \quad \lim_{n\to\infty}\psi_n = \pi. \tag{2.26}$$

This leads to the following discrete Bogomolny argument

$$0 \le \frac{h}{4}\sum_{n\in Z}(D_n - F_n)^2 \tag{2.27}$$

$$= E_P + \frac{1}{2}\sum_{n\in Z}(\cos\psi_{n+1} - \cos\psi_n) \tag{2.28}$$

$$= E_P - 1, \tag{2.29}$$

so $E_P \ge 1$, with equality given by the Bogomolny equation, $D_n = F_n$, *i.e.* provided

$$\begin{aligned} \frac{2}{h}\sin\frac{1}{2}(\psi_{n+1} - \psi_n) &= \sin\frac{1}{2}(\psi_{n+1} + \psi_n) \\ \text{or,}\quad \psi_n &= 2\tan^{-1}\exp a(nh - b). \end{aligned} \tag{2.30}$$

The constant $a = h^{-1}\ln[\frac{2+h}{2-h}]$ is the kink's slope and $b \in \mathbb{R}$ is the position. Equation (2.30) is the static kink solution. So the moduli space of static solutions for the TDSG is isomorphic to $\mathbb{R}$ rather than $\mathbb{Z}$, which is what one usually expects for a lattice system. Moreover, E_P is independent of b suggesting that the model has no

PN barrier. This means that the kink can move along the lattice arbitrarily slowly without getting pinned.

The Euler-Lagrange equation gives the following equation of motion,

$$\ddot{\psi}_n = \frac{4-h^2}{4h^2}\cos\psi_n(\sin\psi_{n+1}+\sin\psi_{n-1}) - \frac{4+h^2}{4h^2}\sin\psi_n(\cos\psi_{n+1}+\cos\psi_{n-1}). \tag{2.31}$$

Equation (2.31) can then be used to study the behaviour of a moving kink,

$$\psi_n(t) = 2\tan^{-1}\exp[a(nh-b)-vt]. \tag{2.32}$$

Note that (2.32) is not a solution of the equation of motion (2.31); nevertheless it can be used as an initial condition in the simulations. The results show that for small initial velocities the kink wobbles with a period h/v as it moves along the lattice [42]. This is a purely dynamical effect since there is no PN barrier.

For fast moving kinks it is found that the kink radiates as it moves along the lattice. This is observed through a gradual decrease in the kink velocity. But it is found that there is certain velocity threshold below which the radiation from the kink is significantly reduced.

The existence of such a velocity threshold can be understood by considering the linearised equation of motion,

$$\ddot{\psi}_n = \frac{4-h^2}{4h^2}(\psi_{n+1}+\psi_{n-1}) - \frac{4+h^2}{2h^2}\psi_n. \tag{2.33}$$

Equation (2.33) can be used to derive a dispersion relation for small amplitude travelling waves, given by

$$\omega^2 = \frac{4+h^2}{2h^2} - \frac{4-h^2}{2h^2}\cos kh, \tag{2.34}$$

where k is the wavenumber. Since $0 < h < 2$, we have $1 < \omega < 2/h$. The case $\omega = 1$ corresponds to the threshold velocity. The frequency at which the kink hits the lattice sites is v/h per unit time. So provided $v \geq h/2\pi$, the kink will radiate (at $\omega = 2\pi v/h$). But if $v < h/2\pi$ then $\omega < 1$ and the kink radiates very slowly. Hence there is a "preferred" velocity for the kink. Since this velocity depends only on h, it can be regarded as a feature of the lattice.

The choice of the functions D_n and F_n is not unique. For instance, D_n could be multiplied by a function $f(x,h)$ and F_n by $f(x,h)^{-1}$ and the product is independent of f so one would still have a topologically stable kink solution. The only condition on $f(x,h)$ is that $\lim_{h\to 0} f = 1$. Similarly there is freedom in the choice of the kinetic energy term in the Lagrangian. Zakrzewski [53] has investigated the effects on the kink motion when this choice is exploited.

2.3 Kink-antikink Interactions in the TDSG System

2.3.1 Preliminaries

In this section we present results of kink-antikink interactions in the Speight-Ward model. The results are obtained by solving (2.31) with the initial condition corresponding to Galilean boosted static kink and antikink solutions at each end of the lattice grid, *i.e.*

$$\psi(x,0) = 2\tan^{-1}\exp a(x+b) - 2\tan^{-1}\exp a(x-b), \tag{2.35}$$

$$\dot{\psi}(x,0) = -av(\operatorname{sech} a(x+b) + \operatorname{sech} a(x-b)). \tag{2.36}$$

The boundary condition is taken to be $\psi(x_{min}) = \psi(x_{max}) = 0$, i.e. the ends of the kink and anti-kink are held fixed at all times.

The kink and antikink move towards each other with relative velocity $2v$. Equation (2.31) is solved using a 4th-order Runge-Kutta algorithm. The programme is run with various lattice spacings h. The time step is chosen to be 0.05. This conserves the energy to within 0.05% in a simulation which runs for 1000 units. We use the same time step for all values of $0.1 \leq h \leq 1.5$.

Our choice of the boundary condition means that any radiation emitted by the kink will reflect off the edges and eventually interact with the kinks. This is easily avoided by making the grid sufficiently large.

As mentioned already, the amount of radiation emitted by the kink depends on the kink velocity and also on the lattice spacing. For large velocities and coarser

lattices the amount of radiation is significantly greater. In these cases we have damped the first few lattice sites at each end of the grid. That is, the value of $\dot{\psi}$ at these sites is decreased by a constant amount (10%) for the entire duration of the simulation. The total energy of the system is of course no longer conserved. The energy loss depends on the initial velocity of the kink and on the lattice spacing, but it is usually within 10% of the initial energy, for a simulation running for 1000 units.

2.3.2 Simulation Results

The simulations showed that the outcome of an interaction depends on the impact velocity of the kinks. The velocity of the kink (or the antikink) is defined to be the rate of change of $X(t)$, where $X(t)$ is the "average" position of the kink (or the antikink). $X(t)$ for the kink is given by

$$X(t) = \frac{\sum_{i=-N}^{0} x_i e_i}{\sum_{i=-N}^{0} e_i}. \tag{2.37}$$

Here e_i is the total energy of the field and the radiation at the i^{th} lattice site, where $x_i = x_{min} + ih$. The quantity $\sum_{-N}^{0} e_i$ is the total energy of the field and the radiation for the single kink. We found that for cases when the phonon radiation from the kinks is not significant, $X(t)$ makes a good approximation to the kink position. We define the velocity of the kink to be $\dot{X}(t)$, which is computed using the forward difference, $\dot{X}(t) = \frac{1}{\Delta t}(X(t + \Delta t) - X(t))$.

Since the kink wobbles as it moves along the lattice, $\dot{X}(t)$ is an oscillating function. The period of oscillation is the wobble period, h/v, where v is the velocity used in the initial condition (2.36). This wobble can be understood by considering the geodesic motion on the kink moduli space. This moduli space has a periodic metric [42].

Figure 2.1 shows various plots of how the kink velocity changes with time for a single kink starting at different positions on the grid. The kink is on a lattice with

$h = 1.4$ and the initial velocity of the kink is $v = 0.197$. In all cases the average velocity of the kink is significantly decreased. This is due to phonon radiation from the kinks. The plots show that the kink velocity depends on the initial position of the kink, modulo h.

The outcome of an interaction has sensitive dependence on the velocity of the kink. In particular, there are three different outcomes:

(a) If the kink impact velocity is above a certain critical velocity, v_c, then the kinks simply pass through each other, i.e. there is a smallest number v_c such that the outcome of the interaction for all $v \geq v_c$ is always a passing through behaviour. The value of v_c depends on the lattice spacing and also on b. Figure 2.2 shows the dependence of v_c against h. The dotted curve represents the quadratic $0.073h^2 + 0.036h$. This curve is an empirical fit to the data points and is not derived from the theory.

The dependence of v_c on the position of the kinks is due to dynamical dressing and the kink wobble. For small initial velocities (figure 2.1), the kink velocity oscillates with a period (h/v). The amplitude of oscillation is of the order of 10^{-2}. For large velocities, the phonon radiation make the oscillations erratic and also significantly decrease the overall velocity of the kink. The initial velocity also changes due to the readjustment of the kink field to suit the lattice distribution (dynamical dressing). The initial propagating velocity of the kink is not always v, the velocity used in expression (2.36). In some cases it is larger than v and in others it is less than v. This change depends on the magnitude of v and on the lattice spacing. The effect can be seen in figure 2.1.

For initial kink velocities which give impact velocities below v_c, we found that the outcome is either *(b)* a bounce or *(c)* a trapped breather-like state (a bion). The bounce is essentially a kink-antikink scattering, where the kinks after the first collision pass through each other but fail to escape to infinity. Instead, they travel a small distance and then turn around for another collision. After the second collision the kinks either escape to infinity or turn around again for more collisions. For a 2-bounce event (meaning the kinks pass each other twice) the ultimate outcome of this scattering would be a reflection, and for a 3-bounce a transmission.

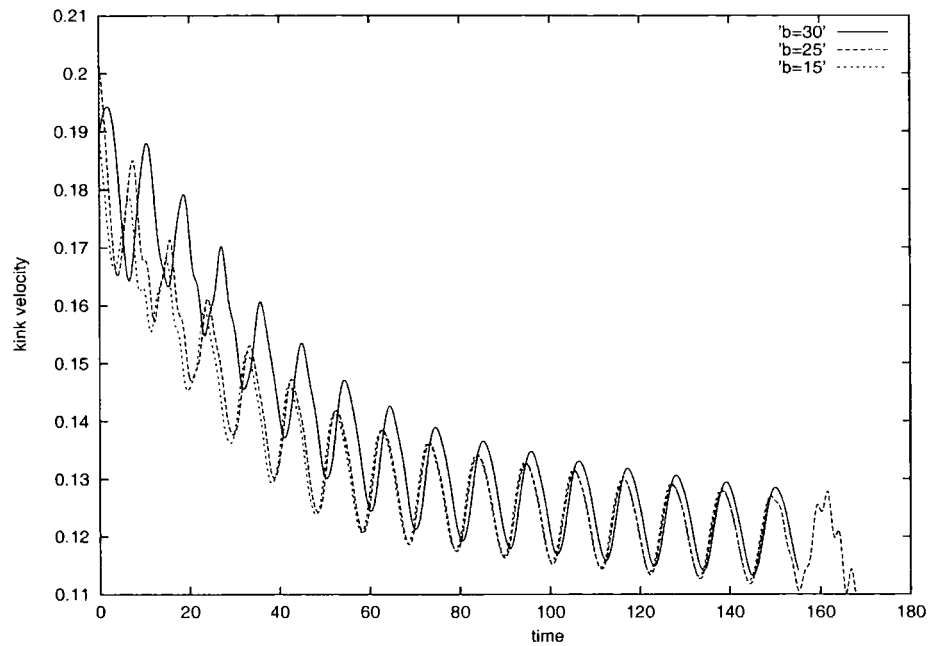

Figure 2.1: A plot of the kink velocity against time. The three curves represent velocities of a kink on a lattice with $h = 1.4$ and with an initial velocity of 0.197 but starting at different points on the lattice. The solid curve represents a kink with $b = 30$, the dashed curve a kink with $b = 25$ and the dotted curve is for $b = 15$.

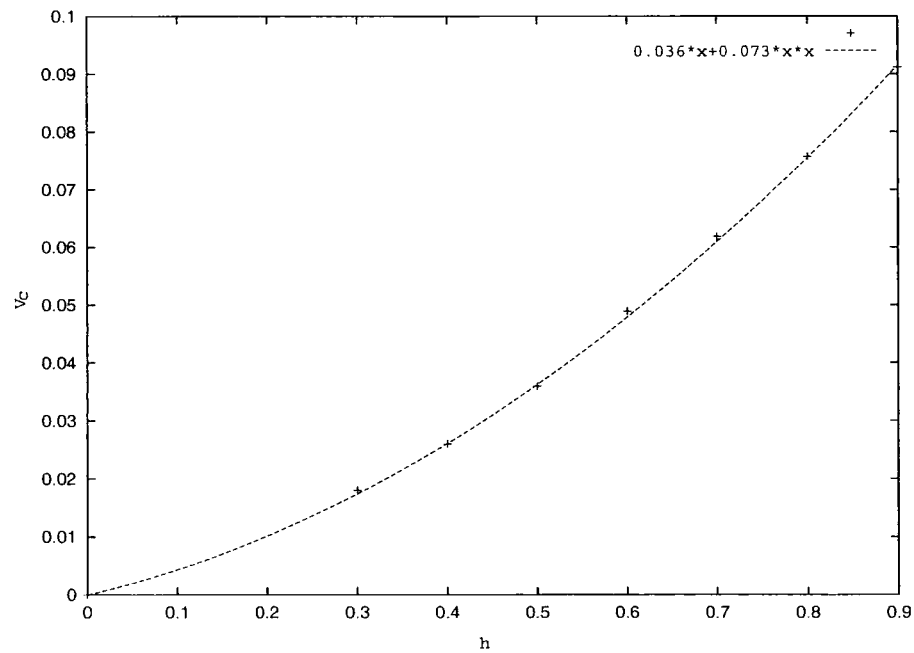

Figure 2.2: A plot of critical velocity against lattice spacing. The crosses represent data points found numerically. The curve represents a theoretical fit of $v_c = 0.073h^2 + 0.036h$.

The velocities for the bounces occur in small intervals. For velocities outside of these intervals the outcome is always a bound state. This is similar to the result of the ϕ^4 model presented in section 2.1.2 except in this case the outcome does not depend fractally on the impact velocity. We have only seen 2, 3 and 4-bounce events. But the velocities at which the bounces occur are not easy to find and the intervals are small (10^{-7} for a 4-bounce), so it may be that higher bounce events occur but we have not seen them.

Figure 2.3 shows an example of the 2-bounce event. In this figure we have plotted the field $\psi(0,t)$ against t. $\psi(0,t)$ is the field at the centre of mass of the kink-antikink system.The kinks are on a lattice of unit spacing with an initial separation of 10 units. v_c for this combination is found to be 0.100. The kinks bounce for all initial velocities in the range $0.0969 \leq v \leq 0.0972$ (2-bounce window).

Figures 2.4 and 2.5 show examples of three and four bounce events. In figure 2.4 the kinks transmit whereas in 2.5 they reflect off each other. As can be seen from the figure for the 2-bounce case, the kink and antikink collide, pass through each other and travel a small distance before stopping, turning around and travelling in the other direction. The kinks then collide again, pass through each other and this time escape to infinity. Figure 2.6 is a graph of $\psi(0,t)$ against t representing the oscillations at the centre of mass of a bion. This is essentially an n-bounce event for n very large. The erratic oscillations suggest that the system might be chaotic. The period of oscillations become constant after about 10 cycles and the bion then oscillates for a long time (i.e for hundreds of cycles). We have calculated the maximum Lyapunov exponent of the time series $\psi(0,t)$, using the algorithm of Wolf *et al* [57]. Its value is approximately 0.18, suggesting that the oscillations are mildly chaotic. In general, a positive maximum Lyapunov exponent is taken as a formal definition of chaos.

The results of the simulation can be understood using the resonance energy exchange mechanism. This requires the TDSG kink to support shape modes. We show next that the TDSG kink does support such a mode. The frequency of this mode is calculated in two ways, by using a collective coordinate approximation and also numerically, by Fourier analysing the deformations of a perturbed static kink.

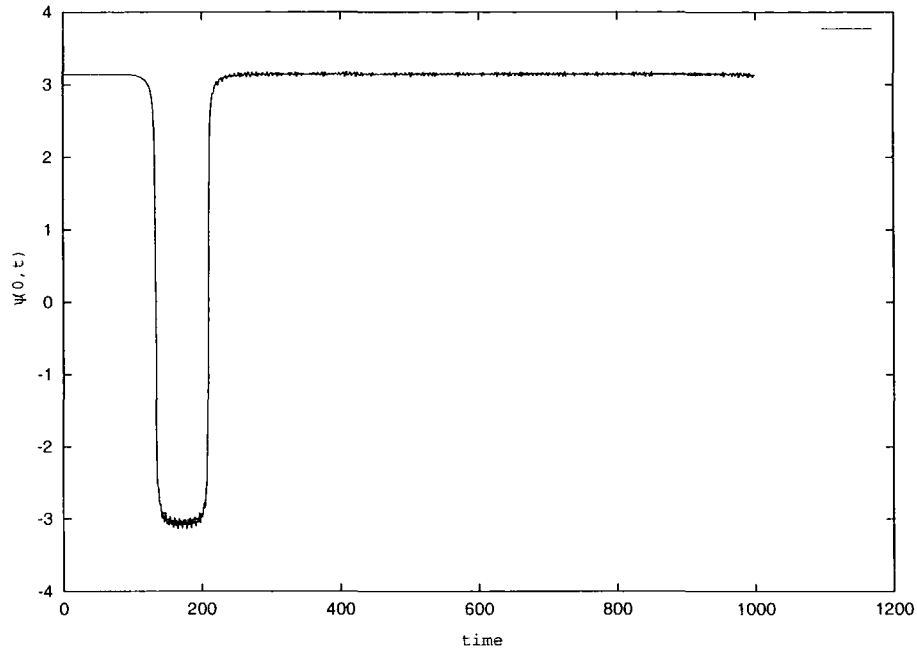

Figure 2.3: A figure representing the 2-bounce event. The kinks collide and essentially reflect off each other.

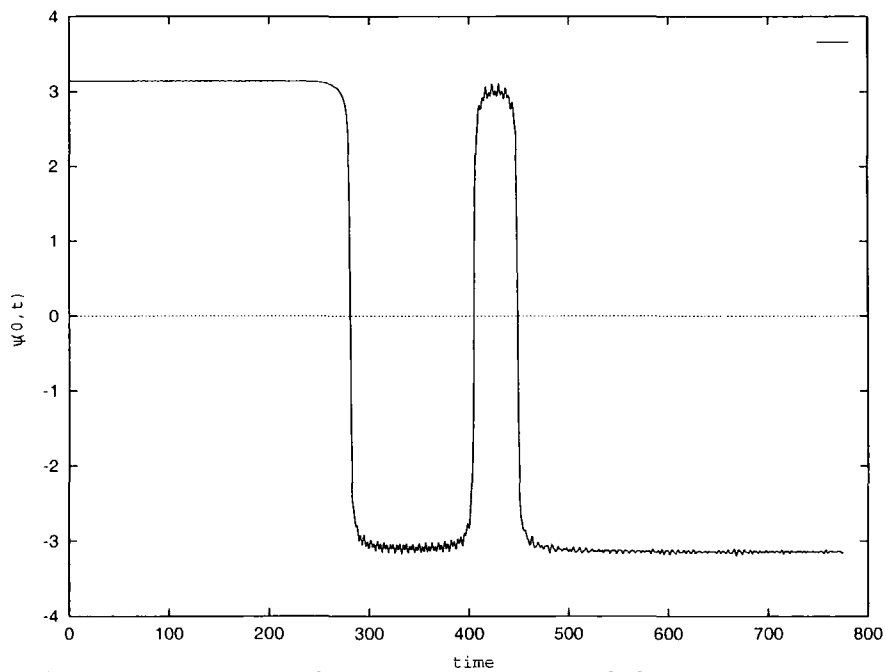

Figure 2.4: A 3-bounce event where the scattering of the kinks results in a transmission.

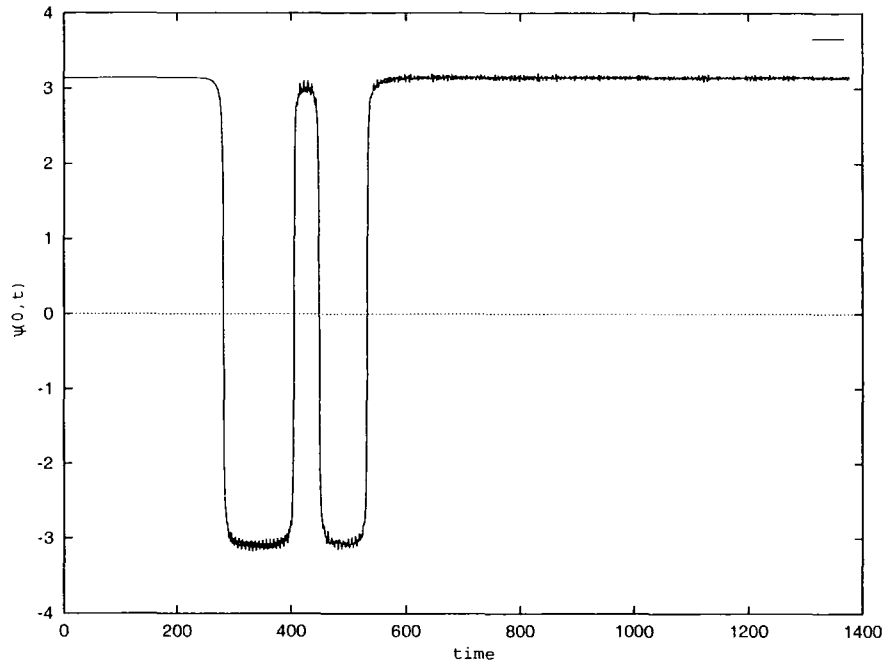

Figure 2.5: A plot showing a 4-bounce event.

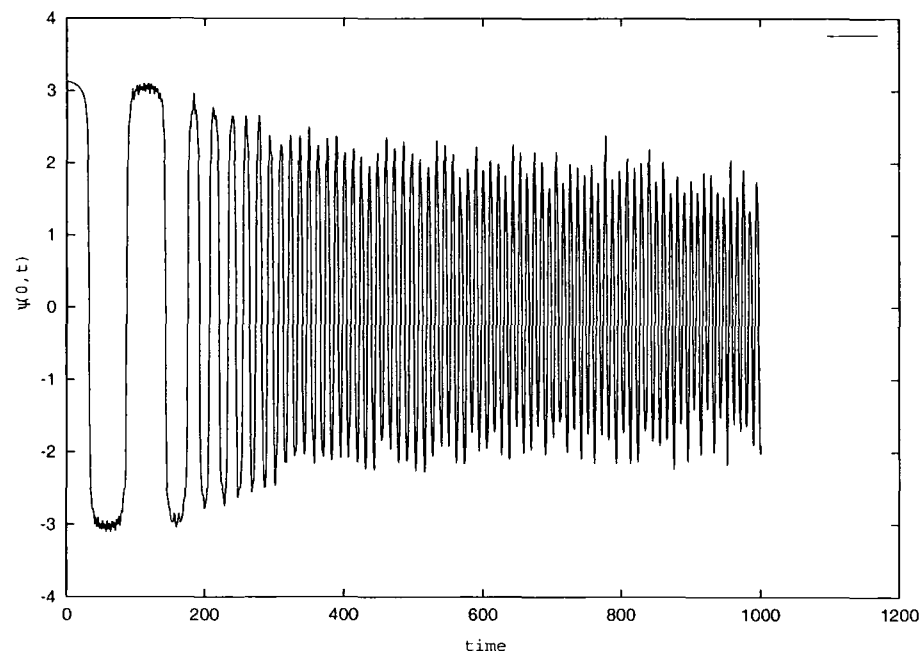

Figure 2.6: A plot of $\psi(0,t)$ against time, representing the oscillations at the centre of mass of the bion.

Note that we could also have used a matrix-based approach similar to the one used by Speight in [58], where it was used to calculate the Casimir energy of the TDSG kink.

2.3.3 Kink Internal Shape Mode

Collective Coordinate Approximation

We can obtain a collective coordinate approximation of the TDSG system by treating the scale factor a in the kink as a dynamical variable. This reduces the number of degrees of freedom from infinity to one. The Lagrangian of the reduced system is given by

$$\mathcal{L} = f(a,b)\dot{a}^2 - g(a,b), \tag{2.38}$$

where $f(a,b)$ and $g(a,b)$ are functions given by

$$f(a,b) = \frac{h}{4}\sum_x (x-b)^2 \mathrm{sech}^2 a(x-b), \tag{2.39}$$

$$g(a,b) = \frac{1}{h}\tanh(\frac{1}{2}ah) + \frac{h}{4}\coth(\frac{1}{2}ah). \tag{2.40}$$

The corresponding equation of motion is

$$2f\ddot{a} + f'\dot{a}^2 - g' = 0. \tag{2.41}$$

where the prime denotes differentiation with respect to a. $g(a,b)$ has a minimum (stable equilibrium) at $a = s := \frac{2}{h}\tanh^{-1}\frac{h}{2}$. Small amplitude oscillations $a(t) = s + \epsilon(t)$ satisfy the linearised equation,

$$2f(s,b)\ddot{\epsilon} = g''(s,b)\epsilon. \tag{2.42}$$

Hence the waves oscillate with frequency

$$\nu = \frac{1}{2\pi}\sqrt{\frac{g''(s)}{2f(s,b)}}. \tag{2.43}$$

$g''(s) = (1-\frac{1}{4}h^2)^2$, so the frequency of the shape mode depends on the lattice spacing. For $h = 1$, the shape mode frequency is 0.152. Table 2.1 shows the dependence of frequency on the lattice spacing h.

h	frequency
0.1	0.175
0.2	0.175
0.5	0.170
0.8	0.161
0.9	0.157
1.0	0.152
1.2	0.143

Table 2.1: The collective coordinate predictions for the shape mode frequency for various values of h

As a check on the accuracy of the collective coordinate approach, we have used it to calculate the frequency of the shape mode of the ϕ^4 kink. The value found is $\sqrt{(1.55)}$, which is fairly close to the actual value $\sqrt{(1.5)}$.

Numerical method

Numerically, the shape mode frequency is obtained by Fourier analysing the deformations of the perturbed static kink. We set the initial condition for equation (2.31) to be

$$\begin{aligned} \psi(x,0) &= \psi_K(x,0) + \epsilon \\ \dot{\psi}(x,0) &= 0, \end{aligned} \tag{2.44}$$

where $\psi(x)$ is the static kink solution and ϵ is the pertubation. The value of ϵ is chosen to be -0.03. The field $\psi(x,t)$ is sampled at various values of x. From this we obtain the variations in the field, $\delta\psi(x,t) = \psi(x,t) - \psi(x,0)$, for each of the sampled values of x. $\delta\psi(x,t)$ were then Fourier analysed using the MATLAB FFT routine.

In figure 2.7 we have plotted the power spectrum for the data sampled at $x = 0$ for a kink on an $h = 1$ lattice. The power spectrum of the data for other values of x give identical power spectra. Moreover, we get identical power spectra for cases

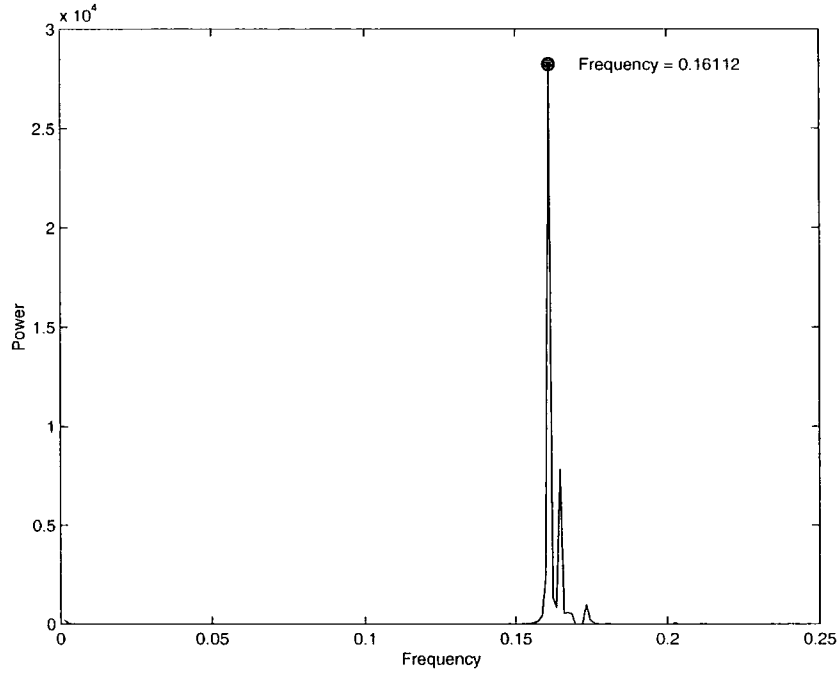

Figure 2.7: Power spectrum of the fluctuations around a perturbed static kink

when the kink is located exactly on a lattice point or somewhere in between points, *i.e.* there is no dependence on b.

Figure 2.7 was constructed using $N = 2^{14} = 16384$ data points. Aliasing of the power does not occur since the amplitude at the Nyquist frequency is essentially zero. There is a peak at $\nu = 0$ corresponding to the Goldstone mode, and a peak at $\nu = 0.161$ corresponding to the shape mode.

This procedure is repeated for other values of h. In contrast to the results suggested by the collective coordinate approach, we find that the frequency of the shape mode is more or less independent of h. For $0.5 \leq h \leq 1.2$, we found $0.158 < \nu < 0.161$. The value of the frequency (for $h = 1$) however is within the range of frequencies found using the collective coordinate method.

In the continuum limit the TDSG shape mode frequency is precisely the quasi-mode frequency of the continuum sG system found by Rice [47], $\omega_R = 0.175$, which corresponds to an angular frequency of 1.0996. This finding seems to be in contradiction with the very recent work of Quintero, Sanchez and Mertens [49], whose numerical simulations show that the quasimode reported by Rice does not exist.

However, it can be argued that the simulations done by Quintero *et al* are not accurate since they allow phonons to be reflected off the boundaries and interfere with subsequently emitted phonons from the kink [59].

It is interesting to compare the situation with other discrete sine-Gordon systems. The well-known Frenkel-Kontorrova model does not support a kink with an internal shape mode for all values of the discreteness parameters. The sine-Lattice model however does support one, as long as the system is only weakly discrete [39]. The shape mode for the sine-Lattice system lies just below the lower phonon band suggesting that it is a genuine kink shape mode rather than just a phonon resonance. Moreover, in the continuum limit this shape mode converges to the sine-Gordon quasimode frequency.

2.4 Kink-antikink Interactions in Topological Discrete ϕ^4 System

In this section we present the results of kink-antikink interactions for the topological discrete ϕ^4 system. The model is defined by the Lagrangian

$$L = h\sum_{n\in\mathbb{Z}} \frac{1}{2}\dot{\phi}_n^2(t) - (\frac{1}{2}D_n^2 + \frac{1}{8}F_n^2), \tag{2.45}$$

with,

$$D_n = (\phi_{n+1} - \phi_n)/h \quad \text{and} \quad F_n = 1 - \frac{1}{3}(\phi_{n+1}^2 + \phi_{n+1}\phi_n + \phi_n^2), \tag{2.46}$$

say. With this choice of D_n and F_n, the equation of motion is given by

$$\begin{aligned}\ddot{\phi}_n &= \frac{1}{h^2}(\phi_{n+1} - 2\phi_n + \phi_{n-1}) + \frac{1}{12}[(2\phi_n + \phi_{n-1})(1 - \frac{1}{3}(\phi_n^2 + \\ &\quad \phi_n\phi_{n-1} + \phi_{n-1}^2)) + (2\phi_n + \phi_{n+1})(1 - \frac{1}{3}(\phi_n^2 + \phi_n\phi_{n+1} + \phi_{n+1}^2))].\end{aligned} \tag{2.47}$$

The model admits genuine lattice static kink solutions provided $h < 2$, and the moduli space of these solutions is isomorphic to $\mathbb{R}$, suggesting that the kink can be positioned anywhere on the lattice and that there is no Pierels-Nabarro barrier [54]. However, we use the Galilean boosted continuum static kink and anitikink solutions as our initial conditions in the simulation, as has been done for the conventional

discrete ϕ^4 system. This will enable us to compare the results we obtain here with the results presented in section 2.1.3.

2.4.1 The Setup

The results of this section were obtained by solving (2.47) using a 4^{th}-order Runge-Kutta algorithm. The initial condition was set as

$$\begin{aligned} \phi(x,0) &= \tanh\frac{1}{2}(x+15) - \tanh\frac{1}{2}(x-15) - 1, \\ \dot{\phi}(x,0) &= -\frac{v}{2}[\text{sech}^2\frac{1}{2}(x+15) + \text{sech}^2\frac{1}{2}(x-15)], \end{aligned} \tag{2.48}$$

so the kink is located at $x = -15$ and the antikink at $x = +15$. The simulations were performed with a time step of $\Delta t = 0.05$ and the grid was chosen to have 900 points. The results of the simulations are very sensitive to any interference from the radiation from the kinks. The best way to avoid this is to make the grid large so that the radiation does not have enough time to reflect off the boundaries and interfere with the kinks. This is of course at the expense of computational time; the chosen grid size and time spacing were found to be the best compromise. With this time step the energy is conserved to about 2%.

The boundary condition was chosen so that at the first and last points of the grid the field was fixed at $\phi = -1$ for all time. The results were then obtained by a programme that solved (2.47) with (2.48) (using a 4^{th}-order Runge-Kutta algorithm) for particular value of v. The programme began with some $v_{initial}$ and ran in steps of $\Delta v = 0.001$ until v_{final}. For each v the outcome of the interactions was recorded, in particular the number of bounces were recorded. The total energy of the kink-antikink system, $E = \sum_{i=0}^{899} e_i$, is a minimum whenever the kinks bounce, so the number of bounces can be recorded by finding the number of minima[2] of E.

It is important to choose the correct duration length T of the simulation. This is because for some cases the time gap between the first and the second collision is rather large, so it is easy to mistake these as a single collision event if T is not large

[2]The "minimum" is recorded only if the energy goes sufficiently below some average value. This is because E is an oscillating function in time and therefore has many minima.

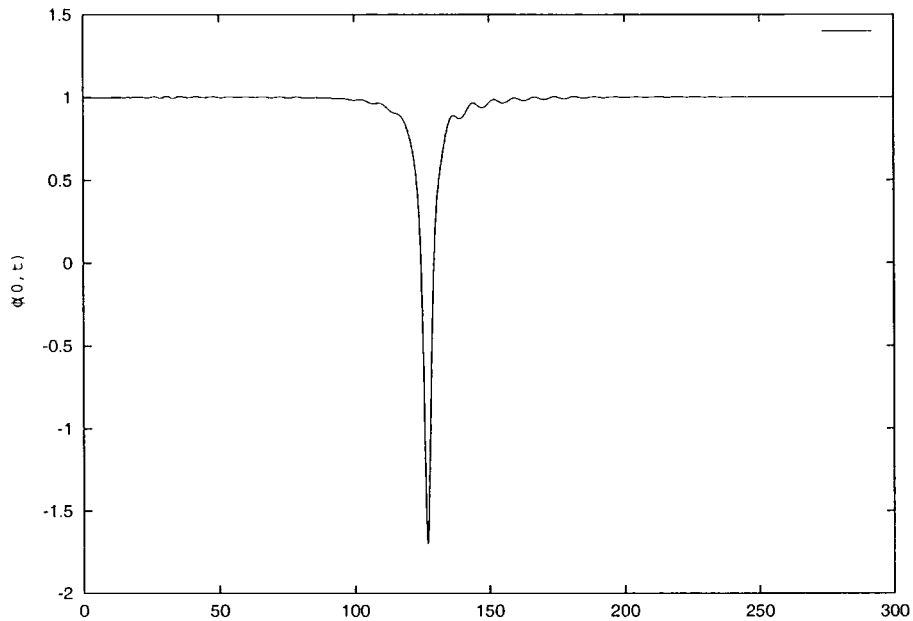

Figure 2.8: A plot showing a "reflection" event ($n = 1$): the kink and antikink simply bouncing off each other.

enough. We have chosen $T = 400$ for most part of the programme except at the beginning (when v is small) where $T = 1500$ was chosen.

2.4.2 Simulation Results

The above setup was run for various values of the lattice spacing h. In general, we found that as the lattice spacing is increased the effect of the kink shape mode on the outcome of the interaction is decreased. That is, for coarser lattices the outcome is more likely to be a "reflection" (*i.e.* where the kinks collide once only, as depicted in figure 2.8). Figure 2.10 is the plot of v_r against the lattice spacing h. v_r is the velocity at which the kinks first reflect off each other, and such that for all subsequent v, $v \geq v_r$, the outcome is always a reflection. For $v \leq v_r$ there are reflection events but they occur in between "trapped" states (where the kinks collide more than once, as shown in figure 2.9).

In fact, the general pattern of the outcome of an interaction for all v and h is similar to that of the conventional discrete ϕ^4 system. That is, there are "trapped" states (where the kinks collide more than once) in between reflection states. Fig-

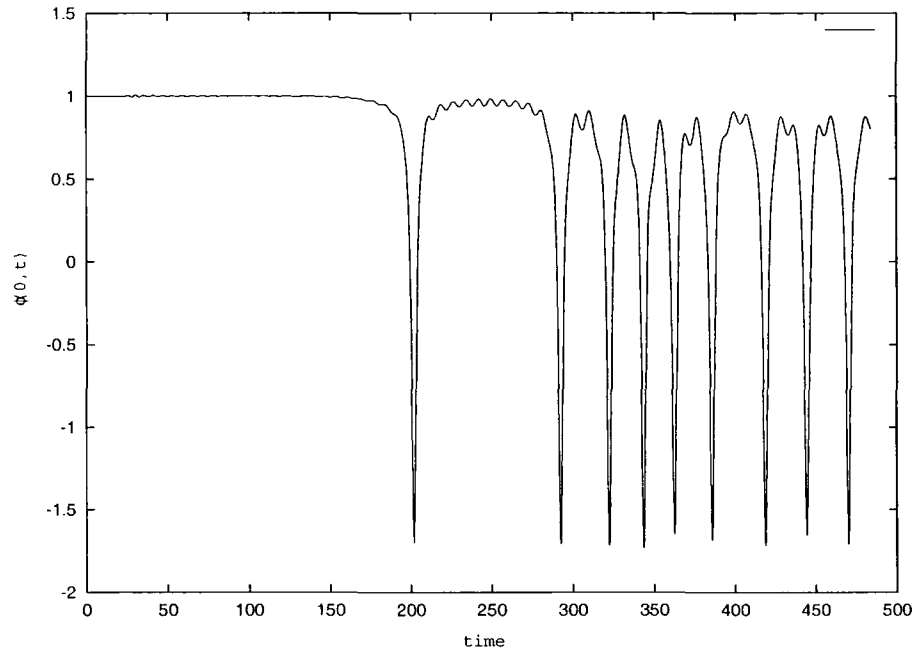

Figure 2.9: A plot showing a "trapped" event. In this case $n = 9$, but a trapped event is one for which $n \geq 2$.

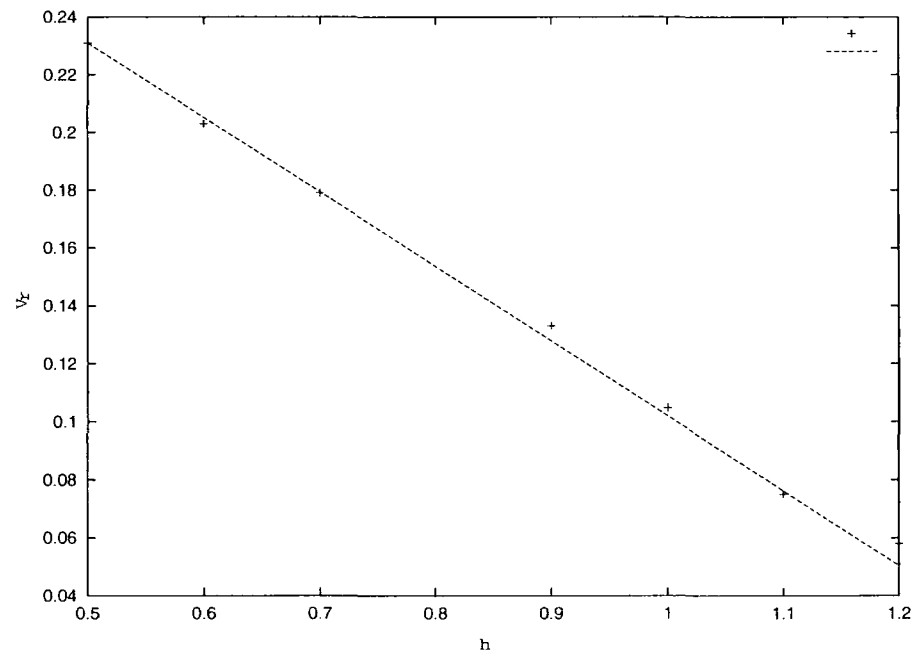

Figure 2.10: A plot showing the relationship between v_r and the lattice spacing.

Figure 2.11: A plot showing the general pattern of the outcome of an interaction (regardless of the lattice spacing). The dark bands represent a trapped state and the light ones a reflection.

ure 2.11 depicts this general pattern,

For instance, for $h = 1.5$, the velocities for which this happens are given in table 2.2.

We have also seen the "windows" behaviour that was reported for the conventional discrete ϕ^4 system. In each of the "trapped" velocity intervals there are "windows" for a given n-bounce event. For instance, the first four 2-bounce windows for the "trapped" interval 0.1031-0.1080 (as shown in table 2) are represented in figures 2.12- 2.15.

A similar structure exists for a 3-bounce, 4-bounce etc, events. One feature that

Velocity range	Outcome
< 0.0850	trapped
0.0851 - 0.0856	reflection
0.0857 - 0.0895	trapped
0.0896 - 0.0910	reflection
0.0911 - 0.0948	trapped
0.0949 - 0.0966	reflection
0.0967 - 0.1008	trapped
0.1009 - 0.1030	reflection
0.1031 - 0.1080	trapped
0.1080 - 0.1112	reflection
0.1113 - 0.1161	trapped
0.1161 - 0.1204	reflection
0.1205 - 0.1250	trapped
0.1251 - 0.1303	reflection
0.1304 - 0.1349	trapped
0.1350 - 0.1422	reflection
0.1423 - 0.1460	trapped
> 0.1461	reflection

Table 2.2: The results of kinks-antikink collisions for $h = 1.5$. The reflection state is one for which the kinks collide once only ($n = 1$), whereas a trapped state is when $n \geq 2$. Here $v_r = 0.1461$.

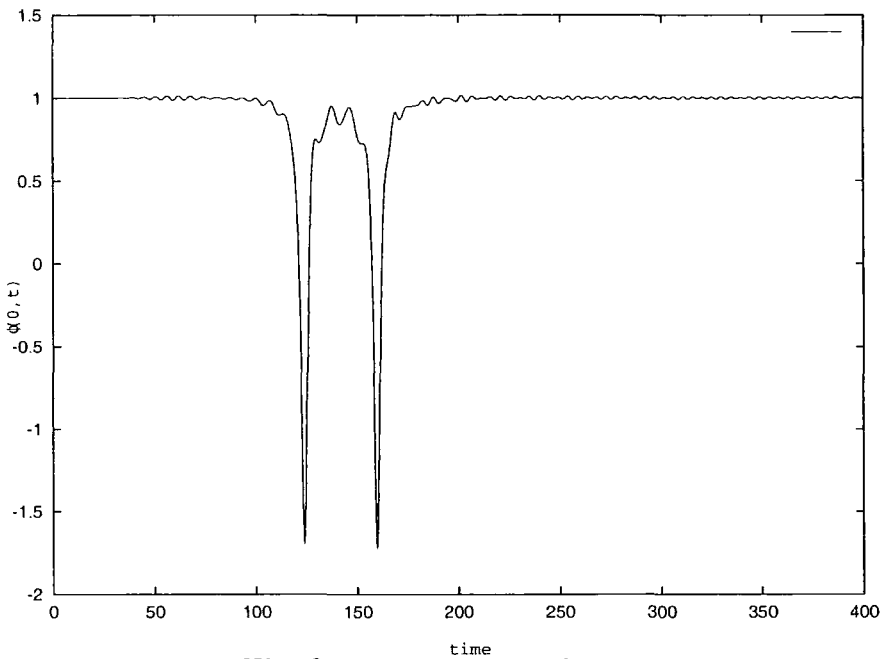

Figure 2.12: The first 2-bounce window at $v = 0.1066$.

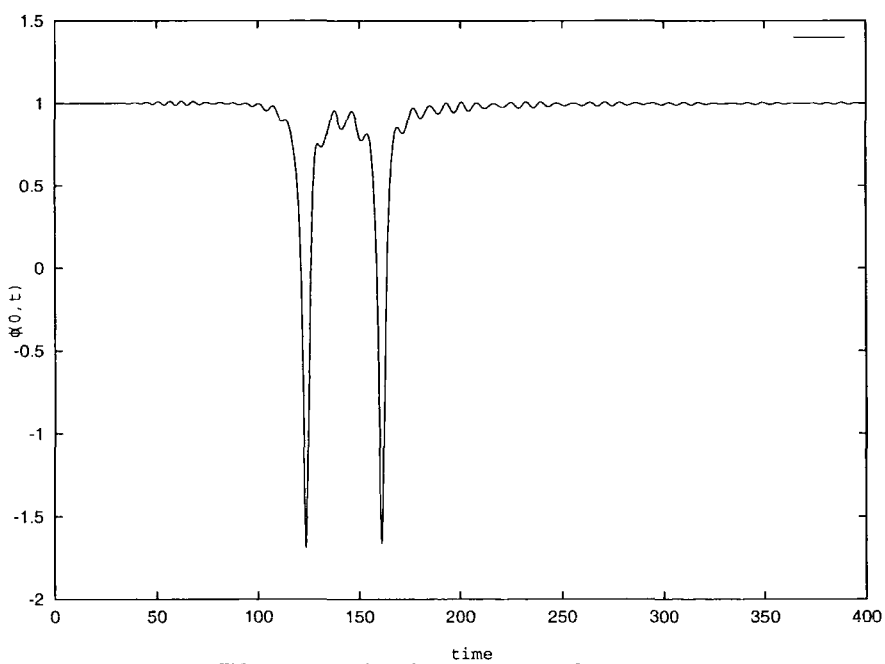

Figure 2.13: The second 2-bounce window at $v = 0.10673$.

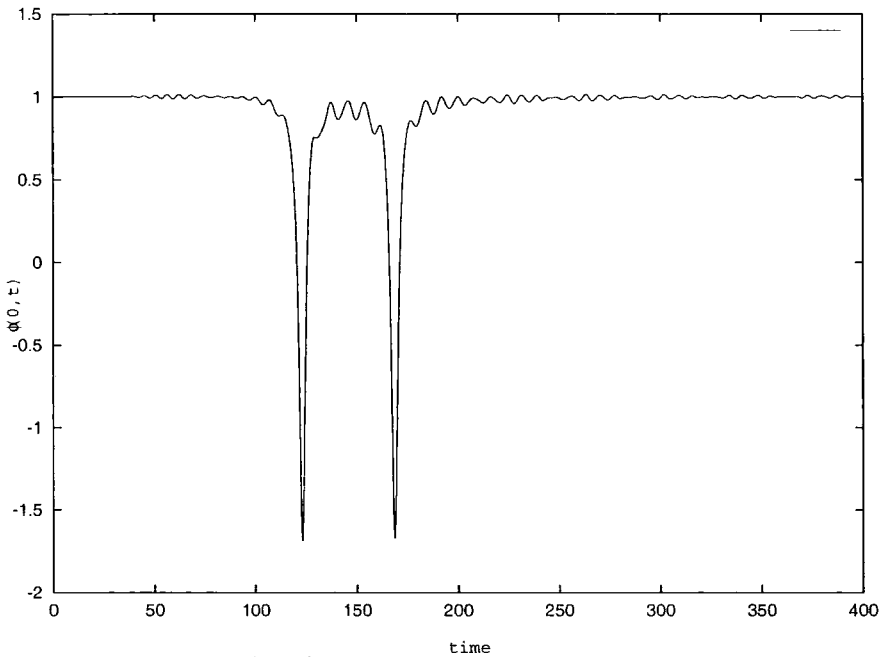

Figure 2.14: The third 2-bounce windows at $v = 0.1072$.

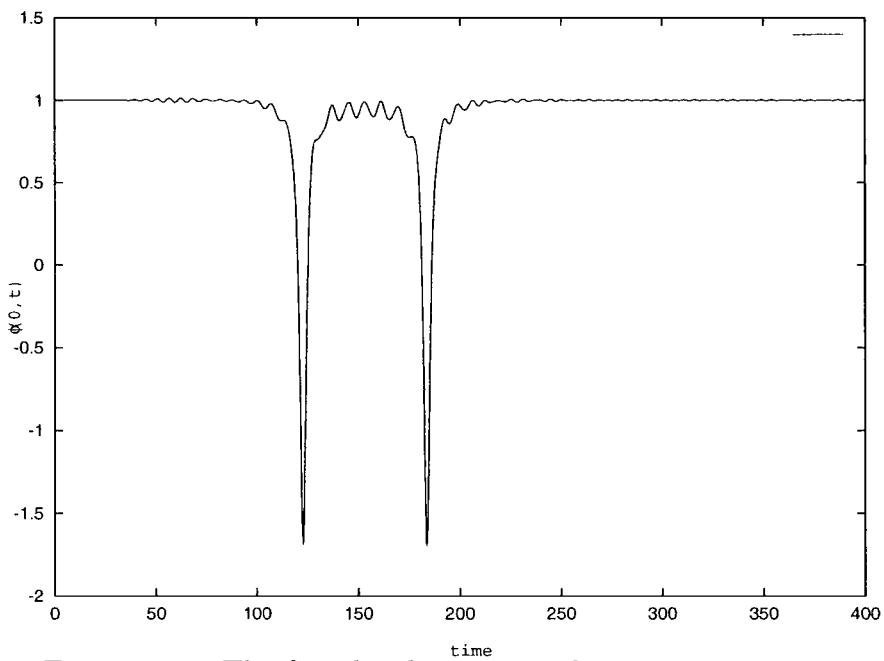

Figure 2.15: The fourth 2-bounce windows at $v = 0.1076$.

is absent in the TDϕ^4 system is the fractal structure. For the conventional discrete ϕ^4 system, the boundary between any two reflection and trapped intervals can be blown up and one sees a similar pattern (figure 2.11) for the velocities that form the boundary [36]. This feature has not been seen for the TDϕ^4 system.

2.5 Conclusion

In this chapter we have discussed the behaviour of kink-antikink interactions in the continuum sine-Gordon and ϕ^4 systems. We have also seen the outcome of kink-antikink interactions in the TDSG and the TDϕ^4 systems.

We found that the kink-antikink interactions in the TDSG system exhibit resonance phenomena similar to those in the continuum ϕ^4 system. In particular, we found that for certain initial kink and anti-kink velocities, the kinks either pass through each other, reflect off each other or form a long-lived bound state. The initial velocities for which the kinks first reflect off each other are found to increase as the lattice spacing is increased. These resonance phenomena may be due to the excitation of an internal mode of the TDSG kink. A collective coordinate analysis shows that the frequency of this mode depends on the lattice spacing, and in the continuum limit ($h \longrightarrow 0$) the frequency seems to approach the quasimode frequency predicted by Rice. The analysis done in [49] however says that there cannot be a quasimode for the continuum sine-Gordon kink, but they do predict the existence of a quasimode for a lattice sine-Gordon kink. This is not the quasimode we have found, so this is something genuinely new. Further numerical simulations are required to determine what is happening in the limit $h \longrightarrow 0$.

Also, as we have mentioned already, there is a modified TDSG system [53] which admits an exact travelling-kink solution (with a fixed velocity). It would be interesting to perform kink-antikink interactions for this system. Since the expressions we have used to perform the interactions are only an approximation to the equation of motion, it would be interesting to see the difference.

The simulation results for the TDϕ^4 system are similar to the conventional discrete ϕ^4 system, though the fractal structure that was reported for the latter has

not been seen here. This conclusion was drawn by explicitly checking the behaviour at the boundary between the trapped and reflection intervals.

Chapter 3

Travelling Kink Solutions in Lattice Systems

3.1 Introduction

The subject of the existence of exact travelling kink solutions for lattice systems is clearly an important one. The immediate application is in condensed matter physics where one is interested in the dynamics of the lattice kink. In general one does not expect lattice systems to admit an exact travelling kink solution: the presence of the Peierls-Nabarro barrier means that the kink loses energy through emission of radiation and slows down. Moreover, lattice systems in general are not invariant under Galilean and Lorentz transformations. Besides, travelling kinks obtained this way require fixing the kink velocity from the outset so the velocity cannot be considered as a parameter.

Nevertheless, there are lattice systems which admit travelling-kink solutions. The first example of such a system was from Schmidt [60], who derived a travelling-kink expression essentially by "reverse engineering": by writing down a travelling-kink solution first and then deriving the potential for which this was a solution. He derived a tanh-shaped kink for a nonlinear lattice system which had a double-minimum on-site potential. This procedure was then extended to other (reaction-diffusion-type) systems by Bressloff [61]. Recently, a systematic procedure for obtaining various travelling-wave solutions (pulses, kinks, breathers) has been put forward by Flach,

Kaldko, and Zolotaryuk [62]. Their "Inverse Method" is fairly general and applies to higher dimensional systems as well.

Interestingly, one can find exact travelling-pulse solutions for many nonintegrable lattice systems. A recent existence theorem by Friesecke and Wattis suggests that this is due to the inherent nonlinearity of the system rather than its integrability [63]. This theorem however has not been extended to include topological solitons (kinks, breathers etc). Note that the TDSG system is an example of a nonlinear system where the particular choice of inter and on-site potentials has resulted in an exact static kink solution. But the TDSG system together with other nonintegrable lattice sine-Gordon systems do not admit exact travelling-kink solutions. In this chapter we will show that an integrable lattice sine-Gordon system does admit such a solution. Other integrable lattice systems which also support travelling-kink solutions are the Toda system [64] and the Ablowitz-Ladik system [65].

The aim of this chapter is therefore two-fold: to briefly survey the situation regarding exact travelling-kink solution for various lattice sine-Gordon systems and to show that an integrable lattice sine-Gordon system does support the travelling-kink solution.

3.2 Lattice sine-Gordon systems

In this section we will summarise the situation regarding travelling-kink solutions in various lattice sine-Gordon systems. Let us begin with the Hamiltonian for the continuum sine-Gordon system,

$$H[\phi,\pi] = \int \left[\frac{1}{2}\pi^2 + \frac{1}{2}\left(\frac{\partial\phi}{\partial x}\right)^2 + (1-\cos\phi)\right] dx. \tag{3.1}$$

Here $\phi(x,t)$ and $\pi(x,t)$ are the canonical coordinates which satisfy the Poisson bracket relation $\{\pi(x),\phi(y)\} = \delta(x-y)$. There are many lattice versions of (3.1). The most natural one seems to be the following,

$$H[\phi_n,p_n] = h\sum_n [p_n^2/2h^2 + (\Delta\phi_n)^2 + V(\phi_n)], \tag{3.2}$$

where Δ is the difference-operator on the lattice and h is a constant (the discreteness parameter). The potential $V(\phi_n)$ is usually taken to be $V(\phi_n) = 1-\cos\phi_n$, but it

is not restricted to this; it could, for instance, be a two-point function $V(\phi_n, \phi_{n+1})$. The difference-operator Δ can be a number of things, with the most common choice being the forward-difference operator, $\Delta f = (f(x+h) - f(x))/h$. Taking Δ to be this gives a lattice sine-Gordon system known as the Frenkel-Kontorova system [66]. Other choices of Δ give other systems such as the TDSG system (and its modifications) [42], [53]. One could also have a lattice sine-Gordon system where the p_n are replaced by its two-point equivalent.

Let us now consider some of these systems in detail.

The Frenkel-Kontorova system

The Frenkel-Kontorova is the most studied lattice sine-Gordon system and is given by the differential-difference equation

$$\frac{d^2\phi_n}{dt^2} = \phi_{n+1} + \phi_{n-1} - 2\phi_n - h^2 \sin\phi_n, \tag{3.3}$$

where $n \in \mathbb{Z}$ is the position on the lattice and h is the discreteness parameter. Equation (3.3) is successfully used to model a number of phenomena including a network of Josephson junctions, certain molecular crystals and the behaviour of DNA [67]. A kink solution of the static system,

$$\phi_{n+1} + \phi_{n-1} - 2\phi_n = h^2 \sin\phi_n, \tag{3.4}$$

can be obtained numerically using shooting methods. For a time-dependent solution one would need to solve

$$v^2\varphi''(z) = \varphi(z+1) + \varphi(z-1) - 2\varphi(z) - h^2 \sin\varphi(z), \tag{3.5}$$

where $z = (n - vt)$ so that $\phi_n(t) = \varphi(z)$. A moving kink solution of (3.3) would require the usual continuum sine-Gordon kink boundary conditions (as discussed in chapter 1). Equation (3.5) has no mathematically exact solutions that represent a moving kink [68]. Of course in the continuum limit $h \longrightarrow 0$, there is such a solution given by

$$\phi = 4\tan^{-1}\exp[\gamma(x - vt)], \tag{3.6}$$

where γ is the Lorentz factor. But for all other h the closest one gets to a moving kink is a solution that has the basic shape of the kink but where the tails are replaced by a small amplitude wave (corresponding to the phonon radiation); the amplitude of the tail-wave increases as the lattice spacing is increased [68].

The "reverse engineering" argument shows that to obtain a moving kink solution $\phi = 4\tan^{-1}\exp(kn - vt - b)$ for a system with the Hamiltonian (3.2) and where Δ is the forward-difference operator, we need potential $V(\phi_n)$ to be

$$V(\phi_n) = \frac{1}{h^2}\int \left[4\tan^{-1}(e^k \tan\frac{1}{4}\phi) - 2\phi + 4\tan^{-1}(e^{-k}\tan\frac{1}{4}\phi) - v^2h^2\sin\phi\right] d\phi. \tag{3.7}$$

The potential depends on k and u and therefore on the speed uh/k of the kink.

The sine-Lattice system

The sine-Lattice system is a modification of the Frenkel-Kontorova system [69], [70]. The modification is the replacement of the difference factor $\Delta\phi = \phi_{n-1} + \phi_{n+1} - 2\phi_n$ with sinusoidal functions. This means that the on-site and inter-site potentials in the sine-Lattice Hamiltonian are now both sinusoidal functions,

$$H = \sum_n (\dot{\phi}_n^2/2) + [1 - \cos(\phi_{n+1} - \phi_n)] + [g(1 - \cos\phi_n)], \tag{3.8}$$

where $\phi_n = \phi_n(t)$ and $g = g(x,t)$. The equation of motion can be found from Hamilton's equations,

$$\frac{d\phi_n}{dt} = \frac{\partial H}{\partial p_n} \quad \text{and} \quad \frac{dp_n}{dt} = -\frac{\partial H}{\partial \phi_n}, \tag{3.9}$$

giving

$$\sin(\phi_{n+1} - \phi_n) - \sin(\phi_n - \phi_{n-1}) - \ddot{\phi}_n = g\sin(\phi_n). \tag{3.10}$$

According to Hirota theory [21], to find soliton solutions of a given nonlinear equation, it is sufficient to cast it into a suitable bilinear operator equation. The bilinear form for the sine-Lattice equation is very similar to the one for the continuum sine-Gordon equation [70]. Consequently the soliton properties of the sine-Lattice system are very close to the sine-Gordon system. But due to the nonintegrability

of the sine-Lattice equation, the solitons are well-defined but not mathematically exact, *i.e.* they are restricted to certain ranges of the kink width and velocity. The system supports a well-defined moving kink of relatively short wavelength, and it also has approximate solutions for kink-antikink and breather-like states. The analogous SLO system [71], obtained by setting the right hand side of (3.10) to zero,

$$\sin(\phi_{n+1} - \phi_n) - \sin(\phi_n - \phi_{n-1}) - \ddot{\phi}_n = 0 \tag{3.11}$$

gives the explicit solutions

$$\phi_n(t) = A \tan^{-1} \exp(\alpha_n/\beta_n), \tag{3.12}$$

where A is the (arbitrary) amplitude, and α_n and β_n are functions of n and t.

The TDSG system

As we have already seen in chapter 2, by exploiting the choice in Δ one can obtain a lattice sine-Gordon system that maintains the Bogomolny bound of the continuum system. The static kink of the system is obtained by solving the discrete Bogomolny equation. A moving kink configuration is obtained by Lorentz boosting the static kink. But this configuration is only an approximation; it does not satisfy the equation of motion (2.31). Since there is freedom in the choice of the expressions for D, F, and in the way the kinetic energy of the kink is defined, one can hope to find suitable expressions for these leading to a (modified) TDSG system that yields explicit moving solutions. This is indeed the case [53]. One can find these expressions by "reverse engineering". The Hamiltonian for the modified TDSG system is given by

$$\begin{aligned} H_n &= -\frac{1}{\beta^2} \log \cos\left(\frac{\beta p_n}{h}\right) + \frac{8}{h^2} \sin^2 \frac{1}{4}(\phi_n - \phi_{n-1}) + \\ &\quad 2 \sin^2 \frac{1}{4}(\phi_{n+1} + \phi_n), \end{aligned} \tag{3.13}$$

and the equation of motion follows from Hamilton's equations [53]. A moving kink solution of the equation of motion is given by

$$\phi_n(t) = 4 \tan^{-1} \exp[\gamma(kn - vt - b)], \tag{3.14}$$

where k, v and b are constants. Substituting this into Hamilton's equations (3.9) we find that they are satisfied provided

$$4\gamma^2 \sinh^2(\frac{k}{2}) - 8h^3v^2\gamma - h^2 \cosh^2(\frac{k}{2}) = 0, \tag{3.15}$$

and for $v \neq 0$,

$$2\beta v = \sinh k. \tag{3.16}$$

Note that for $v = 0$, condition (3.15) reduces to $k = \frac{h}{2} \tanh^{-1} \frac{2}{h}$ [42], the expression for a in chapter 1. So we find that the modified TDSG system does support a travelling kink but its velocity is fixed, determined by β and h. A kink with this velocity is found to propagate on the lattice with no emission of radiation [53].

3.3 Integrable Lattice Systems

We expect integrable lattice systems to support explicit travelling kink solutions; examples of such systems which have long been known are the discrete Toda [64] equation and the Ablowitz-Ladik [65] system. The Ablowitz-Ladik system also supports moving discrete breathers. The subject of integrable lattice systems has been tackled using a number of approaches; these include the AKNS method [25], Hirota's bilinear operator formalism [21], etc. Here we will consider the point of view that a lattice system is integrable if it can be expressed as the consistency condition of a Lax pair. The Lax pair is a linear system defined by two (2×2) matrices $L(n, t, \zeta)$ and $V(n, t, \zeta)$ [72],

$$\begin{aligned} \Psi_{n+1} &= L_n \Psi_n, \\ \frac{d\Psi_n}{dt} &= V_n \Psi_n, \end{aligned} \tag{3.17}$$

where the dependence on t and ζ is taken to be understood; $\Psi(n, t, \zeta)$ is a column 2-vector and $\zeta \in \mathbb{C}$ is the spectral parameter. From (3.17) we see that L_n and V_n provide the spatial and time evolution of the system respectively. The consistency condition for (3.17) is

$$\frac{dL_n}{dt} = V_{n+1}L_n - L_nV_n. \tag{3.18}$$

Notice that (3.18) gives an evolution equation for L_n only; in particular, there is none for V_n. The system however is well-defined because the matrix V_n can be found from L_n. The details of how this is done can be found in [72].

This is, of course, analogous to the r-matrix description of integrable systems, where one finds the r-matrix from the L-operator [73]. In this case, one has the Hamiltonian H written in terms of the basic fields $\phi_n(t)$ and $\eta_n(t)$, which satisfy the Poisson relation $\{\phi_n, \eta_m\} = \delta_{nm}$. Associated with the L-operator (or the matrix $L_n(\zeta)$) are two matrices, an r-matrix and a matrix $M(\zeta)$. The r-matrix is constructed in such a way that the fundamental lattice Poisson bracket relation is satisfied. For instance, for the lattice sine-Gordon system, this relation is given by[1]

$$\{L_n(\zeta) \underset{,}{\otimes} L_m(\lambda)\} = [r(\zeta - \lambda), L_n(\zeta) \otimes L_n(\lambda)]\delta_{nm}. \tag{3.19}$$

The matrix $M(\zeta)$, known as the monodromy matrix, is given by

$$M(\zeta) = \prod_{n=-\infty}^{\infty} L_n(\zeta). \tag{3.20}$$

If we have $\zeta_1, \zeta_2, \ldots, \zeta_N$ such that $\det \mathrm{L}_\alpha = 0$ for all α, then the trace of the monodromy matrix, $\tau(\zeta)$, can be related to the Hamiltonian,

$$H = \sum_{\alpha=1}^{N} c_\alpha \tau(\zeta_\alpha), \tag{3.21}$$

where c_α is a constant. If $\frac{\partial(\tau(\zeta_\alpha))}{\partial t} = 0$ then the Hamiltonian admits an infinite number of conserved quantities. This condition will be met provided V is local [72].

3.3.1 Integrable Lattice sine-Gordon system

The integrable lattice sine-Gordon system is given by the L-operator [73],

$$L_n(\zeta) = \begin{pmatrix} \zeta f(\phi_n) e^{i\eta_n} & \frac{1}{4}h(e^{-i\phi_n/2} - \zeta^2 e^{i\phi_n/2}) \\ \frac{1}{4}h(\zeta^2 \exp^{-i\phi_n/2} - e^{i\phi/2}) & \zeta f(\phi_n) e^{-i\eta_n} \end{pmatrix},$$

[1] At present a generalised form of the fundamental Poisson relation exists only for continuum systems [74]. Equation (3.19), however, is the relation for the lattice Landau-Lifshitz model, of which the lattice sine-Gordon system is a limiting case [73].

where $\phi_n(t)$ and $\eta_n(t)$ are the canonical coordinates; $f(\phi_n) = \sqrt{1 + \frac{1}{8}h^2 \cos\phi_n}$, and h is the lattice spacing. The corresponding r-matrix is similar to that of the continuum sine-Gordon system [73],

$$r(\zeta) = \frac{1}{16\sinh(\zeta)} \begin{pmatrix} 0 & 0 & 0 & 0 \\ 0 & \cosh(\zeta) & -1 & 0 \\ 0 & -1 & \cosh(\zeta) & 0 \\ 0 & 0 & 0 & 0 \end{pmatrix},$$

and the L-operator together with this r-matrix satisfy the fundamental lattice Poisson relation (3.19). The Hamiltonian for this system is given by

$$H[\phi_n(t), \eta_n(t)] = -\frac{4}{s}\sum_n \log\left(\frac{H_n}{2+s^2}\right), \tag{3.22}$$

where,

$$H_n = f(\phi_n)f(\phi_{n+1})\cos\frac{1}{4}(\eta_{n+1}+\eta_n) + \frac{1}{2}s^2\cos\frac{1}{2}(\phi_{n+1}+\phi_n) + \cos\frac{1}{2}(\phi_{n+1}-\phi_n). \tag{3.23}$$

Here $s \in (0, \sqrt{2})$ is a parameter related to the lattice spacing h; namely, $h = 2s$. Note that as $h \longrightarrow 0$ we retrieve the continuum expressions; the L-operator (3.3.1) becomes the infinitesimal L-operator on the infinitesimal lattice

$$L_n(\zeta) = \begin{pmatrix} \zeta(1+i\eta_n) & \frac{1}{4}h(e^{-i\phi_n/2} - \zeta^2 e^{i\phi_n/2}) \\ \frac{1}{4}h(\zeta^2\exp^{-i\phi_n/2} - e^{i\phi/2}) & \zeta(1-i\eta_n) \end{pmatrix},$$

where

$$\phi_n = \frac{1}{h}\int_{x_{n-1}}^{x_n} \phi(x)\,dx, \quad \text{and} \quad \eta_n = \int_{x_{n-1}}^{x_n} \pi(x)\,dx, \tag{3.24}$$

such that $\{\pi(x), \phi(y)\} = \delta(x-y)$. The lattice Hamiltonian (3.3.1) reduces to the continuum Hamiltonian (3.1).

3.3.2 Derivation of the Travelling Kink Solution

The vacuum solutions of the integrable lattice sine-Gordon system may be constructed by taking ψ_n (the 2×2 augmented matrix) to have the form

$$\psi_n = UD(\zeta)^n, \tag{3.25}$$

with

$$U = \frac{1}{\sqrt{2}} \begin{pmatrix} 1 & i \\ i & 1 \end{pmatrix}, \quad \text{and} \quad D = \begin{pmatrix} f_0 - ik_0 & 0 \\ 0 & f_0 + ik_0 \end{pmatrix}.$$

Here $f_0 = \sqrt{1 + \frac{1}{8}h^2}$ and $k_0 = \frac{1}{2}s(\zeta - \zeta^{-1})$. Substituting (3.25) into $L_n\psi_n = \psi_{n+1}$ and equating the powers of ζ leads to the vacuum solutions $\phi_n = 2n\pi$.

A travelling kink solution of the integrable lattice sine-Gordon system may be constructed by analogy with the continuum case [73]. In particular, let ψ_n be of the form

$$\psi_n = A_n B_n^{-1}(\zeta) D(\zeta)^n, \tag{3.26}$$

where A_n is a 2×2-matrix independent of ζ, and $B_n(\zeta)$ is the Blaschke-Potapov factor,

$$B_n = I + \frac{\bar{\zeta}_o - \zeta_o}{\zeta - \bar{\zeta}_o} P_n. \tag{3.27}$$

Here P_n is a projection operator given by,

$$P_n = \frac{1}{1 + |\Theta_n|^2} \begin{pmatrix} |\Theta_n|^2 & \Theta_n \\ \bar{\Theta}_n & 1 \end{pmatrix},$$

so that $P_n^2 = P_n$. For a travelling-kink solution, ζ_o may be taken to be purely imaginary, *i.e.*, $\zeta_o = i\mu$, where μ is a real number (related to the speed of the kink). The expressions for ϕ_n and η_n can now be found by considering $L_n = \psi_{n+1}\psi_n^{-1}$ and calculating the residue at $\zeta = i\mu$. This gives

$$\phi_n = 2\tan^{-1}\Theta_n + 2\tan^{-1}\Theta_{n+1} \tag{3.28}$$

$$\eta_n = -4\tan^{-1}\frac{h\sinh\mu\Theta_n}{(f_0 - \frac{1}{2}\cosh\mu)(1 + \Theta_n\Theta_{n+1})}, \tag{3.29}$$

where $g = (2f_0 + h\cosh\mu)/(2f_0 - h\cosh\mu)$, $u = 4f_0\sinh\mu/(4f_0^2 - h^2\cosh^2\mu)$ and $\Theta_n = e^{-ut}g^n$. Equation (3.28) is a kink solution provided $\cosh(2\mu) < 8/h^2$, but such a μ always exists since $0 < h < \sqrt{2}$. By taking $\mu = 0$ we have $u = 0$ and $\eta_n = 0$, so this gives the static kink solution

$$\phi_n = 2\tan^{-1}(cg^n) + 2\tan^{-1}(cg^{n+1}), \tag{3.30}$$

where c is a constant. Equation (3.30) is the solution of the following equation

$$X(\phi_{n+1}) = \frac{f_0 + s}{f_0 - s} X(\phi_n), \tag{3.31}$$

where

$$X(\phi_n) = \frac{f(\phi_n) - f_0 \cos \frac{1}{2}\phi_n}{f_0 \sin \frac{1}{2}\phi_n}. \tag{3.32}$$

Equations (3.31) are the Bogomolny equations.

3.4 Conclusions

In this chapter we have briefly reviewed the situation regarding travelling kink solutions in various lattice sine-Gordon systems. We have seen that a number of non-integrable lattice sine-Gordon systems are unable to support explicit travelling kink solutions. However, certain integrable lattice systems are known to support such solutions. We have therefore sought to find travelling kink solutions for the integrable lattice sine-Gordon system. Explicit forms of such solutions are not believed to have previously existed in the literature. We have found these expressions (3.28) by analogy with the continuous sine-Gordon case [73]. It can be verified (using MAPLE for instance) that the given expressions indeed satisfy Hamilton's equations.

It is conceivable that a double soliton solution or a breather can also be constructed using a similar procedure, again by analogy with the continuum case.

Chapter 4

Yang-Mills-Higgs Solitons on De Sitter Space-Time

4.1 Introduction

As was mentioned in chapter 1, it is a conjecture by Richard Ward that all the known integrable systems in $(1+1)$ and $(2+1)$-dimensional flat space-times arise as reductions of the self-dual Yang-Mills equations [33]. In this chapter we will show that an appropriate reduction of the self-dual Yang-Mills equations generates an integrable system which is covariantly coupled to a curved space-time. Such a reduction procedure can be carried out only for space-times which have constant curvature. So there are three possibilities, namely, the positive definite hyperbolic space-time and its Lorentzian versions, the de Sitter and anti-de Sitter (AdS) space-times. The positive definite case has been dealt with by Atiyah, and gives rise to the so-called hyperbolic monopoles [75], [76]. The AdS case has been considered also, by Ward [77], and both the positive definite case and the AdS case are being investigated further by Hickin [78]. Here we will consider the remaining possibility, namely we will construct an integrable system on de Sitter space-time. The method used to generate solutions for the other two cases, namely the 'Riemann problem with zeros' method [73] does not work so well here. Instead, we will use twistor methods to generate the solutions [22].

The chapter is divided into 6 sections. In section 4.2 we will consider some

details of the twistor correspondence and the Atiyah-Ward ansatz. In section 4.3 we consider the (2+1)-dimensional de Sitter space-time itself. In section 4.4 we consider various integrable equations on the de Sitter space-time. Section 4.5 contains various explicit solutions of the Yang-Mills-Higgs equations with gauge groups U(1) and SU(2), and section 4.6 ends with some concluding remarks.

4.2 The Twistor Construction

It is a conjecture that one can in principle construct solutions of any integrable equation on a space-time M using the twistor construction and via the Penrose transform. Here we will use twistor methods to construct solutions of the reduced Yang-Mills system on the $(2+1)$-dimensional de Sitter space-time.

Twistor space itself was introduced by Roger Penrose as an attempt to unify quantum theory with general relativity [79]. The basic idea is that twistor space acts as an auxiliary manifold to the space-time manifold. The various equations and physical quantities on the 4-dimensional (complex) space-time manifold correspond to various geometrical structures on the 3-dimensional (complex) twistor space. For example, solutions of linear field equations such as the wave equation, the massless Klein-Gordon equation, Maxwell's source-free equation, Dirac-Weyl neutrino equation all correspond to cohomologies (or integral representations) of functions on the twistor space [80]. Solutions of gauge theories correspond to holomorphic vector bundles over the twistor space [81].

The Penrose transform can be used to move back and forth between the twistor space and space-time pictures. It can be expressed using the following construction: Consider a 5-dimensional complex space $\mathbb{F}$ with the following double fibration,

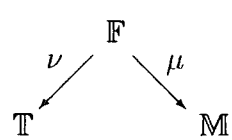

where $\mathbb{T}$ is the 3-dimensional twistor space for the 4-dimensional space-time manifold $\mathbb{M}$. The space $\mathbb{F}$ is a fibre bundle over both $\mathbb{T}$ and $\mathbb{M}$ and is known as the correspondence space. The Penrose transform is given by the composite map

$\mu \circ \nu^{-1}$. The concrete form of the transform is typically a Cauchy-type integral along the fibres of ν.

An important application of the Penrose transform arises in the context of gauge fields and is known as the Penrose-Ward transform. The Penrose-Ward transform is derived from the observation that the anti-self-dual Yang-Mills equations are equivalent to the vanishing of the curvature on α-planes. This idea is incorporated into Ward's theorem which relates solutions of the self-dual Yang-Mills equations on a region of complex space-time U to holomorphic vector bundles over the twistor space of U. This is what we use to find solutions of the Bogomolny equations on de Sitter space-time. In order to do this we consider first some basic facts about the geometry of twistor space. We will consider the twistor correspondence primarily for the ultrahyperbolic space-time [22]. Details for the Euclidean case can be found in [80], [22].

4.2.1 The Geometry of Twistor space

Consider the complexified Minkowski space-time $\mathbb{CM}$, with double null coordinates $(w, z, \tilde{z}, \tilde{w})$. The metric on $\mathbb{CM}$ is given by

$$ds^2 = 2(dz\, d\tilde{z} - dw\, d\tilde{w}), \tag{4.1}$$

and the volume element is

$$\nu = dw \wedge d\tilde{w} \wedge dz \wedge d\tilde{z}. \tag{4.2}$$

The ultrahyperbolic space-time $\mathbb{R}^{2+2}$ is a real slice of $\mathbb{CM}$ given by the correspondence

$$\begin{pmatrix} \tilde{z} & w \\ \tilde{w} & z \end{pmatrix} = \frac{1}{\sqrt{2}} \begin{pmatrix} x^1 + ix^2 & x^3 - ix^4 \\ x^3 + ix^4 & x^1 - ix^2 \end{pmatrix},$$

where the coordinates (x^0, x^1, x^2, x^3) are real. The reality conditions on the double null coordinates are $\bar{z} = \tilde{z}$ and $\bar{w} = \tilde{w}$.

A point on $\mathbb{R}^{2+2}$ has a spinor representation given by

$$x^\mu = x^{AA'} = \begin{pmatrix} x^{00'} & x^{01'} \\ x^{10'} & x^{11'} \end{pmatrix} = \frac{1}{\sqrt{2}} \begin{pmatrix} x^1 + ix^2 & x^3 - ix^4 \\ x^3 + ix^4 & x^1 - ix^2 \end{pmatrix}.$$

A null 2-plane $Z \subset \mathbb{CM}$ is either an α-plane or a β-plane depending on whether its tangent bivector is self-dual or anti-self-dual. The tangent bivector is defined to be $\pi^{ab} = v^{[a}w^{b]}$, where v^a and w^a are independent tangent vectors. So Z is an α-plane if $\pi^{ab} = +{}^*\pi^{ab}$ and a β-plane if $\pi^{ab} = -{}^*\pi^{ab}$.

An α-plane is the set of $(w, z, \tilde{z}, \tilde{w}) \in \mathbb{CM}$ satisfying

$$Z^0 = \tilde{z}Z^2 + wZ^3 \tag{4.3}$$

$$Z^1 = \tilde{w}Z^2 + zZ^3, \tag{4.4}$$

where (Z^0, Z^1, Z^2, Z^3) are complex constants. Let $\lambda = Z^0/Z^2$, $\mu = Z^1/Z^2$ and $\zeta = Z^3/Z^2$ for $Z^2 \neq 0$. Then equations (4.3) and (4.4) are equivalent to

$$\zeta w + \tilde{z} = \lambda, \tag{4.5}$$

$$\zeta z + \tilde{w} = \mu. \tag{4.6}$$

The α-planes for which $Z^2 \neq 0$ have a tangent space spanned by the vector fields

$$\partial_1 = \partial_w - \zeta\partial_{\tilde{z}} \tag{4.7}$$

$$\partial_2 = \partial_z - \zeta\partial_{\tilde{w}}, \tag{4.8}$$

and those with $Z^2 = 0$ are spanned by $\partial_{\tilde{z}}$ and $\partial_{\tilde{w}}$. From this we see that the α-plane are parametrized by three complex numbers λ, μ, and ζ (provided ζ is finite), and the set of all α-planes through a point in space-time has the structure of a Riemann sphere with affine coordinate ζ.

The space of all α-planes in $\mathbb{CM}$ is a complex 3-manifold $\mathbb{T}$ known as the twistor space of $\mathbb{CM}$, given by $\mathbb{T} = \mathbb{CP}^3 \backslash \mathbb{CP}^1$. $\mathbb{T}$ has inhomogeneous coordinates (λ, μ, ζ) if $\zeta \neq \infty$ and $(\tilde{\lambda} = Z^0/Z^3, \tilde{\mu} = Z^1/Z^3, \tilde{\zeta} = Z^2/Z^3)$ if $\zeta \neq 0$. The $\mathbb{CP}^1$ is the set of all points in $\mathbb{CP}^3$ which lie on $Z^2 = Z^3 = 0$.

The twistor space of $U \subset \mathbb{CM}$ is defined to be the subset

$$\mathcal{P} = \{Z \in \mathbb{T} : Z \cap U \neq \emptyset\} \tag{4.9}$$

of $\mathbb{CP}^3$. The space-time patch U and its twistor space $\mathcal{P}$ are both quotients of $\mathbb{F}$. The space $\mathbb{F}$ is a set of pairs (x, Z), where x is a space-time point and Z is an α-plane through x. The projections μ and ν as defined by the diagram in the previous

section are then given by

$$\mu : (x, Z) \mapsto x \tag{4.10}$$

$$\nu : (x, Z) \mapsto Z, \tag{4.11}$$

or using coordinates,

$$\mu : (w, z, \tilde{z}, \tilde{w}, \zeta) \mapsto (w, z, \tilde{z}, \tilde{w}) \tag{4.12}$$

$$\nu : (w, z, \tilde{z}, \tilde{w}, \zeta) \mapsto (\zeta w + \tilde{z}, \zeta z + \tilde{w}, \zeta). \tag{4.13}$$

From this we infer that an α-plane in $\mathbb{CM}$ is represented by a point in $\mathbb{T}$, and a point of $\mathbb{CM}$ is represented by a line in $\mathbb{T}$. This is the famous Klein correspondence.

To find the twistor space for $\mathbb{R}^{2+2}$, we have to impose a reality structure on $\mathbb{CM}$. As mentioned already, $\mathbb{R}^{2+2}$ can be obtained from $\mathbb{CM}$ by setting $\tilde{w} = \bar{w}$ and $\tilde{z} = \bar{z}$. So if σ is an anti-holomorphic involution on $\mathbb{CM}$, then the required reality structure on $\mathbb{CM}$ may be given by

$$\sigma : (w, z, \tilde{w}, \tilde{z}) \mapsto (\bar{\tilde{w}}, \bar{\tilde{z}}, \bar{w}, \bar{z}). \tag{4.14}$$

This induces a map $\sigma : \mathbb{T} \mapsto \mathbb{T}$,

$$\sigma : (Z^0, Z^1, Z^2, Z^3) \longrightarrow (\bar{Z}^1, \bar{Z}^0, \bar{Z}^3, \bar{Z}^2). \tag{4.15}$$

There are fixed points of the action of σ on $\mathbb{CP}^3$. This set of fixed points is the set of real α-planes in $\mathbb{R}^{2+2}$. The space of all real α-planes through a point in $\mathbb{R}^{2+2}$ is S^1, and the space of all α-planes in compactified $\mathbb{R}^{2+2}$ is $\mathbb{RP}^3$. It should be noted that each α-plane in $\mathbb{R}^{2+2}$ compactifies to $\mathbb{RP}^2$ which is not simply connected and has fundamental group $\mathbb{Z}_2$. The upshot of this is that the Penrose transform applied to the compactification of $\mathbb{R}^{2+2}$, $\tilde{M} = S^2 \times S^2/\mathbb{Z}_2$, does not yield globally smooth solutions of linear field equations [22]. However, the double cover of $\tilde{M}$, $\bar{M} = S^2 \times S^2$, has corresponding α-planes homeomorphic to S^2 which is simply connected. So to find globally smooth solutions of equations in a split $(2, 2)$ signature space-time, we need to consider the space-time $\bar{M}$.

4.2.2 Solutions of Massless Field Equations

As an illustration of the use of the Penrose transform, we consider its use in generating solutions of massless field equations [80].

The idea behind the use of the Penrose transform to solve massless field equations is the following: Consider a function $f(Z)$ defined on the twistor space $\mathbb{T}$. Let $Z^\alpha = (\omega^A, \pi^{A'})$, and let $\hat{f}$ denote the function f restricted to α-planes (*i.e.* the pullback of f to $\mathbb{F}$), given by

$$\hat{f} = f(ix^{AA'}\pi_{A'}, \pi_{A'}). \tag{4.16}$$

Taking the integral of $\hat{f}$ along the fibres of ν (*i.e.* integrating out the dependence on $\pi_{A'}$) then gives a function on M. The function $\hat{f}$ satisfies various differential equations which are inherent in the double fibration. For instance, consider the contour integral of $\hat{f}$ given by

$$\phi(x) = \frac{1}{2\pi i} \oint f(ix^{AA'}\pi_{A'}, \pi_{A'})\pi_{C'}\, d\pi^{C'}, \tag{4.17}$$

where the contour is chosen so that all singularities of $\hat{f}$ lie outside of it. Let ρ_x denote the restriction of all subsequent twistors to an α-plane, then

$$\frac{\partial}{\partial x^{AA'}}\rho_x f = i\pi_{A'}\rho_x \frac{\partial f}{\partial \omega^A} \tag{4.18}$$

and,

$$\frac{\partial^2 \phi}{\partial x^{AA'} x^{BB'}} = \frac{1}{2\pi i} \oint (-1)\rho_x \frac{\partial^2 f}{\partial \omega^A \partial \omega^B} \pi_{A'}\pi_{B'}\pi_{C'}\, d\pi^{C'}, \tag{4.19}$$

so it follows that $\Box\phi = 0$.

Other massless field equations are solved in a similar way by choosing an appropriate contour integral and the function f. See Ward and Wells for a full description [80].

4.2.3 The Ward Correspondence

In this section we will give details of the twistor correspondence for gauge fields for the Euclidean and ultrahyperbolic space-times. The difference between the two is essentially due to the treatment of the boundary condition at infinity. S^4 is a natural one-point compactification of $\mathbb{E}^4$. So solutions of all integrable equations on $\mathbb{E}^4$ can be extended smoothly across infinity to solutions in S^4. The points at infinity in $\tilde{M}$ form a null hypersurface and it is not always possible to extend solutions on $\mathbb{R}^{2+2}$

smoothly across this surface. For example, the solutions of Maxwell's equations do not have this property.

The central idea behind the twistor correspondence for gauge fields is Ward's theorem which relates solutions of the anti-self-dual Yang-Mills equations (section 1.2.1) to holomorphic vector bundles over $\mathbb{CP}^3$ [82].

Theorem (Ward 1977) 1 *There is a one-to-one correspondence between:*
(a) anti-self-dual $SU(2)$−gauge fields on S^4 up to gauge equivalence and
(b) inequivalent 2-dimensional algebraic vector bundles E over $\mathbb{CP}^3$ such that
(i) E has a symplectic structure, and
(ii) $E|_{\hat{x}}$ is trivial.

The proof for this theorem can be found in [80].

Remarks

- The bundle E does not have a connection. The information about the Yang-Mills connection is coded into its complex structure.
- The anti-holomorphic involution $\sigma : \mathbb{CP}^3 \to \mathbb{CP}^3$ given by (4.15) induces a symplectic structure on E as $\sigma^2 = -1$.
- Here $\hat{x}$ is the fibre over the compactified space S^4 and we require $E|_{\hat{x}}$ is trivial for all $x \in S^4$. Since the space S^4 is compact one can use Serre's theorem to construct bundles with these properties.

It turns out that one can consider the Penrose-Ward transform for the $(2,2)$ split-signature space-times by considering a non-Hausdorff doubling of $\mathbb{CP}^3$ over the open sets of the two copies of $\mathbb{RP}^3$ [83]. This is effectively the second requirement in Mason's theorem in [83]. We will denote a holomorphic bundle over this space by $\tilde{E}$.

We now give the procedure used to extract the Yang-Mills potentials from the holomorphic vector bundle $\tilde{E}$. Following Corrigan *et al* [84], let U and $\hat{U}$ be an open cover for $\mathbb{CP}^3$, which has homogeneous coordinates $Z^\alpha = (Z^0, Z^1, Z^2, Z^3)$ and inhomogeneous coordinate ζ. The sets U and $\hat{U}$ are defined as

$$U := \{\zeta : |\zeta| < 2\}, \tag{4.20}$$
$$\hat{U} := \{\zeta : |\zeta| > 1\},$$

and $U \cap \hat{U}$ is the annular region $1 < |\zeta| < 2$. We see from (4.15) that σ is a one-to-one map of U to $\hat{U}$. Now let η and $\hat{\eta}$ be column vectors on U and $\hat{U}$. They can be considered to be the components of the fibres over U and $\hat{U}$ respectively. On $U \cap \hat{U}$ they are patched by $\eta = F(Z^\alpha)\hat{\eta}$, where $F(Z^\alpha)$ is a (2×2)-matrix defined on $U \cap \hat{U}$ and satisfying

$$\begin{aligned} F(Z)^\dagger &= F(Z), \\ \det F(Z) &= 1. \end{aligned} \tag{4.21}$$

One class of matrices $F(Z^\alpha)$ which satisfy the above condition are the upper-triangular matrices,

$$\tilde{F}(Z^\alpha) = \begin{pmatrix} \zeta^k e^f & \Gamma(x,\zeta) \\ 0 & \zeta^{-k} e^{-f} \end{pmatrix},$$

where k is a positive integer, $\Gamma(x,\zeta) = \Gamma^\dagger(x,\zeta^{-1})$, and $f(Z^\alpha)$ is real. This class of matrices is known as the Atiyah-Ward ansatze and is particularly useful for constructing soliton solutions. The matrix $\tilde{F}(Z^\alpha)$ does not satisfy (4.21) for any Γ and f but it is always equivalent to a matrix which does. That is, there is a (2×2)-matrix R which is holomorphic on $\hat{U}$ such that $F = \tilde{F}R$ satisfies (4.21). The existence of R is not guaranteed. However, if we take f to be real and $\Gamma = (e^f + e^{-f})/Q$, where $Q = P/(Z^2 Z^3)$ and $P(Z^\alpha)$ is a real homogeneous polynomial of degree $2k$, then the matrix R given by

$$R(Z^\alpha) = \begin{pmatrix} 0 & -1 \\ 1 & \zeta^k Q \end{pmatrix},$$

does yield a $F(Z^\alpha)$ with properties (4.21). Note that $\bar{\zeta} = \zeta^{-1}$.

Given the patching matrix F on the holomorphic vector bundle $\tilde{E}$, one can now extract the information about the anti-self-dual gauge field that is coded into $\tilde{E}$.

The crucial step in this procedure is the splitting of F restricted to α-planes, into two matrices H and $\hat{H}$,

$$F(ix^{AA'}\pi_{A'}, \pi_{A'}) = \hat{H}H^{-1}, \tag{4.22}$$

where $H(x,\zeta)$ is a (2×2)-matrix holomorphic on $\mathbb{R}^{2+2}\times U$ and $\hat{H}$ is holomorphic on $\mathbb{R}^{2+2}\times \hat{U}$. If such a splitting exists (which it must if the triviality condition on $\tilde{E}$ is satisfied) then the gauge potentials may be calculated using the following argument: Let $D_A = (\partial_{A0'} - \zeta\partial_{A1'})$ be a differential operator such that $D_A(x^{AA'}\pi_{A'}) = 0$, where $\partial_{AA'} = \partial/\partial x^{AA'}$. Then we have

$$\hat{H}^{-1}D_A\hat{H} = H^{-1}D_AH. \tag{4.23}$$

Now, since the left hand side of equation (4.23) is holomorphic on $\mathbb{R}^{2+2}\times\hat{U}$ and the right hand side on $\mathbb{R}^{2+2}\times U$, then by using a generalised form of Liouville's theorem we have that both sides are holomorphic on $\mathbb{R}^{2+2}\times\mathbb{CP}^1$ and linear in ζ. By appropriately defining the functions $A_{BB'}$ we have

$$\hat{H}^{-1}D_B\hat{H} = A_{B0'} - \zeta A_{B1'}, \tag{4.24}$$

where $A_{BB'}$ are the su(2) gauge potentials. The first step in the splitting of F multiplicatively is to split f additively,

$$f = \hat{h} - h, \tag{4.25}$$

where $\hat{h}$ and h are holomorphic on $\mathbb{R}^{2+2}\times\hat{U}$ and $\mathbb{R}^{2+2}\times U$ respectively. The functions $\hat{h}$ and h can be found using complex analysis to be given by the contour integrals

$$h = \frac{1}{2\pi}i\oint \frac{f(x^{AA'}\pi_{A'},\pi_{A'})}{(\zeta-\zeta')}\,d\zeta, \tag{4.26}$$

$$\hat{h} = \frac{1}{2\pi}i\oint \frac{f(x^{AA'}\pi_{A'},\pi_{A'})}{(\zeta-\zeta')}\,d\zeta, \tag{4.27}$$

where the contour in the first equation is taken over $|\zeta|<2$ and in the second over $|\zeta|>1$. The explicit expressions for the gauge potential $A_{BB'}$ can now be calculated in a particular gauge known as Yang's R-gauge. The following theorem gives the procedure [80].

Theorem 2 *Let B_a be a potential for a $GL(n,C)$ gauge field and let $\{\Delta_r\}_{r=1-k}^{k-1}$ be a set of fields satisfying*

$$\begin{aligned} &if \quad k=1: \quad (\nabla_a + 2B_a)(\nabla^a + 2B^a) &&= 0, \\ &if \quad k>1: \quad (\nabla_{A0'} + 2B_{A0'})\Delta_r &&= (\nabla_{A1'} + 2B_{A1'})\Delta_{r+1}, \\ &\qquad where \quad 1-k \leq r \leq k-2. \end{aligned} \tag{4.28}$$

where Δ_r and B_a are holomorphic on a region $U \subset \mathbb{CM}$. Let M be the $k \times k$ matrix

$$\begin{pmatrix} \Delta_{1-k} & \cdots & \Delta_0 \\ \vdots & \ddots & \vdots \\ \Delta_0 & \cdots & \Delta_{k-1} \end{pmatrix}.$$

Also let $E = (M^{-1})_{11}$, $F = (M^{-1})_{1k}$ and $G = (M^{-1})_{k1}$, then the SU(2) valued gauge potentials are given by

$$\Phi_{A0'} = \frac{1}{2F} \begin{pmatrix} \eth_{A0'}F & 0 \\ -2\eth_{A0'}G & -\eth_{A0'}F \end{pmatrix},$$

$$\Phi_{A1'} = \frac{1}{2F} \begin{pmatrix} -\eth_{A1'}F & -2\eth_{A1'}E \\ 0 & \eth_{A1'}F \end{pmatrix},$$

where $\eth_a = \nabla_a - 2B_a$.

The Maxwell potential B_a is determined by the relationship

$$\pi_{A'} B_{AA'} = \pi^{A'} \nabla_{AA'} h = \pi^{A'} \nabla_{AA'} \hat{h}. \tag{4.29}$$

Note that if $f = 0$ then $B_a = 0$. The fields Δ_r are given by [84]

$$\Delta_r = \frac{1}{2\pi i} \oint_{|\zeta|=1} \rho(\zeta) \zeta^{1-r} \, d\zeta, \tag{4.30}$$

where $\rho = \Gamma e^{-h-\hat{h}}$. Δ_r are the components of a free massless field of helicity $k-1$ coupled to the Maxwell field. So for instance for $k=2$, $\Delta_{-1}, \Delta_0, \Delta_1$, are components of the $\phi_{AA'}$, *i.e.* $\Delta_0 = \phi_{00'}, \Delta_1 = \phi_{01'}, \Delta_{-1} = \phi_{10'}$, and $\phi_{AA'}$ satisfies

$$(\nabla^{AA'} + 2B^{AA'})\phi_{AB'} = 0. \tag{4.31}$$

4.3 (2 + 1)-Dimensional De Sitter Space-Time

(2 + 1)-dimensional de Sitter space-time M is the manifold $\mathbb{R} \times S^2$ which has the metric [85]

$$ds^2 = \cosh^2 T(d\theta^2 + \sin^2\theta d\varphi^2) - dT^2, \tag{4.32}$$

where T is a time coordinate and (θ, φ) are polar coordinates on the spatial sphere. It is a space of constant curvature, and scalar curvature $R = 6$.

In view of Mason's theorem in [83], it is useful to regard M as being a reduction of a (2 + 2)-dimensional space, namely one conformal to $\bar{M} = S^2 \times S^2$. The space $\bar{M}$ has the metric

$$ds^2_{\bar{M}} = d\Omega_1^2 - d\Omega_2^2, \tag{4.33}$$

where $d\Omega_1^2$ and $d\Omega_2^2$ are the metrics on the two spheres. If we use polar coordinates (θ, φ) on the first sphere and $(\tilde{\theta}, \tilde{\varphi})$ on the second, then the metric is given by

$$ds^2_{\bar{M}} = (d\theta^2 + \sin^2\theta d\varphi^2) - (d\tilde{\theta}^2 + \sin^2\tilde{\theta} d\tilde{\varphi}^2). \tag{4.34}$$

To recover the ultrahyperbolic space-time from $\bar{M}$ we use the complex quantities u and v defined by,

$$u = \frac{(\sin\theta)e^{-i\varphi}}{(\cos\theta + \cos\tilde{\theta})}, \qquad v = \frac{(\sin\tilde{\theta})e^{i\tilde{\phi}}}{(\cos\theta + \cos\tilde{\theta})} \tag{4.35}$$

and in the region where $\cos\theta + \cos\tilde{\theta}$ is positive, so

$$du\, d\bar{u} - dv\, d\bar{v} = \frac{2ds^2_{\bar{M}}}{(\cos\theta + \cos\tilde{\theta})}, \tag{4.36}$$

which is the metric for $\mathbb{R}^{2+2}$. We get the reduced de Sitter space-time from $\bar{M}$ by factoring out by the Killing vector $\partial/\partial\tilde{\varphi}$, *i.e.* by a rotation of the second sphere. First we remove $\tilde{\theta} = 0$ and $\tilde{\theta} = \pi$, which are the fixed points of the rotation. On the complement of these fixed points, we can write

$$ds^2_{\bar{M}} = \sin^2\tilde{\theta}(\mathrm{cosec}^2\tilde{\theta}(d\theta^2 + \sin^2\theta d\varphi^2 - d\tilde{\theta}^2) - d\tilde{\varphi}^2). \tag{4.37}$$

So $\bar{M} - \{\tilde{\theta} = 0 \cup \tilde{\theta} = \pi\}$ is conformal to the product of S^1 and a space with topology $\mathbb{R} \times S^2$ and metric

$$ds^2 = \mathrm{cosec}^2\tilde{\theta}(d\theta^2 + \sin^2\theta d\varphi^2 - d\tilde{\theta}^2). \tag{4.38}$$

This is the $(2+1)$-dimensional de Sitter space-time and the metric is essentially equation (4.3) once we have identified $\cos\tilde{\theta} = \tanh T$.

Let us now consider the reduced $(2+1)$-dimensional space obtained directly from $\mathbb{R}^{2+2}$. This space is obtained from the conformal equivalence

$$\mathbb{R}^{2+2} - \mathbb{R}^2 \sim S^1 \times H^3,$$

where the space $H^3 = \{(x, y, t) : t > 0\}$ is a $(2+1)$-dimensional space-time known as the Poincare space-time (or the $(2+1)$-dimensional steady state universe [85]). The $\mathbb{R}^2$ that is being factored out is the plane $t = 0$. The space-time H^3 has the metric

$$ds^2 = \frac{dx^2 + dy^2 - dt^2}{t^2}, \tag{4.39}$$

and it has constant curvature and scalar curvature $R = 6$. It is incomplete and extends to the de Sitter space-time. It is in fact "half" of the de Sitter space-time. Figure 4.1 shows the Penrose diagram for the two cases.

The completion of H^3 is obtained by setting

$$\begin{aligned} t^{-1} &= \cosh T \cos\theta + \sinh T, \\ xt^{-1} &= \cosh T \sin\theta \cos\varphi, \\ yt^{-1} &= \cosh T \sin\theta \sin\varphi, \end{aligned} \tag{4.40}$$

where (T, θ, φ) are the coordinates on $\mathbb{R} \times S^2$. In the new coordinates H^3 is given by $H^3 = \{(T, \theta, \varphi) : \cos\theta > -\tanh T\}$. The intersection of a space-like surface $\theta = 0$ (a two sphere) in $\mathbb{R} \times S^2$ with H^3 is the southern hemisphere $0 \leq \theta \leq \pi/2$. This hemisphere corresponds to a hyperboloid in Poincare space-time given by $t = +\sqrt{1 + x^2 + y^2}$, and the circle at infinity on this hyperboloid corresponds to the equator $\theta = \pi/2$.

To keep things simple, we will denote the coordinates on the submanifold H^3 by u and v as well, and in this case they are given by $u = (x + iy)$ and $v = te^{i\alpha}$; (t, x, y, α) are the coordinates on $\mathbb{R}^{2+2}$.

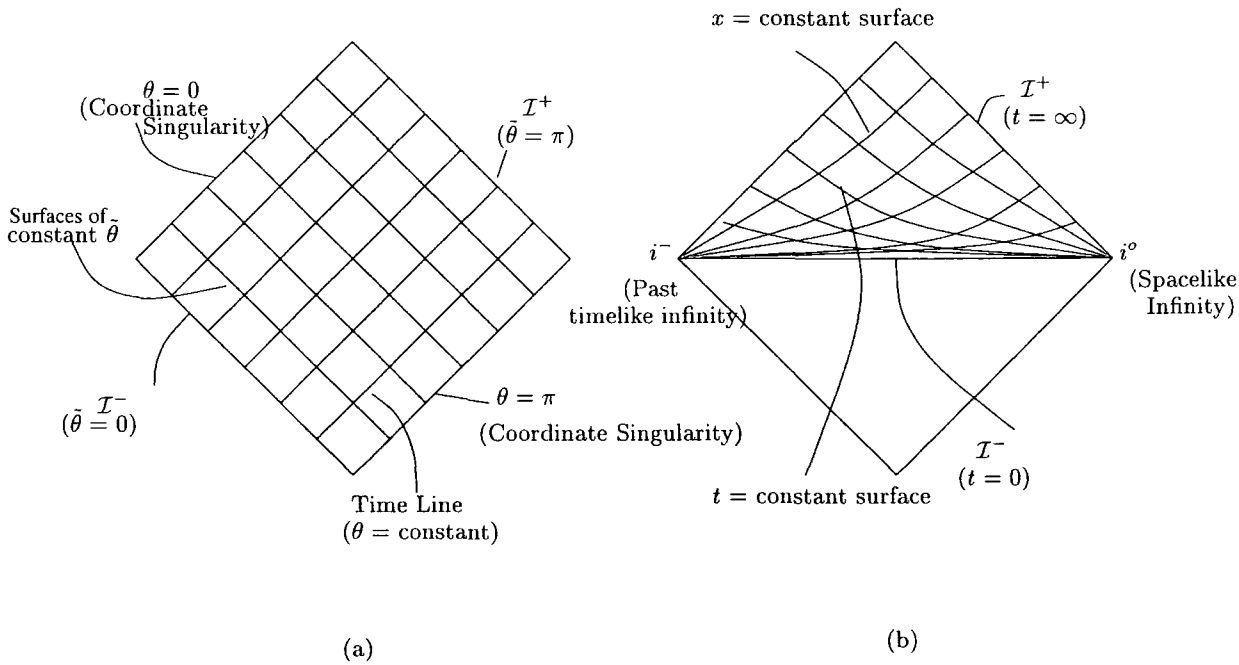

Figure 4.1: Penrose diagram for (a) de Sitter space-time and (b) Poincare space-time.

For both the de Sitter space-time and H^3, the twistor correspondence that relates the space-time to the twistor manifold is given by

$$\omega(\zeta) = \frac{v(\zeta - u + \bar{v})}{\zeta - u}, \tag{4.41}$$

where ω and ζ are the coordinates on the twistor space $\mathbb{CP}^3 \times \mathbb{CP}^3$.

In the following sections we will consider conformally-invariant integrable equations on the de Sitter space-time. We will find that there are certain solutions which are smooth only on the submanifold H^3, *i.e.,* they are nonsingular provided $\cos\theta > -\tanh T$.

4.4 Integrable Equations on De Sitter Space-Time

4.4.1 Conformally-Invariant Wave-Equation

In this section we will consider certain integrable equation on the de Sitter space-time M. The equations we will consider are all conformally invariant and completely

integrable. The idea is to study the solutions which are smooth and independent of $\tilde{\varphi}$. The simplest conformally-invariant equation on $\bar{M}$ is the conformally-invariant wave equation. In view of the product form of the metric and the absence of scalar curvature, this has the form

$$\Delta\chi - \tilde{\Delta}\chi = 0, \tag{4.42}$$

where Δ and $\tilde{\Delta}$ are the Laplacians on the two spheres. The $\tilde{\varphi}$-independent solutions of (4.42) correspond to solutions of the conformally-invariant wave equation on M, namely

$$g^{\mu\nu}\nabla_\mu\nabla_\nu\Psi - \Psi = 0, \tag{4.43}$$

where χ and Ψ are related by $\Psi = (\operatorname{sech} T)\chi$. Using coordinates we get

$$\operatorname{sech}^2 T[-((\cosh^2 T)\Psi_T)_T + (\operatorname{cosec}\theta)(\sin\theta\Psi_\theta)_\theta + (\operatorname{cosec}^2\theta)\Psi_{\varphi\varphi}] = \Psi. \tag{4.44}$$

Solutions of equation (4.44) can be obtained by separating variables or using twistor methods [86]. To use the latter method we need to solve the following contour integral,

$$\Psi = \frac{1}{2\pi i}\oint f(iX^{AA'}\pi_{A'}, \pi_{A'})\pi_{C'}\, d\pi^{C'} \tag{4.45}$$

where f is homogeneous of degree 2 in Z^α and is independent of $\tilde{\varphi}$. One can then use, for instance, the procedure described in Penrose and Rindler [87] to calculate the standard spherical harmonics.

The simplest solution is given by $\chi = 1$ and this leads to $\Psi = \operatorname{sech} T$, *i.e.* a solution that is spatially constant. The $l = 1$ spherical harmonics give the solutions $\Psi = \operatorname{sech} T \tanh T \cos\theta$ and $\Psi = \operatorname{sech} T \tanh T \sin\theta\cos\varphi$. The $l = 2$ spherical harmonics give the solutions $\Psi = \operatorname{sech} T \tanh T(2\cos^2\theta - \sin^2\theta)$, $\Psi = \operatorname{sech} T \tanh T \cos\theta \sin\theta\cos\varphi$, and $\Psi = \operatorname{sech} T \tanh T \sin^2\theta\cos 2\varphi$, and so forth.

4.4.2 Self-Dual Yang-Mills Equations

The self-dual Yang-Mills equations on the manifold $S^2 \times S^2$ are given by

$$\begin{aligned} F_{\theta\phi} &= (\sin\theta/\sin\tilde{\theta})F_{\tilde{\theta}\tilde{\phi}}, \\ F_{\phi\tilde{\theta}} &= (\sin\theta/\sin\tilde{\theta})F_{\theta\tilde{\phi}}, \\ F_{\theta\tilde{\theta}} &= (1/\sin\theta\sin\tilde{\theta})F_{\phi\tilde{\phi}}. \end{aligned} \tag{4.46}$$

When we reduce to the $(2+1)$-dimensional space-time M, the self-dual Yang-Mills field becomes a Yang-Mills-Higgs system (Φ, A_μ). The reduction is carried out by the requirement that the self-dual potential be invariant under a conformal symmetry, in this case under the rotation of the second sphere, $\partial/\partial\tilde{\varphi}$. The reduced system satisfies the Bogomolny-type equations

$$D_\alpha\Phi = \frac{1}{2}\eta_{\alpha\beta\gamma}F^{\beta\gamma}. \tag{4.47}$$

The Higgs field Φ takes values in the Lie algebra of the gauge group G. It can be identified with the $\tilde{\varphi}$-component of the gauge field $A_{\tilde{\varphi}}$. The remaining three components of A_μ become a gauge potential on the $(2+1)$-dimensional space M. As usual, D_α denotes the covariant derivative $D_\alpha\Phi = \partial_\alpha\Phi + [A_\alpha, \Phi]$, and $\eta_{\alpha\beta\gamma} = -[\det(g_{\mu\nu})]^{-1/2}\epsilon_{\alpha\beta\gamma}$ is the volume 3-form on M. In terms of the polar coordinates $(\theta, \tilde{\theta}, \varphi)$, eqn (4.47) is given by

$$\begin{aligned} D_{\tilde{\theta}}\Phi &= (\sin\tilde{\theta}/\sin\theta)F_{\theta\varphi}, \\ D_\theta\Phi &= (\sin\tilde{\theta}/\sin\theta)F_{\tilde{\theta}\varphi}, \\ D_\varphi\Phi &= (\sin\tilde{\theta}\sin\theta)F_{\theta\tilde{\theta}}. \end{aligned} \tag{4.48}$$

On the space-time H^3 (4.47) is

$$\begin{aligned} D_x\Phi &= t^{-1}F_{yt} \\ D_y\Phi &= t^{-1}F_{tx} \\ D_t\Phi &= -t^{-1}F_{xy}. \end{aligned} \tag{4.49}$$

Equation (4.47) is integrable with the Lax pair (in terms of (x, y, t)) given by

$$\begin{aligned} L &= 2D_t + (\zeta - u)t^{-1}D_u \\ M &= D_{\bar{u}} - 2(\zeta - u)t^{-1}D_t, \end{aligned} \tag{4.50}$$

where $u = x + iy$.

In the remaining sections of this chapter we will construct solutions of (4.48) and (4.49).

4.5 Solutions of SDYM Equations

4.5.1 U(1) Examples

We start with the abelian (linear) case G=U(1). The equations of (4.47) reduce to

$$\partial_\alpha \Phi = \eta_{\alpha\beta\gamma} F^{\beta\gamma}, \tag{4.51}$$

where $F_{\mu\nu} = \partial_\mu A_\nu - \partial_\nu A_\mu$. This case is related to, but different from, that of the wave equation (4.43) discussed in the section (4.4.1). Indeed, from (4.43) it follows immediately that $g^{\mu\nu}\nabla_\mu \nabla_\nu \Phi = 0$. Another feature is that there can be non-trivial topology: the space in this case is a sphere S^2, and U(1) gauge fields over S^2 are classified topologically by an integer

$$k = \frac{-i}{2\pi} \int_\Sigma F_{\mu\nu} dx^\mu \wedge dx^\nu, \tag{4.52}$$

where Σ is a space section (space-like surface with topology S^2).

We shall construct various U(1) examples of solutions to the Yang-Mills-Higgs system using the twistor construction outlined earlier. In this case the twistor matrix is a (1×1)-matrix, *i.e.* just a smooth real function (patching function) $f(Z)$ on the twistor space. To get solutions which are independent of $\tilde{\varphi}$, f needs to be invariant under the action of

$$K = Z^3 \frac{\partial}{\partial Z^3} - Z^2 \frac{\partial}{\partial Z^2} + Z^1 \frac{\partial}{\partial Z^1} - Z^0 \frac{\partial}{\partial Z^0}. \tag{4.53}$$

For instance, the conditions of smoothness, K-invariance and homogeneity of degree zero in Z^α are met by the function $Q = (Z^0 Z^1 + Z^2 Z^3)/(Z^2 Z^3)$. Using the correspondence (4.3 and 4.4) and with $z = u$ and $\bar{w} = v$ (u and v are given by either (4.35) or in Cartesian coordinates $u = x + iy$ and $v = te^{i\alpha}$), we have $Q = a\zeta + b + c\zeta^{-1}$

where

$$\begin{aligned} a &= u\bar{v}, \\ b &= |u|^2 + |v|^2 + 1, \\ c &= \bar{u}v. \end{aligned} \tag{4.54}$$

Example 1 Let us take $f = Q^k$, where $k \in \mathbb{Z}$. Consider first the case $k \in \mathbb{Z}^+$. The splitting of $f = \hat{h} - h$ (4.25) gives

$$\begin{aligned} \hat{h} &= G_1(\zeta^{-1}) + H, \\ h &= -(G_2(\zeta) + H), \end{aligned} \tag{4.55}$$

where G_1 and G_2 are functions which are holomorphic on $\hat{U}$ and U respectively. H is a function of the space-time coordinates only and is given by

$$H = \frac{1}{2} \sum_{\{l \in \mathbb{Z}^+ : k-2l \geq 0\}} \binom{k-l}{l} \binom{k}{l} a^l c^l b^{k-2l},$$

where $\binom{n}{r}$ is the binomial coefficient. The gauge potentials can now be readily calculated using the procedure given in section (4.2.3). For instance, the Higgs field is given by

$$\Phi = i(v\,\partial_v \hat{h}(\infty) - \bar{v}\,\partial_{\bar{v}} h(0)). \tag{4.56}$$

Substituting (4.55) gives

$$\Phi = i \sum_{\{l \in \mathbb{Z}^+ : k-2l \geq 0\}} \left[\binom{k-l}{l} \binom{k}{l} (l a^l c^l b^{k-2l} + (k-2l) a^l c^l b^{k-2l-1} |v|^2) \right].$$

This gives a smooth Maxwell-Higgs field on the Poincare space-time. Clearly it is singular on M due to the denominator in u and v of (4.35). Note that the $k = 1$ case is spatially homogeneous.

Consider now the case when $k \in \mathbb{Z}^-$. Before looking at the general case let us consider the $k = -1$ case; f can be split into

$$\begin{aligned} \hat{h} &= \frac{\zeta_1/p}{\zeta - \zeta_1}, \\ h &= \frac{\zeta_2/p}{\zeta - \zeta_2}, \end{aligned} \tag{4.57}$$

where $\zeta_1 = (b-p)/2a$, $\zeta_2 = -(b+p)/2$ and $p = \sqrt{b^2 - 4ac}$. This yields the following gauge potentials on the de Sitter space-time,

$$\begin{aligned} \Phi &= \frac{1}{4} i(\cos^2\tilde{\theta} - 1)\cos\theta, \\ A_\varphi &= -\frac{1}{4} i(\cos^2\theta - 1)\cos\tilde{\theta}, \\ A_\theta &= -\frac{1}{4} i \sin\theta, \\ A_{\tilde{\theta}} &= -\frac{1}{4} i \sin\tilde{\theta}. \end{aligned} \tag{4.58}$$

So for $f = Q^{-k}$ we have,

$$f = \left(\frac{\zeta_1/p}{\zeta - \zeta_1}\right)^k + \sum_{l=1}^{k-1} (-1)^l \binom{k}{l} \frac{\zeta_1^l \zeta_2^{k-l}/p^k}{(\zeta - \zeta_1)^l (\zeta - \zeta_2)^{k-l}} + (-1)^k \left(\frac{\zeta_2/p}{\zeta - \zeta_2}\right)^k.$$

For k even we take $\hat{h}$ to be the sum of the first and the third terms and h to be negative of the second term. For k odd we take $\hat{h}$ to be the sum of the first and one-half of the second term and h to be the sum of the third and one-half of the second term. This yields the following gauge potentials on the de Sitter space-time,

$$\begin{aligned} \Phi &= -id(\cos\theta + \cos\tilde{\theta})^{k-1} \sin^2\tilde{\theta}\cos\theta, \\ A_\varphi &= id(\cos\theta + \cos\tilde{\theta})^{k-1} \sin^2\theta\cos\tilde{\theta}, \\ A_\theta &= -id(\cos\theta + \cos\tilde{\theta})^{k-1} \sin\theta, \\ A_{\tilde{\theta}} &= -id(\cos\theta + \cos\tilde{\theta})^{k-1} \sin\tilde{\theta}, \end{aligned} \tag{4.59}$$

where d is given by

$$d = \begin{cases} k/2^k & \text{for } k \text{ even} \\ k/2^{k+1} & \text{for } k \text{ odd} \end{cases}$$

Figure 4.2 shows the plots of Φ^2 against θ and $\tilde{\theta}$ for $k = -1, -5$ and -10.

Some features worthy of mention are: At $\mathcal{I}^+$ and $\mathcal{I}^-$, the Maxwell-Higgs field is zero. Its maximum value increases as k is increased. The maximum value occurs later in "time" as k is increased. The plots of $(D_{\tilde{\theta}}\Phi)^2$ against $\theta, \tilde{\theta}$ (figure 4.3)) show the variation of the Maxwell-Higgs field with "time" for various k cases.

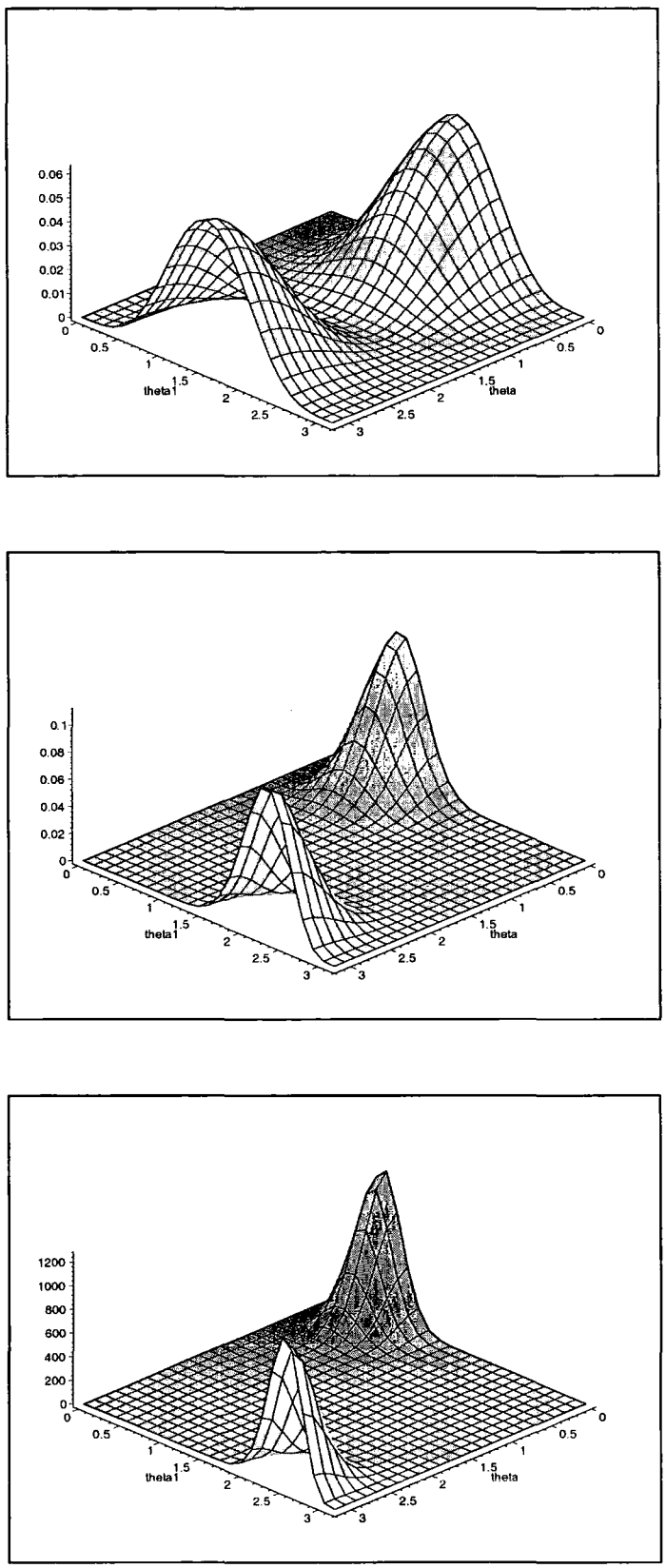

Figure 4.2: A plot of Φ^2 against $\tilde{\theta}$ and θ for $f = Q^{-1}$, Q^{-5} and Q^{-10} respectively.

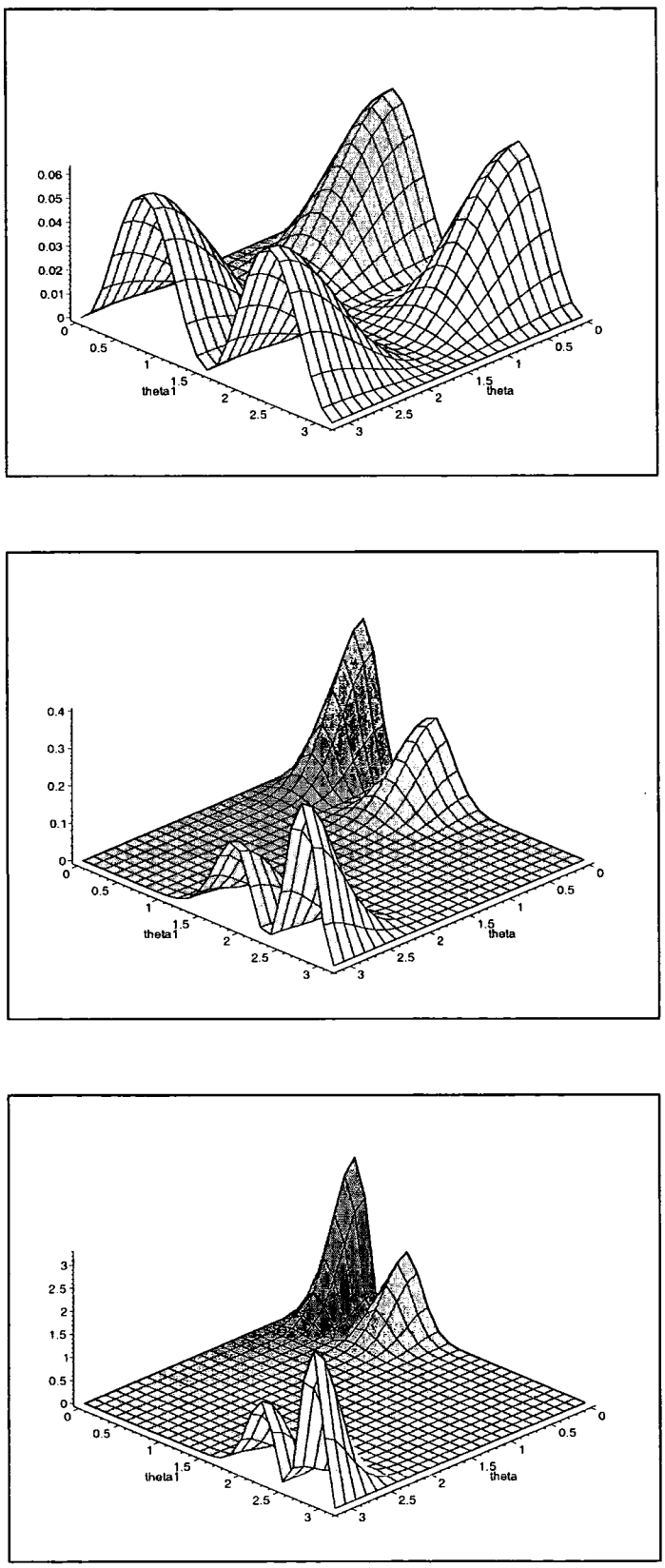

Figure 4.3: A plot of $(D_{\tilde{\theta}}\Phi)^2$ against $\tilde{\theta}$ and θ for $f = Q^{-1}$, Q^{-5} and Q^{-10} respectively.

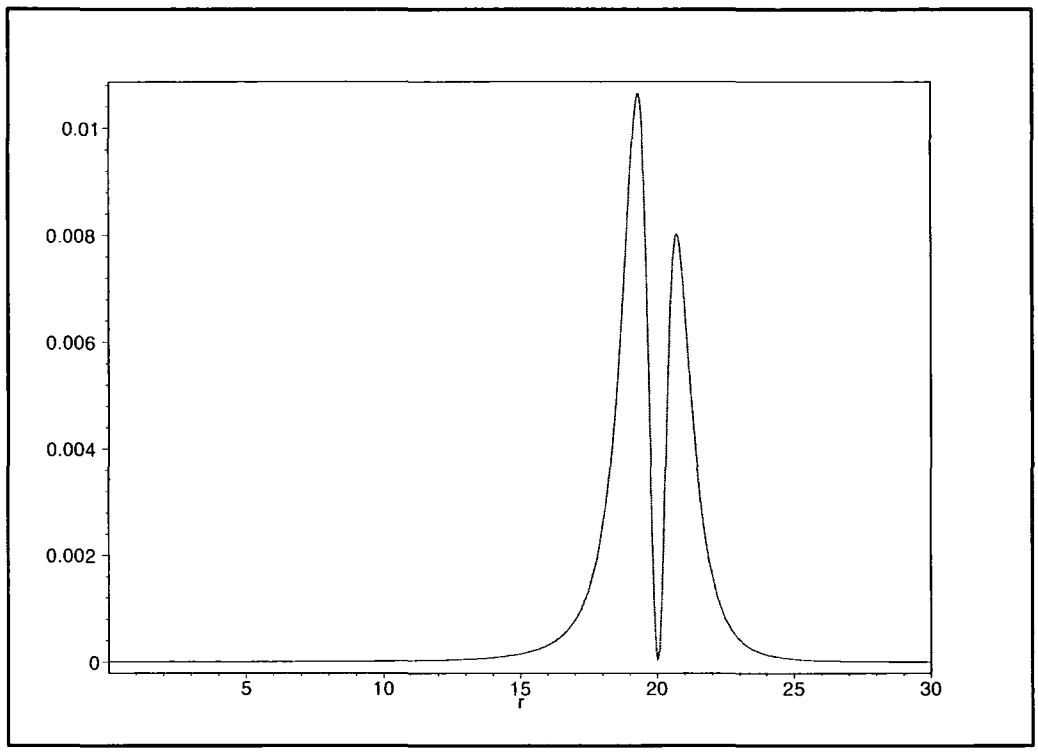

Figure 4.4: A plot of Φ^2 against r for $t = 20$. This is for a solution which is generated by $f = Q^{-1}$.

It is interesting to note that the Maxwell-Higgs field generated by $f = Q^{-k}$ gives an imploding-exploding wave solution on the submanifold H^3. For instance, the $k = -1$ case gives the following gauge fields on the Poincare space-time,

$$\begin{aligned} A_x &= (1 + x^2 + y^2 - t^2)D^{-1}(x - iy), \\ A_y &= iA_x \\ A_t &= -t(x^2 + y^2 - t^2 - 1)D^{-1}, \\ \Phi &= -it^2(x^2 + y^2 - t^2 - 1)D^{-1}. \end{aligned} \tag{4.60}$$

where $D = (1 + x^2 + y^2 + t^2)^2 - 4t^2(x^2 + y^2))^{\frac{3}{2}}$. In figure 4.4 we have plotted Φ^2 against r, where $r = (x^2 + y^2)^{1/2}$ for $t = 20$. The plots for other values of t are similar to 4.4, with the minimum between the two peaks occuring at $r = \sqrt{1 + t^2}$.

Example 2 Consider next the case $f = \log Q^k$. This example gives a topologically

non-trivial solution on the de Sitter space-time. The gauge fields are given by

$$\Phi = \frac{1}{2}ik(\cos\tilde{\theta} - 1), \quad A_\varphi = \frac{1}{2}ik(\cos\theta - 1), \quad A_\theta = 0 = A_{\tilde{\theta}}. \tag{4.61}$$

For smoothness, we require $A_\varphi = 0$ at $\theta = 0, \pi$. So the above gauge potential has a singularity at $\theta = \pi$. But the gauge transformed potential

$$A_\varphi + \exp(-ik\varphi)\partial_\varphi \exp(ik\varphi) = \frac{1}{2}ik(\cos\theta + 1) \tag{4.62}$$

is smooth near $\theta = \pi$. In other words, this Maxwell-Higgs system is smooth throughout the de Sitter space-time. The apparent (Dirac-string) singularities are a consequence of the fact that the gauge field is topologically non-trivial: its magnetic charge equals k. Furthermore, it is spatially-homogeneous: note in particular that Φ depends only on 'time' $\tilde{\theta}$, and that the gauge 2-form (the integrand of (4.52)) is a (time-dependent) multiple of the area element $\sin\theta\, d\theta \wedge d\varphi$.

4.5.2 U(1) Embedding in SU(2)

The case $f = 0$ gives rise to a family of U(1) solutions which are embedded in SU(2) matrices, *i.e.* (2×2) diagonal matrices. The patching matrix $\tilde{F}(Z)$ for the SU(2) case is

$$\tilde{F}(Z^\alpha) = \begin{pmatrix} \zeta^k e^f & \Gamma \\ 0 & \zeta^{-k}e^{-f} \end{pmatrix},$$

where $\Gamma = (e^f + e^{-f})/Q$. Take $f = 0$ and multiply $\tilde{F}$ on the left by a matrix $\hat{K}$ which is holomorphic on $\hat{U}$ and on the right by a matrix K holomorphic on U, where

$$\hat{K} = \begin{pmatrix} \zeta^{-k}Q^k & -2 \\ 1/2 & 0 \end{pmatrix}, \quad K = \begin{pmatrix} 1 & 0 \\ -\zeta^k Q^k/2 & 1 \end{pmatrix}.$$

This gives,

$$F = \begin{pmatrix} Q^k & 0 \\ 0 & Q^{-k} \end{pmatrix},$$

showing that the solutions generated by $f = 0$ are indeed abelian. The gauge potentials for these cases can be calculated using the formulas in theorem 2. For instance, for the $k = 1$ case, the Higgs field is given by

$$\Phi = \frac{i}{2}\begin{pmatrix} -(v\partial_v + \bar{v}\partial_{\bar{v}}) & -2v\partial_u \\ 2\bar{v}\partial_{\bar{u}} & v\partial_v + \bar{v}\partial_{\bar{v}} \end{pmatrix} \log \Delta_0,$$

where Δ_0 is found from (4.30) to be $\Delta_0 = 2p^{-1}$. As it stands, Φ has a superficial dependence on φ (or θ) and it is not abelian. But after a gauge transformation (1.22) using

$$g = \begin{pmatrix} e^{-i\varphi/2} & 0 \\ 0 & e^{i\varphi/2} \end{pmatrix},$$

Φ, and the other three gauge potentials, are independent of ϕ. This gauge applies to solutions with any k. Φ is not abelian since we have calculated it using Yang's R-gauge. There is, of course, a gauge which makes it abelian. The question of regularity of the gauge potentials can be dealt with by considering the determinant of the banded $(k \times k)$ matrix N^k_{rs} [80],

$$N^k_{rs} = \Delta_{r+s-k-1}, \quad r \geq 1, \quad s \leq k.$$

For the gauge potentials to be nonsingular $\det N$ should be nowhere vanishing on the space-time M [80]. In our case this determinant takes the simple form (up to a sign)

$$\det N = 2^k/p^{k^2}, \tag{4.63}$$

which written in de Sitter space-time coordinates is given by

$$\det N = (\cos\theta + \cos\tilde{\theta})^{k^2}/2^{k^2-k}. \tag{4.64}$$

So the matrix N is singular whenever $\theta + \tilde{\theta} = \pi$. Geometrically, this means that the line bundle L_k defined by the patching matrix F, will become nontrivial whenever $\theta + \tilde{\theta} = \pi$, *i.e.* we have a jumping line at $\theta + \tilde{\theta} = \pi$.

On the submanifold H^3,

$$\det N = -2^k((1 + x^2 + y^2 + t^2)^2 - 4(x^2 + y^2)t^2)^{-k^2/2}, \tag{4.65}$$

which is zero only at infinity. So we expect nonsingular solutions on H^3. Some explicit examples are as follows:

$k = 1$: We have $\Delta_0 = 2/p$. The gauge potentials are given by

$$A_x = \begin{pmatrix} -iy(1+x^2+y^2-t^2)g^{-1} & t(-1+x^2+y^2-t^2)g^{-1} \\ t(-1+x^2+y^2-t^2)g^{-1} & iy(1+x^2+y^2-t^2)g^{-1} \end{pmatrix},$$

$$A_y = i\begin{pmatrix} x(1+x^2+y^2-t^2)g^{-1} & -t(-1+x^2+y^2-t^2)g^{-1} \\ t(-1+x^2+y^2-t^2)g^{-1} & -ix(1+x^2+y^2-t^2)g^{-1} \end{pmatrix},$$

$$A_t = \begin{pmatrix} 0 & (x-iy)(1+x^2+y^2-t^2)g^{-1} \\ (x+iy)(1+x^2+y^2-t^2)g^{-1} & 0 \end{pmatrix},$$

$$\Phi = \frac{i}{2}\begin{pmatrix} ((1+x^2+y^2)^2-t^4)g^{-1} & -2t(x-iy)(1+x^2+y^2-t^2)g^{-1} \\ 2t(x+iy)(1+x^2+y^2-t^2)g^{-1} & -((1+x^2+y^2)^2-t^4)g^{-1} \end{pmatrix},$$

so,

$$\text{tr } \Phi^2 = -\frac{1}{2}\frac{g(x,y,t)-2t^2}{g(x,y,t)+2t^2}, \tag{4.66}$$

where $g = 1+2x^2+2y^2+x^4+2x^2y^2-2x^2t^2+y^4-2y^2t^2+t^4$.

$k = 2$: Now the polynomial $Q(Z^\alpha)$ is homogeneous of degree 4. We take $Q = (Z^0Z^1+Z^2Z^3)^2/(Z^2Z^3)^2$, so $\Gamma = 2/[(1-\zeta_1/\zeta)(a\zeta-\zeta_2)]^2$. This leads to

$$\Delta_0 = b/p^3, \quad \Delta_1 = -2c/p^3, \quad \Delta_{-1} = -2a/p^3.$$

Although explicit expressions for the gauge potentials are available, there seems little point in reproducing them here as they are fairly complicated. We will therefore give just the expression of the length of the Higgs field.

$$\begin{aligned} \text{tr } \Phi^2 \;=\; & -1/2\,(1+12\,t^2x^4+4\,t^4x^2+12\,x^4y^2+12\,y^4x^2+24\,t^2y^2+6\,y^4 \\ & +4\,y^6+x^8+4\,x^6+4\,y^6x^2+4\,x^2+4\,y^2+24\,t^2x^2+4\,x^6y^2+6\,y^4x^4 \\ & +y^8+12\,t^2+46\,t^4+60\,t^6+6\,x^4+25\,t^8-42\,t^4x^4+16\,t^6x^2 \\ & +12\,x^2y^2+16\,t^6y^2+4\,t^4y^2+12\,t^2y^4+24\,t^2y^2x^2-42\,t^4y^4-84\,t^4x^2y^2)/ \\ & (1+x^2+y^2+t^2)^2(1+2\,x^2+2\,y^2+2\,t^2+x^4+2\,x^2y^2 \\ & -2\,t^2x^2+y^4-2\,t^2y^2+t^4) \end{aligned} \tag{4.67}$$

4.5.3 Spatially Homogeneous SU(2) Solution

An SU(2) example may be constructed as follows. Temporarily, think of the spatial sphere as the unit sphere in $\mathbb{R}^3$, with coordinates $x^j = (x^1, x^2, x^3)$. Take the Higgs field and gauge potential to have the form

$$\begin{aligned} \Phi &= ig(\tilde{\theta})x^j\sigma_j, \\ A_{\tilde{\theta}} &= 0, \quad \text{(a gauge choice)} \\ A_j &= if(\tilde{\theta})\epsilon_{jkl}x^l\sigma^k. \end{aligned} \tag{4.68}$$

where σ_j denotes the Pauli matrices, and f and g are two scalar functions of $\tilde{\theta}$ only. (The components A_θ and A_φ are obtained from A_j in the usual way.) Substituting (4.69) into (4.48) gives the pair of ordinary differential equations

$$\begin{aligned} g' &= 2f(1-f)\sin\tilde{\theta}, \\ f' &= g(2f-1)/\sin\tilde{\theta}. \end{aligned} \tag{4.69}$$

Eliminating g leaves an equation for f which, after the transformation

$$f(\tilde{\theta}) = \frac{1}{2}(e^{2T}+1)P(T) + \frac{1}{2}, \qquad \tanh T = \cos\tilde{\theta}, \tag{4.70}$$

is

$$P'' = (P')^2/P - 4e^{2T}P^3. \tag{4.71}$$

This is the third Painleve equation P_{III}. In terms of the variable $t = e^T \in (0,\infty)$, it has the more usual form

$$\ddot{P} = (\dot{P})^2/P - \dot{P}/t - 4P^3. \tag{4.72}$$

Solutions of (4.72) therefore determine spatially-homogeneous SU(2) solutions of the Yang-Mills-Higgs-Bogomolny equations (4.48). Note that the gauge invariant quantities are given by

$$-\text{tr}\ \Phi^2 = 2g^2, \tag{4.73}$$

$$D_1\Phi^2 = -\mathbf{tr}(D_{\tilde{\theta}}\Phi)^2 = 2(g'+g)^2. \tag{4.74}$$

We have solved the simultaneous ODE system (4.70) using MATHEMATICA and plotted the two gauge-invariant quantities (4.73) and (4.74) for various boundary conditions $f(\pi/2)$ and $g(\pi/2)$. Some results are plotted in figures 4.5- 4.10.

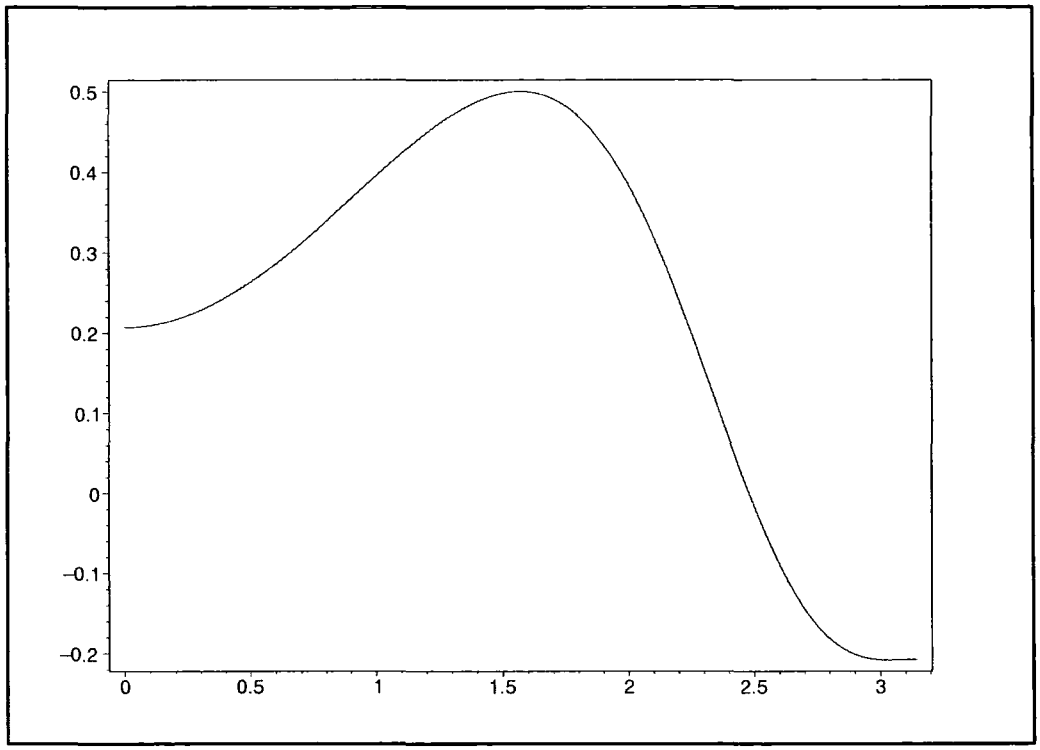

Figure 4.5: A plot of $-\mathbf{tr}\Phi^2$ against 'time' $\tilde{\theta}$ for $f(\pi/2) = 0, g(\pi/2) = 1/2$

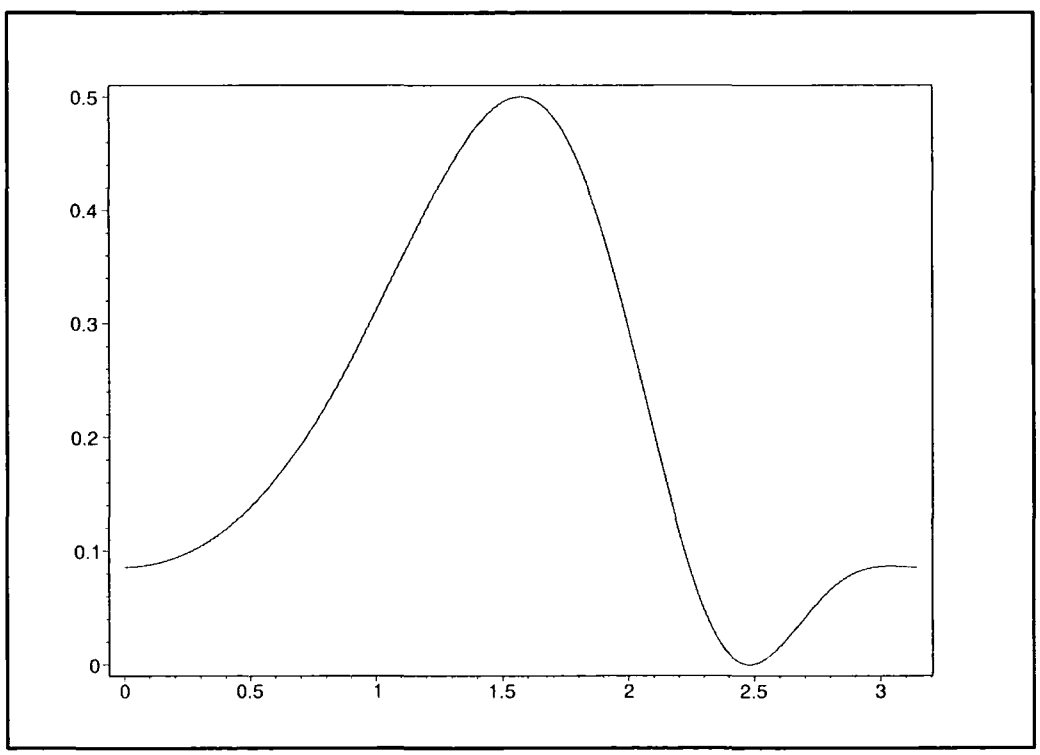

Figure 4.6: A plot of $-\mathbf{tr}(D_{\tilde{\theta}}\Phi)^2$ against $\tilde{\theta}$ for $f(\pi/2) = 0, g(\pi/2) = 1/2$

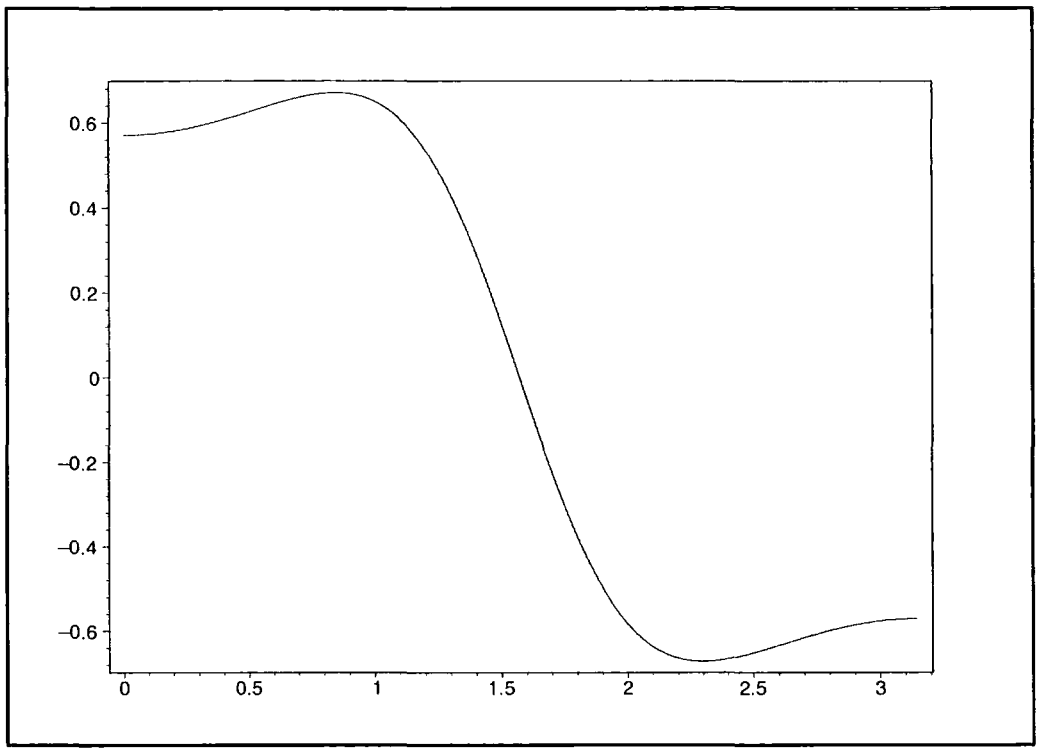

Figure 4.7: A plot of $-\mathbf{tr}\Phi^2$ against $\tilde{\theta}$ for $f(\pi/2) = \pi/2, g(\pi/2) = 0$

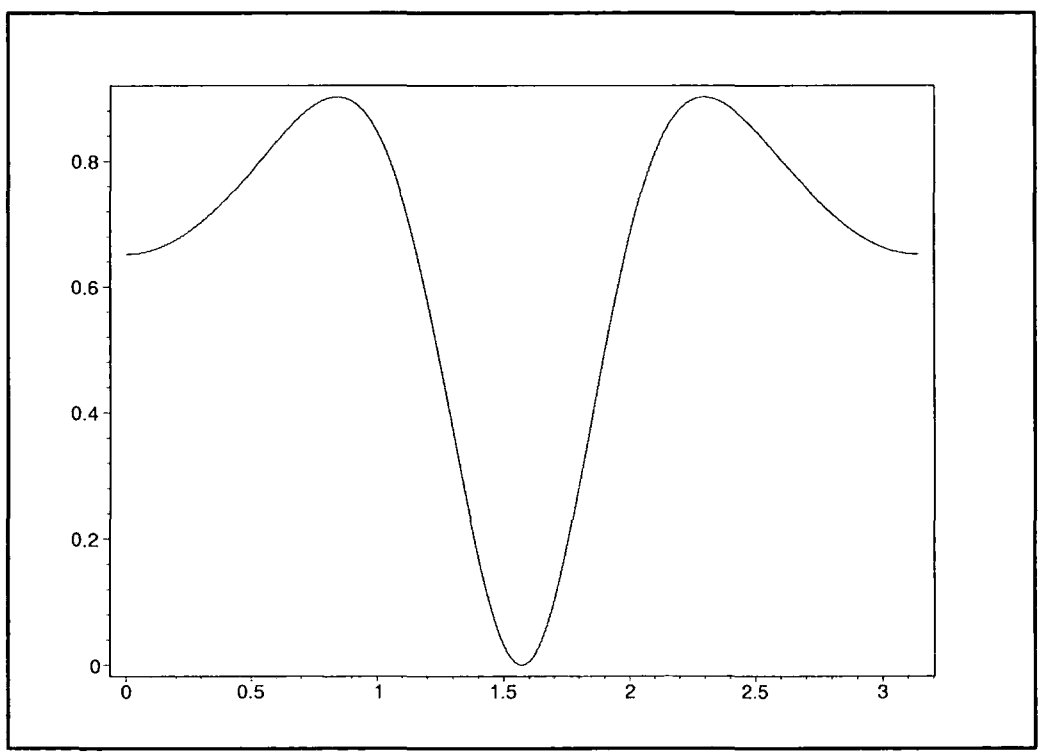

Figure 4.8: A plot of $-\mathbf{tr}(D_{\tilde{\theta}}\Phi)^2$ against $\tilde{\theta}$ for $f(\pi/2) = \pi/2, g(\pi/2) = 0$

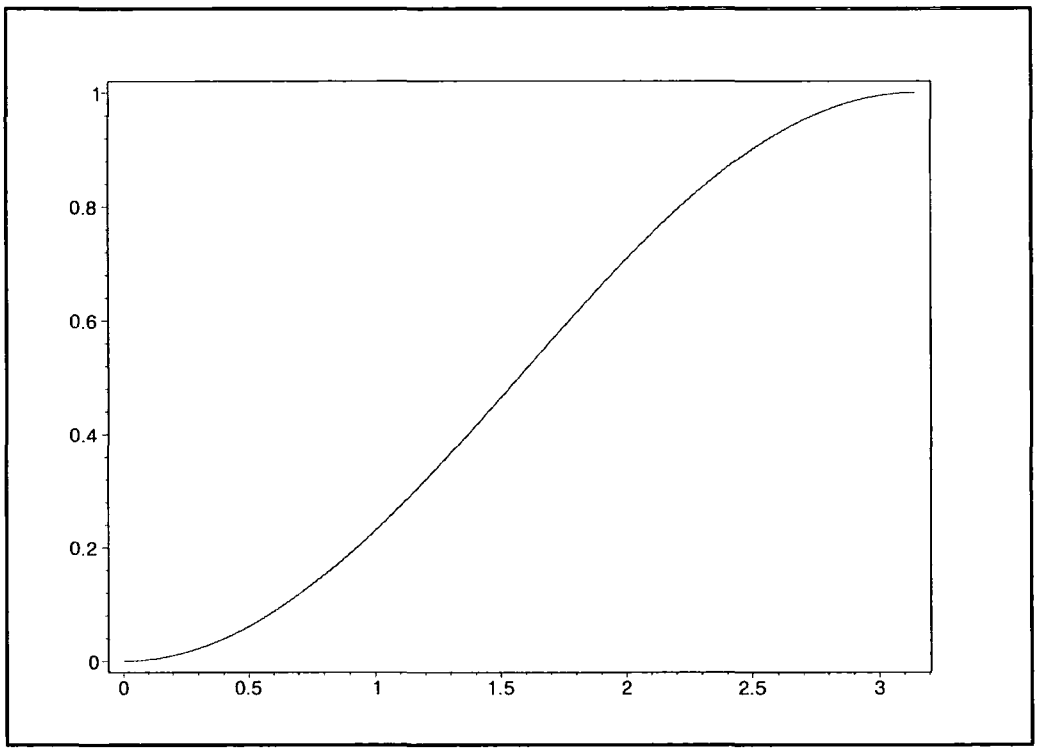

Figure 4.9: A plot of $-\mathbf{tr}\Phi^2$ against $\tilde{\theta}$ for $f(\pi/2) = 1/2, g(\pi/2) = 1/2$

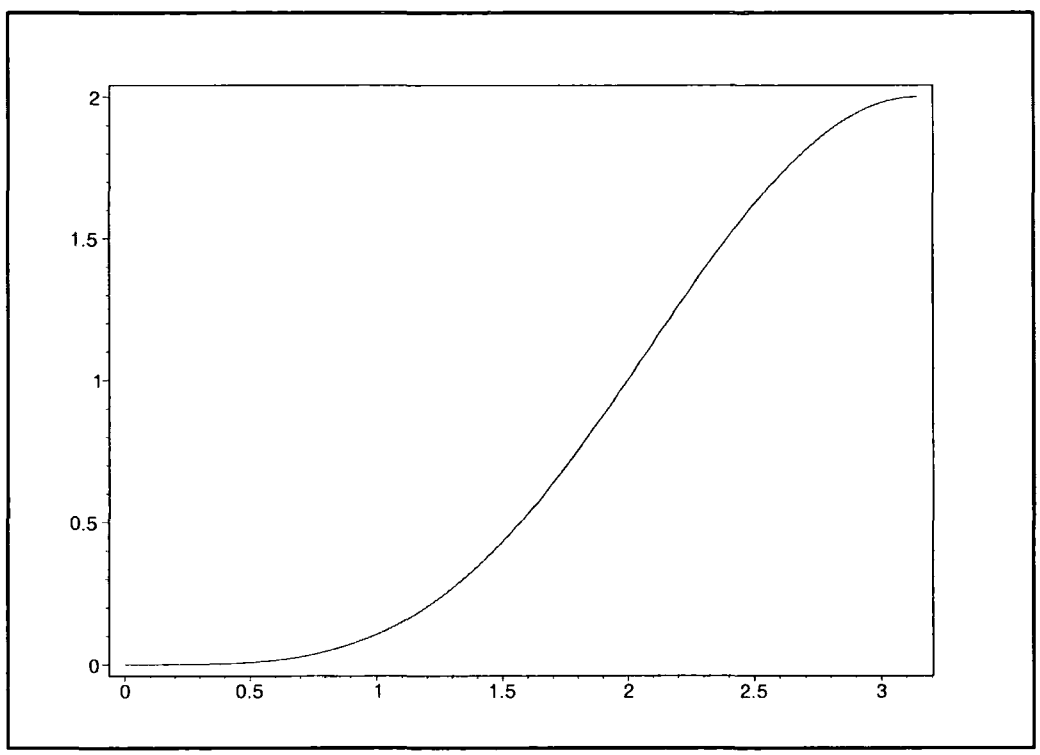

Figure 4.10: A plot of $-\mathbf{tr}(D_{\tilde{\theta}}\Phi)^2$ against $\tilde{\theta}$ for $f(\pi/2) = 1/2, g(\pi/2) = 1/2$

4.5.4 SU(2) Examples

The $k = 1$ Case

To get a SU(2) solution, we may take $P(Z^\alpha) = (Z^0Z^1 + Z^2Z^3)$. This gives $Q(Z^\alpha) = (Z^0Z^1 + Z^2Z^3)/(Z^2Z^3)$. The simplest choice for f, namely $f = 0$ gives an abelian solution as shown in section (4.5.1). To get something genuinely non-abelian, we may take $f = \log Q^n$, where $n \in \mathbb{Z}$. This leads to

$$\tilde{F}(Z^\alpha) = \begin{pmatrix} \zeta Q^n & Q^{n-1} + Q^{-(n+1)} \\ 0 & \zeta^{-1}Q^{-n} \end{pmatrix}.$$

The Birchoff factorization gives the following expressions for $\hat{h}$ and h,

$$\begin{aligned} \hat{h} &= \log(1 - \zeta_1/\zeta)^n(-\zeta_2)^{n/2}, \\ h &= -\log[(a\zeta - \zeta_2)^n/(-\zeta_2)^{n/2}], \end{aligned} \tag{4.75}$$

where $\zeta_1 = (q-p)/2v\bar{u}$ and $\zeta_2 = -(q+p)/2$. The quantities p and q are given by

$$\begin{aligned} p &= 1 + |u|^2 + |v|^2, \\ q &= [(1 + |u|^2 + |v|^2)^2 - 4|u|^2|v|^2]^{1/2}. \end{aligned} \tag{4.76}$$

Using these, we can find an expression for $\rho(\zeta)$,

$$\begin{aligned} \rho(\zeta) &= \frac{e^{-2h} + e^{-2\hat{h}}}{Q(\zeta)} \\ &= \frac{1}{(-\zeta_2)}\left[\frac{\zeta^3}{(\zeta - \zeta_1)^3(a\zeta - \zeta_2)} + \frac{\zeta(a\zeta - \zeta_2)}{(\zeta - \zeta_1)}\right]. \end{aligned} \tag{4.77}$$

Now using the expression for Δ_r (4.30), we can calculate Δ_0. Calculating the residue at $\zeta = \zeta_1$ gives

$$\Delta_0 = \frac{2^n q^{2n-1}}{(p+q)^n} + \frac{(p+q)^n}{2^n q^{2n+1}}. \tag{4.78}$$

Let us consider the $n = 1$ case (or $n = -1$ which gives the same Δ_0). The procedure described in section (4.2.3) then yields explicit (although rather complicated) expressions for Φ and A_μ, as rational functions of $\cos\theta$, $\cos\tilde{\theta}$ and $\exp(i\varphi)$. The dependence on φ can be compensated by a gauge transformation, so in effect the solution depends only on θ and $\tilde{\theta}$. It is effectively an SO(2)-invariant solution of the Yang-Mills-Higgs equations on M.

The functions are somewhat simpler when expressed in terms of X and Y, where $X = \cos^2(\theta/2)$ and $Y = \cos^2(\tilde{\theta}/2)$. X and Y can be thought of as the 'spatial latitude' and the 'time' respectively. Then, for instance the length of the Higgs field is given by

$$\text{-tr } \Phi^2 = \frac{1}{2}H(X,Y)/(1+X^2Y^2)^2, \tag{4.79}$$

where

$$\begin{aligned} H(X,Y) &= 1+16X^4Y^6-24X^4Y^5+9X^4Y^4+16X^2Y^4 \\ &\quad -8X^2Y^3-6X^2Y^2-16XY^4+16XY^3. \end{aligned} \tag{4.80}$$

Figures 4.11- 4.14 show plots of the following gauge-invariant quantities

$$K := \text{-tr } \Phi^2, \tag{4.81}$$

$$L := -\sin^2\tilde{\theta}\text{tr } (D_{\tilde{\theta}}\Phi)^2, \tag{4.82}$$

$$M := -\sin^2\tilde{\theta}\text{tr } [(D_\theta\Phi)^2+(D_\varphi\Phi)^2/\sin^2\theta], \tag{4.83}$$

$$N := L-M = g^{\mu\nu}\text{tr } [(D_\mu\Phi)(D_\nu\Phi)]. \tag{4.84}$$

A couple of things to note are: As $Y \longrightarrow 0,1$, that is in the distant past and future, the Higgs field approaches a 'vacuum value' where $-\mathbf{tr}\ \Phi^2 = \frac{1}{2}$ and $-\mathbf{tr}\ (D_\mu\Phi)^2 = 0$. At the point $X = 0$ on the spatial sphere, we have $-\mathbf{tr}\ \Phi^2 = \frac{1}{2}$, $-\mathbf{tr}\ (D_{time}\Phi)^2 = 0$ and $-\mathbf{tr}(D_{space}\Phi)^2 = 16Y^4(Y-1)^2$.

A topologically nontrivial solution is given by the $n = 2$ case. As the plot for K against X and Y in figure 4.16 shows, the Higgs field in this case is a heteroclinic connection between $\mathcal{I}^-$ ($Y \to 0$) and $\mathcal{I}^+$ ($Y \to 1$). It takes the value of 4.5 at $\mathcal{I}^+$ and a value of 0.5 at $\mathcal{I}^-$. The plots show that the variation of the field in the (spatial) X-direction is not that much. In fact, for fields generated by subsequent n ($n = 3,4\ldots$), this dependence decreases with increasing n so that for a large enough n we have the Higgs field depending only on Y, *i.e.* on 'time' only. So we have (essentially) a spatially homogeneous solution. That this is indeed the case can

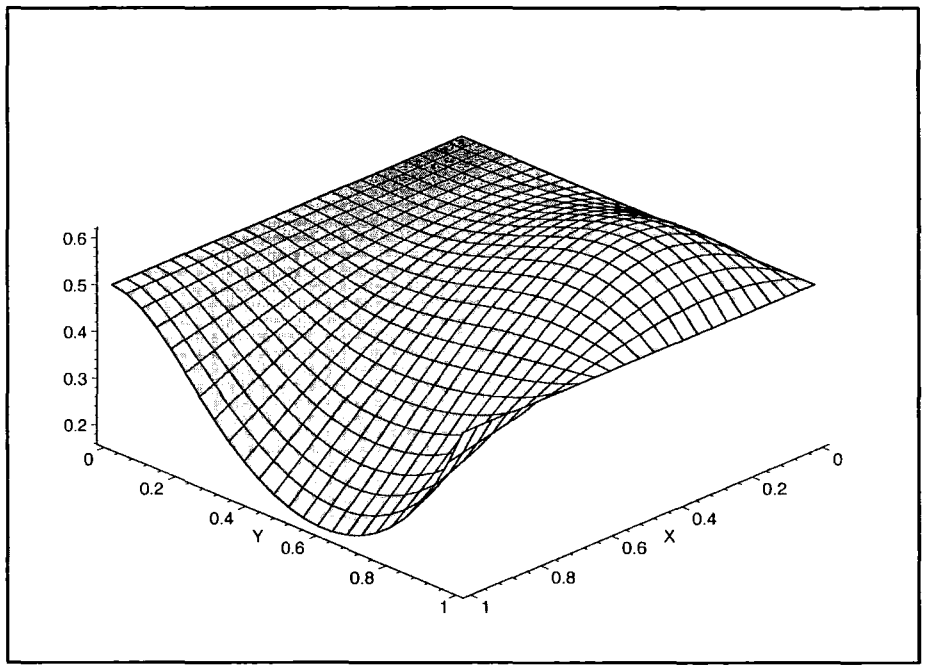

Figure 4.11: A plot of K against 'spatial latitude' X and 'time' Y.

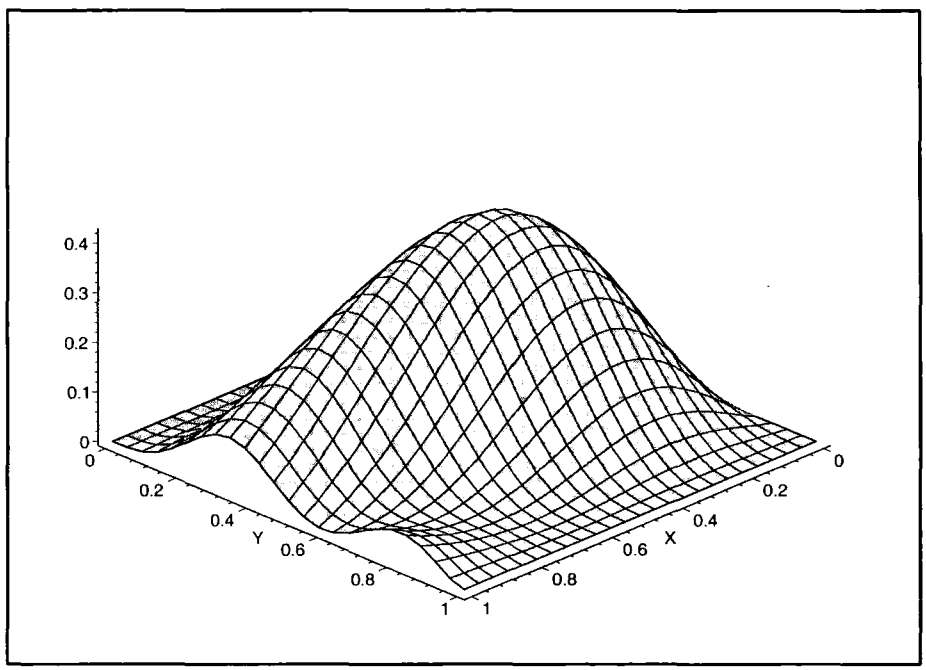

Figure 4.12: A plot of L against X and Y.

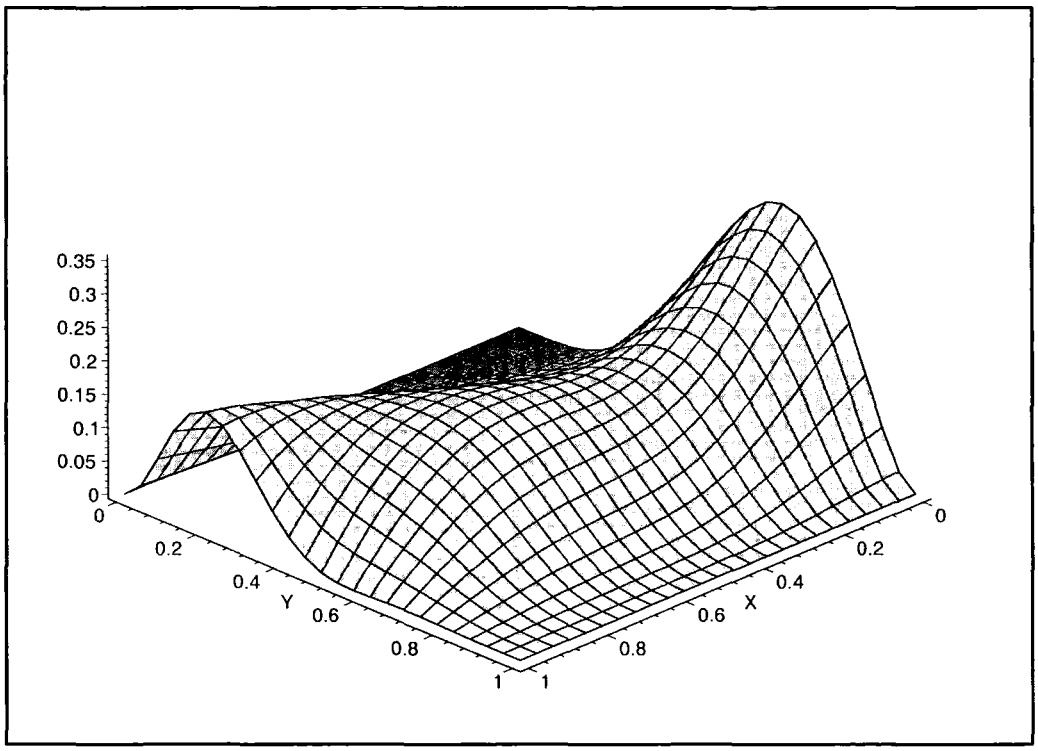

Figure 4.13: A plot of M against X and Y.

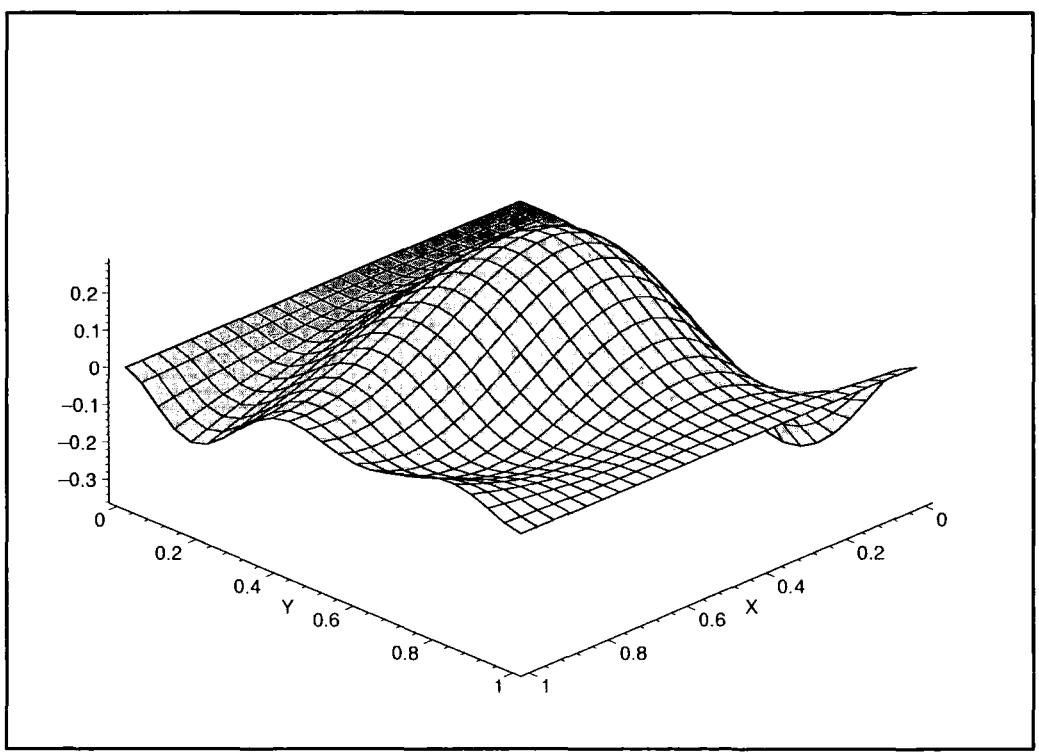

Figure 4.14: A plot of N against X and Y.

be seen by the following argument. For $n \geq 2$, K is given by

$$\begin{aligned} K &= (2n-1)^2 - 4(2n-1)(n-1)Y + (2n-2)^2Y^2 - \\ &\quad (4n-2)(2n+1)X^{2n}Y^{2n} + \\ &\quad (16n^2X^{2n-1} - 8X^{2n})Y^{2n+1} + \\ &\quad (8(n^2+1)X^{2n} - 16n^2X^{2n-1})Y^{2n+2} + \\ &\quad (2n+1)^2X^{4n}Y^{4n} + 2n+2)^2X^{4n}Y^{4n+2} - \\ &\quad 4(2n+1)(n+1)Y^{4n+1}X^{4n} \;/\; 2(X^{2n}Y^{2n}+1)^2. \end{aligned} \tag{4.85}$$

Note that as $Y \to 0$ and 1, $K \to \frac{1}{2}(2n-1)^2$ and $\frac{1}{2}$ respectively. Now consider what happens to K when $0 \leq X \leq 1$, $0 < Y < 1$ and n is very large. K is effectively given by

$$K = \frac{1}{2}((2n-1)^2 - 4(2n-1)(n-1)Y + (2n-2)^2Y^2, \tag{4.86}$$

where the contribution from the other terms is negligible. Figures 4.15- 4.16 shows plots of K against (X, Y) for $n = 2$ 10.

The expression of K is analogous to Prasad's formula for monopoles in $\mathbb{R}^3$. This formula relates the length of the Higgs field to the t'Hooft superpotential [88],

$$||\Phi||^2 = -\frac{1}{4}\Box \log \rho, \tag{4.87}$$

where ρ is the t'Hooft superpotential and $\Box$ is the wave-operator on the Euclidean space-time. In our case the field Δ_0 plays the role of the t'Hooft superpotential. There is a similar formula (equivalent to the expression of K) for the de Sitter solitons,

$$||\Phi||^2 = -\frac{1}{2}[\Box' \log \Delta_0 - r(\tilde{\theta})], \tag{4.88}$$

where $\Box'$ is the Laplacian on $\mathbb{R} \times S^2$,

$$\Box' = \sin^2(\tilde{\theta})[\partial_{\tilde{\theta}}^2 - \partial_\theta^2 - (\cos\theta/\sin\theta)\partial_\theta - (\cos\tilde{\theta}/\sin\tilde{\theta})\partial_{\tilde{\theta}}], \tag{4.89}$$

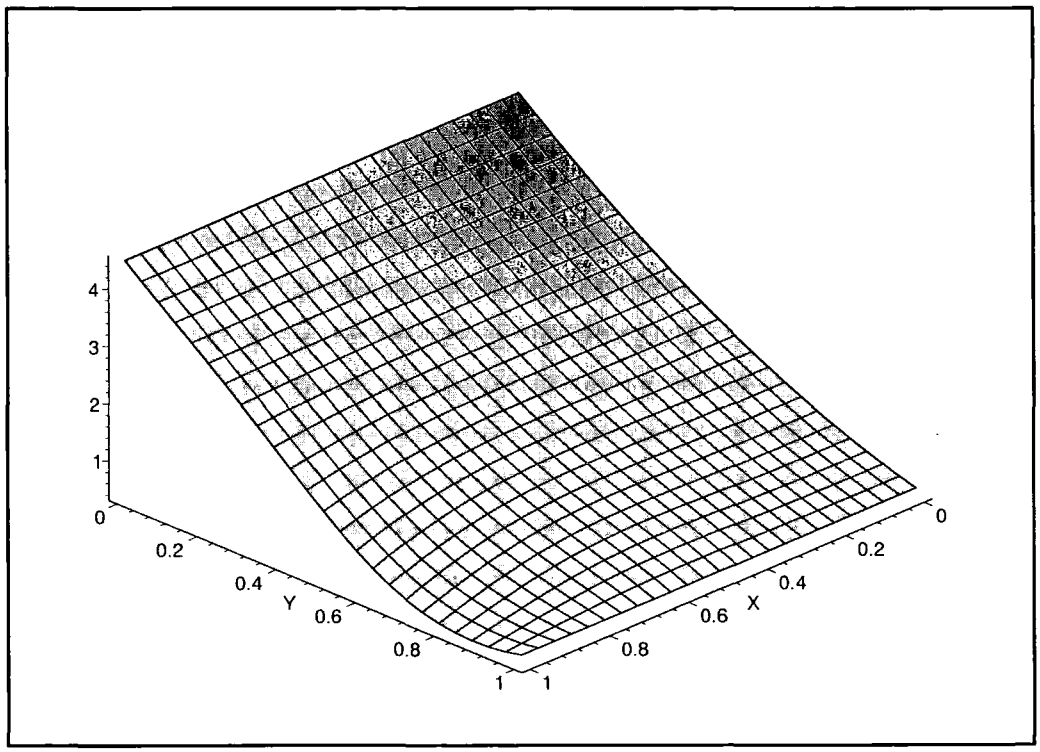

Figure 4.15: K against X and Y for $n = 2$

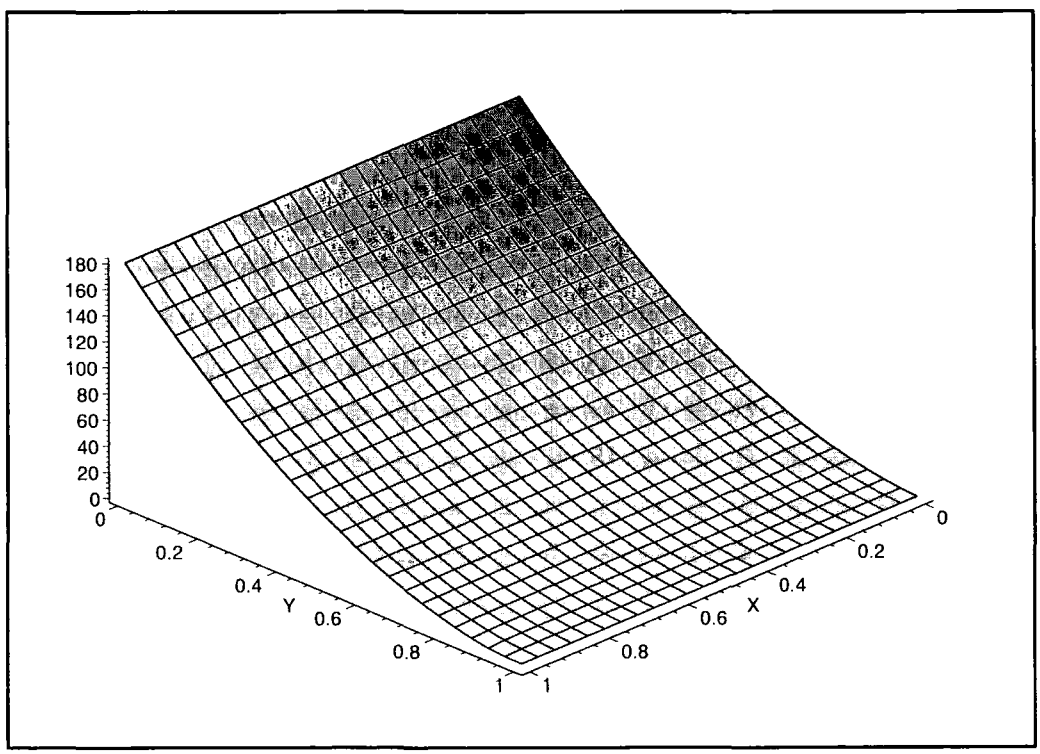

Figure 4.16: K against X and Y for $n = 10$

Δ_0 is given by (4.78), and $r(\tilde{\theta}) = n^2\cos^2(\tilde{\theta}) - 2n^2\cos(\tilde{\theta}) + (n^2+1)$. This formula is not as general as (4.87) since it is only valid for the class of solutions generated by $f = \log Q^n$. There are of course analogous expressions for $r(\tilde{\theta})$ for other choices of f.

The $k = 2$ Case

To obtain a $k = 2$ solution, we need to find a homogeneous polynomial of degree 4, $P(Z)$ which satisfies the reality condition $P^\dagger(Z) = -P(Z)$. The polynomial $Q(Z)$ involved in the patching matrix is then $Q(Z) = P(Z)/(Z^2Z^3)^2$. Note that $\Gamma(x,\zeta)$ is now given by $\Gamma = (e^f - e^{-1})/Q(Z)$, so the patching matrix is

$$\tilde{F}(Z^\alpha) = \begin{pmatrix} \zeta^2 e^f & [e^f - e^{-f})/Q(Z^\alpha)] \\ 0 & \zeta^{-2}e^{-f} \end{pmatrix}.$$

One choice of the polynomial $P(Z^\alpha)$ is $P(Z^\alpha) = i(Z^0Z^1 + Z^2Z^3)^2$. This then gives

$$Q(Z^\alpha) = i[1 + (Z^0Z^1/Z^2Z^3)^2], \tag{4.90}$$

which written in terms of ζ is

$$Q(\zeta) = i(1 - \zeta_1/\zeta)^2(a\zeta - \zeta_2)^2. \tag{4.91}$$

Here ζ_1 and ζ_2 are as before, $\zeta_1 = (q-p)/2v\bar{u}$ and $\zeta_2 = -(q+p)/2$. The previous choice of f namely $f = \log Q$ does not lead to a non-singular solution on the de Sitter space-time; but $f = \log(Q^{-1})$ does. The splitting of this f is analogous to the $k = 1$ case,

$$\begin{aligned} \hat{h} &= \log[(1 - \zeta_1/\zeta)^{-2}(-\zeta_2)^{-1}] \\ h &= -\log[(a\zeta - \zeta_2)^{-2}(-\zeta_2)], \end{aligned} \tag{4.92}$$

and this leads to

$$\rho(\zeta) = -\frac{\zeta^2}{(-\zeta_2)^2(\zeta - \zeta_1)^2(a\zeta - \zeta_2)^2} - \frac{\zeta^2(\zeta - \zeta_1)^2}{(-\zeta_2)^2(a\zeta - \zeta_2)^2}. \tag{4.93}$$

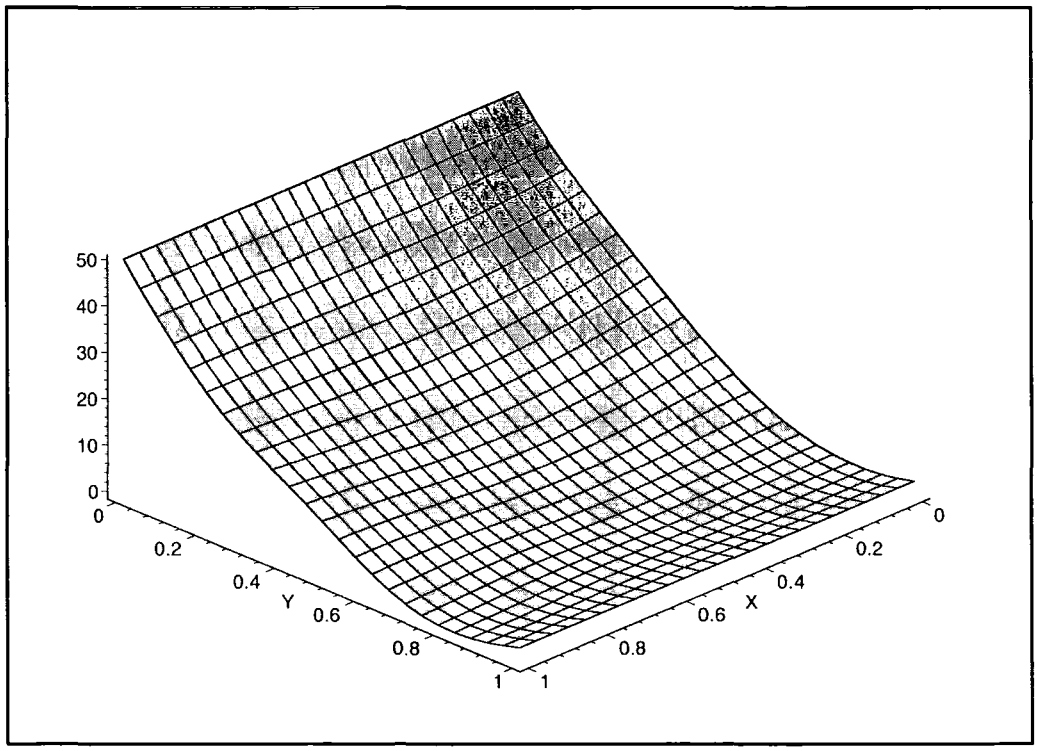

Figure 4.17: A plot showing $-\mathrm{tr}\Phi^2$ against X and Y for a $k = 2$ solution.

To obtain the fields Δ_{-1}, Δ_0 and Δ_{-1}, we need to calculate the residues for $\zeta = \zeta_1$ and $\zeta = 0$,

$$\begin{aligned}
\Delta_{-1} &= \frac{(p-q)^3(3p+q)}{2a^3(p+q)^2q^7}, \\
\Delta_0 &= -\frac{3(p-q)^2p}{a^2q^7(p+q)^2} - \frac{4(p-q)^2}{a^2(p+q)^4}, \\
\Delta_1 &= \frac{2(p-q)(p-3q)}{aq^7(p+q)^2} - \frac{32(p-q)q}{a(p+q)^5}.
\end{aligned} \tag{4.94}$$

It is then straight forward to calculate the gauge fields using the formulas given in section 4.2. The expressions for the gauge fields are rather long and complicated and have therefore not been reproduced here. However the plot of the trace-invariant quantity $-\mathrm{tr}\Phi^2$ is given in figure 4.17. This figure is similar to (but of course different from) the $n = 2$ case of the $k = 1$ solution.

4.6 Conclusions

In this chapter we have seen that the Yang-Mills system on a 4-dimensional space-time can be reduced on a curved space-time to give an integrable system on curved space-time. We have constructed various U(1) and SU(2) examples on both Poincare and de Sitter space-time. For the U(1) case when the patching function is $f = Q^{-k}$, we get an imploding-exploding wave-type solution on de Sitter space-time $\mathbb{R} \times S^2$, where the wave travels between the two antipodal points on the sphere. The U(1) case for $f = \log Q^k$ generates a solution that is homogeneous on S^2. The Maxwell-Higgs field then depends on time only, and the maximum value of the field occurs in the distant past, as $\tilde{\theta} \to \pi$, with magnitude k. The U(1) case with $f = 0$ gives a solution that is singular on de Sitter space-time, but nonsingular on Poincare space-time.

The (one-soliton) SU(2) case can be constructed by taking the function f in the patching matrix to be $f = \log Q^n$, where Q is given by $Q = (Z^0 Z^1 + Z^2 Z^3)/(Z^2 Z^3)$. This soliton is depicted in figure 4.11. The plot shows that in the distant past or future (as $\tilde{\theta} \to \pi$ or $\tilde{\theta} \to 0$), the Higgs field approaches the vacuum value of $-\mathrm{tr}\ \Phi^2 = \frac{1}{2}$. The two-soliton solution has also been constructed. For this we have taken $f = -\log Q$ where $Q = i[1 + (Z^0 Z^1/Z^2 Z^3)^2]$. This soliton is depicted in figure 4.17.

One feature that is absent here for the solitons has been seen in the anti-de Sitter case: the solitons are localised and travel on time-like geodesics. It seems likely that a similar thing happens in the de Sitter case. To investigate this one needs to write the equations in the Q-matrix form [90]. For instance, there is a gauge in which $A_{\bar{u}} = H^{-1}\partial_{\bar{u}} H$ and $A_v = H^{-1}\partial_v H$, where $H \in \mathrm{SL}(2,\mathbb{C})$. The hermitian matrix $Q = HH^*$ then satisfies

$$\partial_u(Q^{-1}\partial_{\bar{u}} Q) - \partial_{\bar{v}}(Q^{-1}\partial_v Q) = 0. \tag{4.95}$$

Equation (4.95) is identical to the Bogomolny equations (4.47). It is possible that this form may also give rise to a conserved quantity on the de Sitter space-time, analogous to the one found by Ward for the flat space-time case. Such a quantity has been found for the anti-de Sitter case as well [78].

Bibliography

[1] V.Kotecha (2001). Resonance effects in Topological discrete sine-Gordon system, nlin.PS/0102037.

[2] V.Kotecha and R.S.Ward (2001). Integrable Yang-Mills-Higgs equations in three-dimensional de Sitter space-time, *J Math Phys* **42** 1018-1025.

[3] J.Scott Russell (1845). Report on waves, *Proc of the British Association for the Advancement of Science, London* 311-390.

[4] P.Drazin and R.Johnson (1989). *Solitons: An Introduction* (CUP).

[5] J.Rubinstein (1970). Sine-Gordon equation, *J Math Phys* **11** 258-266.

[6] L.P.Eisenhart (1909). *A treatise on the differential geometry of curves and surfaces* (Boston).

[7] E.B.Bogomolny (1976). The stability of classical solutions, *Sov J Nucl Phys* **24** 449-454.

[8] A.R.Bishop and T.Scheider (1983) *Solitons and Condensed Matter Physics* (Springer-Verlag).

[9] H.B.Nielsen and P.Olesen (1973). Vortex-line models for dual strings, *Nucl Phys B* **61** 45-61.

[10] T.H.R.Skyrme (1962). A unified field theory of mesons and baryons, *Nucl Phys* **31** 556-569.

[11] E.Witten (1983). Current algebra, baryons and quark confinement, *Nucl Phys B* **223** 433-444.

[12] R.A.Battye and P.M.Sutcliffe (1997). Symmetric Skyrmions, *Phys Rev Lett* **79** 363-366.

[13] G.S.Adkins, C.R.Nappi, E.Witten (1983). Static properties of nucleons in the Skyrme model, *Nucl Phys B* **228** 552-566.

[14] P.Irvin (2000). Zero mode quantization of multi-Skyrmions, *Phys Rev D* **61** 114024-114041.

[15] P.W.Higgs (1966). Spontaneous symmetry breakdown without massless bosons, *Phys Rev* **145** 1156-1163.

[16] C.Tully (2000). Status of LEP-wide Higgs searches, talk Princeton University.

[17] T.W.B.Kibble (1976). Topology of cosmic domains and strings, *J Phys A* **9** 1387-1398.

[18] V.I.Arnold (1980) *Mathematical Methods of Classical Mechanics* Graduate Texts in Mathematics (Sringer-Verlag)

[19] R.S.Ward (1990) Integrable systems in twistor theory, in *Twistors in mathematics and physics*, 246-259, (CUP).

[20] C.S.Gardner, J.M.Greene, M.D.Kruskal and R.M.Miura (1967). Method for solving the Korteweg-de Vries equation, *Phys Rev Lett* **19** 1095-1097.

[21] R.Hirota (1971). Exact solution of the Korteweg-de Vries equation for multiple collisions of solitons, *Phys Rev Lett* **27** 1192-1194.

[22] L.J.Mason and N.M.J.Woodhouse (1996). *Integrability, Self-Duality and Twistor theory*, (OUP).

[23] P.D.Lax (1968). Integrals of nonlinear equations of evolution and solitary waves, *Comm Pure Appl Math* **21** 467-490.

[24] M.J.Ablowitz and P.A.Clarkson (1991). *Solitons, Nonlinear Evolution Equations and Inverse Scattering* (CUP), Chapter 7 and references therein.

[25] M.J.Ablowitz, D.J.Kaup, A.C.Newell and H.Segur (1973). Method for solving the sine-Gordon equation, *Phys Rev Lett* **30** 1262-1264.

[26] V.E.Zakharov and A.B.Shabat (1972). Exact theory of two-dimensional self-focusing and one-dimensional of waves in nonlinear media, *Sov Phys JETP* **34** 62-69.

[27] M.J.Boussinesq (1871). Théorie de l'intumescence appelée onde solitaire ou de translation se propageant dans un canal rectangulaire, *C R Acad Sc Paris* **72** 755-759.

[28] D.J.Korteweg and G.de Vries (1895). On the change of form of Long waves advancing in a rectangular canal, and on a new type of long stationary waves, *Philos Mag Ser 5* **39** 422-443.

[29] A.Davey and K.Stewartson (1974). On three-dimensional packets of surface waves, *Proc Roy Soc London A* **338** 101-110.

[30] B.B.Kadomtsev and V.I.Petviashvili (1970). On the stability of solitary waves in weakly dispersive media, *Sov Phys Dokl* **15** 539-541.

[31] R.M.Miura (1968). Korteweg-de Vries equations and generalisations I. A remarkable explicit nonlinear transformation, *J Math Phys* **9** 1202-1204.

[32] R.S.Ward (1988). Soliton solutions in an integrable chiral model in 2+1 dimensions, *J Math Phys* **29** 386-389.

[33] R.S.Ward (1985). Integrable and solvable systems, and their relations among them, *Phil Trans R Soc Lond A* **315** 451-457.

[34] D.K.Campbell, J.F.Schonfeld and C.A.Wingate (1983). Resonance structure in kink-antikink interactions in ϕ^4 theory, *Physica* **9 D** 1-32.

[35] T.Belova and A.E.Kudryavtsev (1988). Quasiperiodical orbits in the scalar classical $\lambda\phi^4$ field theory, *Physica D* **32** 18.

[36] P.Anninos, S.Oliveira, and R.A.Matzner (1991). Fractal structure in the scalar $\lambda(\phi^2-1)^2$ model, *Phys Rev* **D 44** 1147-1160.

[37] M.J.Ablowitz, M.D.Kruskal and J.F.Ladik (1979). Solitary wave collisions, *Siam J Appl Maths* **36** 428-437.

[38] V.A.Gani and A.E.Kudryavtsev (1998). Kink-antikink interactions in the double sine-Gordon equation and the problem of resonance frequencies, cond-mat/9809015.

[39] Fei Zhang (1997). Kink shape modes and resonant dynamics in sine-lattices, *Physica D* **110** 51-61.

[40] A.E.Kudryavtsev (1975). Solitonlike solutions for a Higgs scalar field., *JETP Lett* **22** 82-83.

[41] D.K.Campbell, M.Peyrard and P.Sodano (1986). Kink-antikink interactions in the double sine-Gordon equation, *Physica* **19 D** 165-205.

[42] J.M.Speight and R.S.Ward (1994). Kink dynamics in a novel discrete sine-Gordon system, *Nonlinearity* **7** 475-484.

[43] W.H.Press *et al* (1988) *Numerical recipes in C* (CUP) p708.

[44] R.Rajaraman, (1982). *Solitons and Instantons* (North-Holland).

[45] P.Morse and H.Feschbach (1953). Methods of mathematical physics, (McGraw-Hill Book Co.).

[46] M.Peyrard and D.K.Campbell (1983). Kink-antikink interactions in the parametrically modified sine-Gordon system, *Physica* **9 D** 33-51.

[47] M.J.Rice (1983). Physical dynamics of solitons, *Phys Rev B* **28** 3587-3589.

[48] R.Boesch and C.R.Willis (1990). Existence of an internal quasimode for a sine-Gordon soliton, *Phys Rev B* **42** 2290.

[49] N.R.Quintero, A.Sanchez and F.G.Mertens (2000). Existence of internal modes of sine-Gordon kinks, *Phys Rev E* **62** R60-R63.

[50] N.Manton (1979). An effective Lagrangian between solitons, emphNuc Phys B **150** 397-412.

[51] R.S.Ward (1992). Discretization of integrable systems, *Phys Lett A* **165** 325-329.

[52] R.Hirota *et al*(1993). Difference scheme of soliton equations. *Future directions of nonlinear dynamics in physical and biological systems*, ed P.L.Christiansen *et al* (New York: Plenum).

[53] W.J.Zakrzewski (1994). A modified discrete sine-Gordon model, *Nonlinearity* **8** 517-540.

[54] J.M.Speight (1997). A discrete ϕ^4 system without a Peierls-Nabarro barrier, *Nonlinearity* **10** 1615-1625.

[55] R.S.Ward (1997). Bogomolny bounds for two-dimensional lattice systems, *Comm Math Phys* **184** 397-410.

[56] T.Ioannidou (1997). Soliton dynamics in a novel discrete $O(3)$ sigma model in $(2+1)$ dimensions, *Nonlinearity* **10** 1357-1369.

[57] A.Wolf, J.B.Swift, H.L.Swinney and J.A.Vastano (1985). Determining Lyapunov exponents from a time series, *Physica D* **16** 285-317.

[58] J.M.Speight (1994). Kink Casimir energy in a lattice sine-Gordon model, *Phys Rev* **D 49** 6914-6919.

[59] C.Willis (2001). Personal Communication.

[60] V.H.Schmidt (1979). Exact solution in the discrete case for solitons propagating in a chain of harmonically coupled particles lying in double-minimum potential wells, *Phys Rev B* **20** 4397-4405.

[61] P.C.Bressloff and G.Rowlands (1997). Exact travelling wave solutions of an "integrable" discrete reaction-diffusion equation, *Physica D* 255-269.

[62] S.Flach, Y.Zolotaryuk and K.Kladko (1999). Moving lattice kinks: An inverse method, *Phys Rev E* **59** 6105-6115.

[63] G.Friesecke and J.A.D.Wattis (1994). Existence theorem for solitary waves on lattices, *Comm Math Phys* **161** 391-418.

[64] M.Toda (1988). *Theory of Nonlinear Lattices* (Springer-Verlag).

[65] M.J.Ablowitz and J.F.Ladik (1975). Nonlinear differential-difference equations, *J Math Phys* **16** 598-603.

[66] Y.Frenkel and T.Kontorova (1939). On the theory of plastic deformation and twinning, *Acad Sci U.S.S.R. J Phys* **1** 137-149.

[67] A.C.Scott (1999). *Nonlinear Science* (OUP).

[68] D.B.Duncan, J.C.Eilbeck, H.Feddersen and J.A.D.Wattis (1993). Solitons on lattices, *Physica D* **68** 1-11.

[69] S.Homma and S.Takeno (1985). Numerical evidence of the existence of approximate kink-antikink states and breather-like modes in sine-form double sine-Gordon equation, *Prog Theo Phys* **74** 618-621.

[70] S.Homma and S.Takeno (1986). a sine-Lattice (sine-form discrete sine-Gordon) equation - one-kink and two-kink solutions and physical models, *J Phys Soc Japan* **55** 65-75.

[71] S.Homma and S.Takeno (1987). Sine-Lattice equation III. Nearly integrable kinks with arbitrary kink amplitude, *J Phys Soc Japan* **56** 3480-3490.

[72] R.S.Ward (1999). Lax pairs for integrable lattice systems, *J Math Phys* **40** 299-308.

[73] L.D.Faddeev and L.A.Takhtajan (1987). *Hamiltonian methods in the theory of solitons*, (Springer-Verlag).

[74] H.Braden (1997). R-Matrices and generalised inverses, *J Phys A* **30** L485-L493.

[75] M.F.Atiyah (1984). Magnetic monopoles in hyperbolic spaces, in *Proceedings on vector bundles on algebraic varieties* (Bombay) 1-34.

[76] A.Chakrabarti (1986). Construction of hyperbolic monopoles, *J Math Phys* **27** 340-348.

[77] R.S.Ward (1999). Two integrable systems related to hyperbolic monopoles, *Asian J Math* **3** 325-332.

[78] D.G.Hickin (2000). Personal Communication.

[79] R.Penrose (1967). Twistor algebra, *J Math Phys* **8** 345-366.

[80] R.S.Ward and R.O.Wells (1990). *Twistor Geometry and Field Theory*, CUP.

[81] R.S.Ward (1977). On self-dual gauge fields, *Phys Lett* **61A** 81-2.

[82] M.F.Atiyah and R.S.Ward (1977). Instantons and algebraic geometry, *Comm Math Phys* **55** 117-125.

[83] L.J.Mason (1995). Generalised twistor correspondences, d-bar problems, and the KP equations. In *Twistor Theory.* Ed S.Huggett. Lecture note in Pure and Applied Maths **169**, Marcell Dekker.

[84] E.F.Corrigan *et al* (1978). The construction of self-dual solutions to SU(2)-gauge theory, *Comm Math Phys* **58** 223-240.

[85] S.W.Hawking and G.F.R.Ellis (1973). *The Large-Scale Structure of Space-Time* (CUP).

[86] N.M.J.Woodhouse (1992). Contour integrals for the ultrahyperbolic wave equation, *Proc Roy Soc London A* **438** 197-206.

[87] R.Penrose and W.Rindler (1984). *Spinors and Space-Time* Vol I, Section 4.15, (CUP).

[88] M.K.Prasad (1980). Instantons and monopoles in Yang-Mills gauge field theories, *Physica D* **1** 167-214.

[89] G. t'Hooft (1974). Magnetic monopoles in unified gauge theories, *Nucl Phys B* 276-284.

[90] P.M Sutcliffe (1993). Yang-Mills-Higgs solitons in (2+1)-dimensions, *Phys Rev D* **47** 5470-5476.